DESIGN AND SIZING METHOD FOR DEPLOYABLE SPACE ANTENNAS

Dissertation

zur Erlangung des akademischen Grades

Doktoringenieur
(Dr.-Ing.)

von Dipl.-Ing. Marco Straubel
geb. am 2. März 1982 in Zerbst

genehmigt durch die Fakultät für Maschinenbau der
Otto-von-Guericke-Universität Magdeburg

Gutachter:
Prof. Dr.-Ing. Michael Sinapius
Prof. Dr.-Ing. habil. Dr. h. c. Ulrich Gabbert
Prof. Dr.-Ing. Joachim Block

Promotionskolloquium am 4. September 2012

Marco Straubel: *DESIGN AND SIZING METHOD FOR DEPLOYABLE SPACE ANTENNAS,* Dissertation

SUPERVISORS:
Prof. Dr.-Ing. Michael Sinapius
Prof. Dr.-Ing. habil. Dr. h. c. Ulrich Gabbert
Prof. Dr.-Ing. Joachim Block

LOCATION:
Braunschweig

SUBMITTED:
July 2nd, 2012
COLLOQUIUM:
September 4th, 2012

ZUSAMMENFASSUNG

Die Dimensionen von Instrumenten-, Antennen- und Solargeneratorstrukturen an Raumfahrzeugen übersteigen des Öfteren die verfügbaren Volumina der existierenden Trägersysteme. Um diese Systeme dennoch zu realisieren, werden die Strukturen mit Faltmechanismen versehen und so während des Orbit-Transfers platzsparend im Trägersystem verstaut.

Ein Nebeneffekt ist dabei, dass auch eine Struktur, die im entfalteten Zustand eine geringe - der Schwerelosigkeit angemessene - Steifigkeit besitzt, im gepackten Zustand kompakter und steifer ist und somit eher den hohen strukturellen Anforderungen während des Starts an eine Nutzlast entspricht.

Dementsprechend erfordert das Auslegen einer solchen Struktur die Berücksichtigung von verschiedenen Konfigurationen derselben, essentiellen Strukturbauteile. Die Arbeit zeigt auf, wie sich dabei die Rollen von einzelnen Komponenten ändern.

So kann eine Komponente in einer Konfiguration einen Hauptteil der Last tragen während sie in einer anderen Konfiguration von einer anderen Strukturkomponente getragen werden muss und diese durch ihre eigene Masse belastet.

Im Kern der Arbeit wird daher das Strukturkonzept der entfaltbaren Membranantenne vorgestellt sowie eine Methode erläutert, die die Auslegung der verschiedenen Komponenten in einer angemessenen Reihenfolge ermöglicht.

Die erhaltene Methode wird im Anschluss genutzt um die Auslegung mit Hilfe der Finiten Elemente Methode (FEM) zu automatisieren. Diese Automatisierung dient zum einen dazu, schnell auf Änderungen in den Anforderungen reagieren zu können. Zum anderen vereinfacht sie aber auch Parameterstudien, deren Auswertung zu einem besseren Strukturverständnis führen.

Als Bestätigung der Methode wird im Anschluss an die Parameterstudie eine weiter verbesserte Variante der Beispielstruktur vorgestellt, die die zuvor definierten Anforderungen sogar übertrifft.

ABSTRACT

The dimensions of spaceborne instrument-, antenna- and solar array structures do often exceed the available envelope of common launch vehicles. To realize such systems anyhow the structures are provided with folding mechanisms that allow a space saving orbit transfer.

A side effect from this deployment concept is the fact that a structure which provides a sufficient deployed stiffness for space environment can also fulfil the stiffness requirements for launcher payload in stowed configuration.

Consequently, the sizing of such structures demands the consideration of different configurations that are composed out of the same essential structural parts. The thesis, thereby, illustrates how the roles of the single components change for the different configurations.

For instance, a component that carries a major part of the load in a first configuration can be nearly offloaded in a second one. Moreover, this component can load another part with its own mass, whereas, this other component is passive in the first configuration and needs to be carried.

Thus, the core of this thesis contains the introduction into an exemplary antenna structure design as well as a method for an adequate sizing of all relevant structural parts.

The developed method is then integrated in a Finite Element Analysis (FEA) aided, closed loop sizing chain. The used automated close loop sizing helps to rapidly react on changed requirements and generates the possibility of performing fast parameter studies to improve the understanding of such a sophisticated structure.

The validity of these approaches is finally proven by presenting a re-sized antenna configuration after the parameter study and its evaluation. This final configuration more than meets the previously defined requirements for the exemplary antenna structure.

In science, being stuck can be a sign that
you are about to make a great leap forward.
The things that don't make sense are,
in some ways, the only things that matter.

— Michael Brooks [14]

ACKNOWLEDGMENTS

The presented thesis is the result of five years of research and development at the DLR Institute of Composite Structures and Adaptive Systems in Braunschweig (Germany), the European Space Research and Technology Centre (ESTEC) in Noordwijk (The Netherlands) of the European Space Agency (ESA) and NASA's Langley Research Center (LaRC) in Hampton, VA.

During this time and all of those stations Prof. Michael Sinapius was a very helpful guide on the way to the final submission of this thesis by always finding the right balance between encouraging and challenging me. Therefore, I want to thank him for his outstanding mentoring and his continuous support of my research as well as the research semester at NASA.

Moreover, a lot of other DLR colleagues need to be thanked for their support of my work. I want to acknowledge Christian Hühne, Prof. Joachim Block and Christine Arlt for their constant support of my work as well as the countless discussions on technical but also on organisational level that were very essential for the final submission of this thesis which happens in combination with upcoming new tasks and running projects of high importance.

I, furthermore, like to thank Prof. Ulrich Gabbert and Prof. Joachim Block for their interest in my work and the offer to act as examiners for the submitted thesis.

Special thanks are also addressed to my former mentor on engineering level, Christoph Sickinger. Christoph supported me in the first years by introducing me into the wide field of gossamer structures and also infected me with his enthusiasm for the extreme lightweight design as well as for the ultimate in gossamer structures - the solar sails.

During my research stays at ESTEC, a lot of ESA staff was helping me by sharing their impressive expertise on their special fields. Hence I want to acknowledge Stéphane Langlois, Torben

Henriksen, Julian Santiago Prowald, Kees van't Kloster, Cyril Mangenot, Lothar Gerlach, and many others.

Moreover, the three months at NASA's LaRC plays a important role in the finalisation of this thesis. Thus, I want to thank W. Keith Belvin from NASA for his support of the research topic as well as his constantly mentoring and very kind hosting during my time in Hampton. Here I also need to thank the DLR board of directors, which awarded me with the DLR research semester and was thereby enabling this experience.

In addition to Keith, a lot of other NASA stuff guided me during this time and opened my mind for new perspectives during many meeting- and lunch break discussions. Hence, I want to thank also Richard S. Pappa, Keats Wilkie, Tom Murphey, Jessica A. Woods-Vedeler and Erik Vedeler.

Moreover, I thank Steffen Opitz, Martin Hillebrandt and Martin Zander for their important support on proofreading.

In addition to the support of experienced persons, this work had also not been possible without a lot of support from students that supported me during their internships or during their master or diploma thesis. I want to thank Andreas Zörnig, Bharadwaj Kodlekere Manjunath Bhat, Christian Sasse, Christian Wenzel, Florian Gräber, Hardy Köke, Kay Sommerwerk, Lars Lindenau, Martin Hillebrandt, Martin Rehwagen, Matthias Bock, Sergej Schneider, Steffen Zerrer, Tobias Reuter, Venkata Yashwanth Kumar Penjuri and Moritz Nitz for their countless helpful contributions.

Away from the professional support, there are some persons from my private environment that need to be mentioned here as well. The most important part at this point is for sure the support of my partner Diana Stoye who encouraged me during my entire research task as well as during the final compilation of the thesis. Moreover, I want to thank my family and friends for their support and the ongoing - sometimes annoying but for sure helpful - questioning on the state of the thesis.

Thank You,
Marco

CONTENTS

LIST OF FIGURES

LIST OF TABLES

LIST OF ACRONYMS

AOCS	Attitude and Orbit Control System
APDL	ANSYS Parametric Design Language
ASD	Acceleration Spectral Density
CFRP	Carbon Fibre Reinforced Polymer
CFS	Constant Force Springs
CTE	Coefficient of Thermal Expansion
DLR	Deutsches Zentrum für Luft- und Raumfahrt e.V.
DOF	Degree of Freedom
ECSS	European Cooperation for Space Standardization
ESA	European Space Agency
FE	Finite Element
FEA	Finite Element Analysis
FEM	Finite Element Method
LEO	Low Earth Orbit addresses usually orbits between 200km and 1200km
LNA	Low Noise Amplifier
MLI	Multi Layer Insulation
MMODs	Micrometeoroids and Orbital Debris
OASPL	Overall Acoustic Sound Pressure Level
PTFE	Polytetrafluoroethylene is a polymer also known as Teflon®
RADAR	Radio Detection and Ranging
RF	Radio Frequency
RMS	Root Mean Square
SAR	Synthetic Aperture Radar

STEM	Storable Tubular Extendible Member
TC	Telecommand
TM	Telemetry
TRL	Technology Readiness Level
UD	Uni Directional fibre layers are characterized by a defined fibre orientation in one direction
UV	Ultra Violet (wavelength of 10 to 400nm)

LIST OF SYMBOLS

Symbols

α	$\left[\frac{1}{K}\right]$	Coefficient of Thermal Expansion (CTE)
Δl	$[m]$	Difference in length
ΔT	$[K]$	Difference in temperature
Δx	$[m]$	Difference in x-direction
ϵ	$[\,]$	Strain
γ	$\left[\frac{kg}{m}\right]$	Specific Mass per Length
λ	$[m]$	Wavelength
μ	$\left[\frac{kg}{m^2}\right]$	Specific Mass per Area
ν	$[\,]$	Poisson's Ration
ψ	$[\,]$	Fibre Volume Content
ρ	$\left[\frac{kg}{m^3}\right]$	Density
σ	$\left[\frac{N}{m^2}\right]$	Compression or Tension Stress
τ	$\left[\frac{N}{m^2}\right]$	Shear Stress
A	$[m^2]$	Area
a	$\left[\frac{m}{s^2}\right]$	Acceleration
c	$\left[\frac{N}{m}\right]$	Spring Constant
	$\left[\frac{m}{s}\right]$	Speed of Light
d	$[m]$	Distance
e	$[m]$	Thickness or Distance
E	$\left[\frac{N}{m^2}\right]$	Elastic Modulus or Young's Modulus
f	$[Hz]$	Frequency
F	$[N]$	Force
G	$\left[\frac{N}{m^2}\right]$	Shear Modulus
h	$[m]$	Height
I	$[m^4]$	Geometrical Moment of Inertia
k	$[\,]$	Factor
l	$[m]$	Length
m	$[kg]$	Mass
M	$[\,]$	Margin

N	$[\,]$	Number or Amount
p	$\left[\frac{N}{m^2}\right]$	Pressure
r	$[m]$	Radius
u	$[m]$	Deflection
U	$\left[\frac{N}{m}\right]$	Distributed Line Load
w	$[m]$	Width

Subscripts and Notations

a	Acceleration
A	Antenna
AA	Antenna array
Alu	Aluminium
ana	Analytic
b	Boom Cross Section
B	Boom or Beam
$crit$	Critical
$circ$	Circumferential
c	Compression
C	Corner or Cable
CFS	Constant Force Springs
CO	Cut-Out
$Core$	Core of a sandwich laminate
D	Deployed
e	Estimated
FEM	Finite Element Method/Model
FS	Face Sheet of a sandwich laminate
h	Hub
(i)	A set of variable during an iteration
i	Inner
IF	Interface
inv	Inverse
K	Kapton® (Kapton® is a trademark of DuPont, chemically Kapton® is a Polyimide)
lat	Lateral

$_{lin}$	Linear
$_{long}$	Longitudinal
$_{L}$	Dimension or a property that is oriented in or related to the *length* direction of the antenna
$_{LNA}$	Low Noise Amplifier
$_{max}$	Maximum
$_{M}$	Membrane or Mechanical
$_{MA}$	Antenna Membrane
$_{MS}$	Service Membrane
$_{o}$	Outer
$_{quad}$	Quadratic
$_{r}$	Radius
$_{ref}$	Reference
$_{s}$	Shell
$_{S}$	Safety or Stowed
$_{SAR}$	Parameters relating to SAR properties
$_{st}$	Stiffener
$_{sup}$	Support Block
$_{t}$	Tension
$_{T}$	Thermal or Tip
$_{vM}$	van Mises
$_{W}$	Dimension or a property that is oriented in or related to the *width* direction of the antenna
$_{x}$	X-direction
$_{y}$	Y-direction
$_{z}$	Z-direction

$\widetilde{x}$	Percentage value of x with respect to reference value x_{ref}
$\|x\|$	Absolute value of x
$max\{x, y\}$	maximum value of x and y

1 INTRODUCTION

Since the beginning of human space flights there are some basic subsystems that all satellites have in common. Besides the essential structure and electronic parts all satellites use *antennas* (see Figure 1). First satellites had used antennas only to communicate to ground stations. Later on, military motivated surveillance and reconnaissance tasks as well as scientific exploration missions required antennas for Radio Detection and Ranging (RADAR) applications.

The performance of RADAR antennas is strongly linked to the physical dimensions of the antenna and the used operational frequency. To enhance the antenna without enlarging the physical dimensions the size can be virtually increased by using interferometric effects of an observing antenna that is in relative motion to the observed object. This RADAR principle is called Synthetic Aperture Radar (SAR) and is today the state of the art for satellite based radar.

However, for a further optimization of SAR antennas, the enlargement of the active antenna surface - the *aperture* - is again a promising option.

Until today, huge antennas are usually designed by utilising classical manifold structure concepts to stow them in a space saving manner for the launch. But the mass and packed size of such antennas is still relatively high and, therefore, the orbit transfer increases the mission costs markedly.

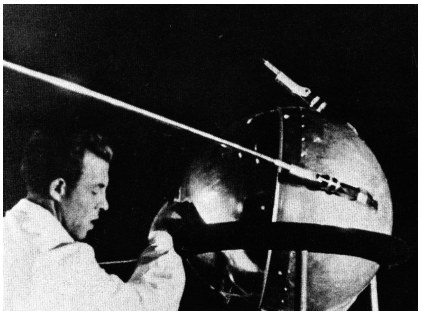

Figure 1.: First man made satellite Sputnik-1 used four radio antennas for sending beacon signals at 20 and 40kHz; launched at October 4th, 1957 [33] (extracted from [3])

To further optimize the structural concepts, one has to consider the expected loads that will apply to the deployed structure. Due to the absence of gravity the required systems stiffness and strength is very low. More detailed, the expected loads on space structures can be assessed quite reliable as translatory and rotatory accelerations that only derive from the on-board Attitude and Orbit Control System (AOCS). Depending on the mission design, those AOCS related loads could be also very small.

Driven by the lightweight design philosophy, the low strength requirements lead to very thin and filigree structures. In addition, folding capabilities are required to comply with the volume constraints for the orbit transfer. During the past years, the name Gossamer Space Structures was established for those filigree collapsible space structures.

Definition of Gossamer Space Structures:

> *Very light structures dedicated to use in space environment. Due to the absence of gravity and the possibility to decrease any translatory and rotatory acceleration of the structure to a minimum by an appropriate Attitude and Orbit Control Systems, the resulting optimal structures are very filigree or* gossamer. *The word* gossamer *is also often an indicator for the use of thin walled shell materials, frameworks of thin rods, or isogrid configurations for construction of hollow members or 3-dimensional structures like habitats*

The opportunity of saving volume and mass by using gossamer space structures leads to different but attractive opportunities:

1. Larger structures can be used/deployed in space
2. A smaller and, therefore, cheaper launcher can be used
   $\Rightarrow$ decrease of mission costs
3. A larger launcher system can carry more than one satellite
   $\Rightarrow$ decrease of multi-satellite mission costs

This thesis contributes a new *mechanical* gossamer antenna concept as well as a sizing strategy for a close-to-optimum structure.

Antennas are only one potential application for Gossamer Structures but due to the strict requirements on contour accuracy they are the most demanding one, as well.

2

FUNDAMENTAL HYPOTHESES

As mentioned above, there is a strong connection between the mass and volume of a space structure and its launch costs. The state of the art of gossamer structures in the next chapter will show the potential of those structures to optimize large antenna structures in order to make them more affordable and, therefore, more attractive for space engineers.

It is the conviction of the author that the past designs are still away from what is possible and can be further optimized using deployable lightweight structures.

The use of lightweight concepts is always driven by a compromise between the required stiffness and the minimum amount of material. Adding the feature of deployability to a lightweight structure, another compromise becomes essential: The structure must be flexible enough to be stowed in a small volume but has to provide the required high stiffness in deployed configuration. So the structure needs to be both stiff and flexible which is unusual but also interesting and challenging.

Therefore, this thesis will propose a novel mechanical design for a membrane antenna that possesses excellent mechanical performance and efficiency.

The regarding design will moreover show that the realization of a gossamer antenna design leads to a sophisticated mass fraction between structural active and passive parts. The electro-magnetic active but structural passive part of the antenna contributes about two-third of the total mass. The remaining one-third represents the support structure.

As the mechanical design bases on a *generic RF concept*, the given final design is considered to be only one example of many possible configurations. To adapt the structure to a later *matured RF concept* a change in the structural concepts is not required. Instead, a re-sizing of all mechanical parts is sufficient.

The demand for a re-sizing capability of the here considered antenna is more or less driven by the given task to provide a mechanical design of an antenna without a previously performed study on the detailed RF concept. This is a suitable approach for a first study in order to keep the costs of such a study within a reasonable limit.

RADIO FREQUENCY *(RF) is a common abbreviation in antenna engineering and addresses every part that is involved in transmitting, receiving or transforming of electromagnetic waves as they derive from radar or communication antennas*

However, the experiences in classical space projects show analogies to everyday project work where engineers of many different fields work together while the developments of each field are influencing all others.

For example, if a team of engineers starts to develop a new satellite, the thermal engineer needs information on the structural setup and the used materials to create a working thermal management that guarantees a safe operation. Contrary, the structural engineer needs information on the mass and position of the planned thermal radiators, heat pipes as well as expected critical temperatures, to choose the appropriate materials and the setup. Therefore, both have to start with making reasonable assessment of a very coarse design to provide the other fields with a foundation for their work. Consequently, it is very usual, that each field updates its requirements every few months and forces the other fields to update their designs. This continuous cycle of re-design and re-sizing is a very essential part of working in large project groups on complex prototypes and is not only limited to space engineering.

Therefore, the thesis shall provide a method for re-sizing that bases mainly on combined parameterised FE-models that allow a rapid and automated reaction on changing requirements. It is assumed, that the implementation of such parameterised models is more complex than the creation of one dedicated one, but from a long term perspective this *time investment* shall pay off. The method is illustrated using the designed antenna but it shall be also applicable to other gossamer structures.

From those introduced thoughts, two basic hypotheses and, thereby, the key objectives of this thesis can be defined:

HYPOTHESIS I

> *It is possible to design and size a deployable gossamer SAR membrane antenna for operation in L-band that has a specific mass of* $1.0\,\frac{kg}{m^2}$ *or less and that is lighter than the state of the art concepts but competitive in its performance.*

HYPOTHESIS II

> *There is a method to size and resize all parts of gossamer membrane structure in a successive manner by using a chain of specified closed loop sizing tasks.*

The thesis is providing answers on those hypotheses and is giving insight in the cognitive processes that lead to the final results.

3

THESIS STRUCTURE

Here the basic structure of the thesis core is introduced to enable the reader to easily navigate through the document and understand the required task for the design and sizing. Thereby, the structure of the document is related to an appropriate work flow for the design and sizing process.

The chart in Figure 2 gives an overview on the regarding top level task as well as the required subtasks and their relation to the previously defined hypotheses.

The process starts with the definition of the general mission requirements and the compilation of a list of dedicated technical requirements.

After the requirements have been defined, a state of the art reference study is performed to get an overview on existing space antenna systems in general and their deployment concepts in detail. At the end of the state of the art study, the *gap between the existing concepts and the requirements* can be identified which is in fact the motivation for the here presented new concept.

Consequently, the next step is the development of a new concept that is capable of filling this gap.

In the steps afterwards, the detailed design is performed in a meaningful order. The design starts with the essential element of a membrane antenna - the membranes. As they are supported by the antenna frame structure, it is very appropriate to design and size the frame loading membranes before the frame itself.

In between the membrane and frame design, a detailed design and sizing of the required interfaces is performed to define the boundary conditions properly.

The chart also contains an entry on a closed loop design chain which is a possibility arising from the task before if the general design remains the same but sizing relevant requirements or boundary conditions change.

As the membrane sizing chapter will show, this scenario is very probable for the discussed antenna.

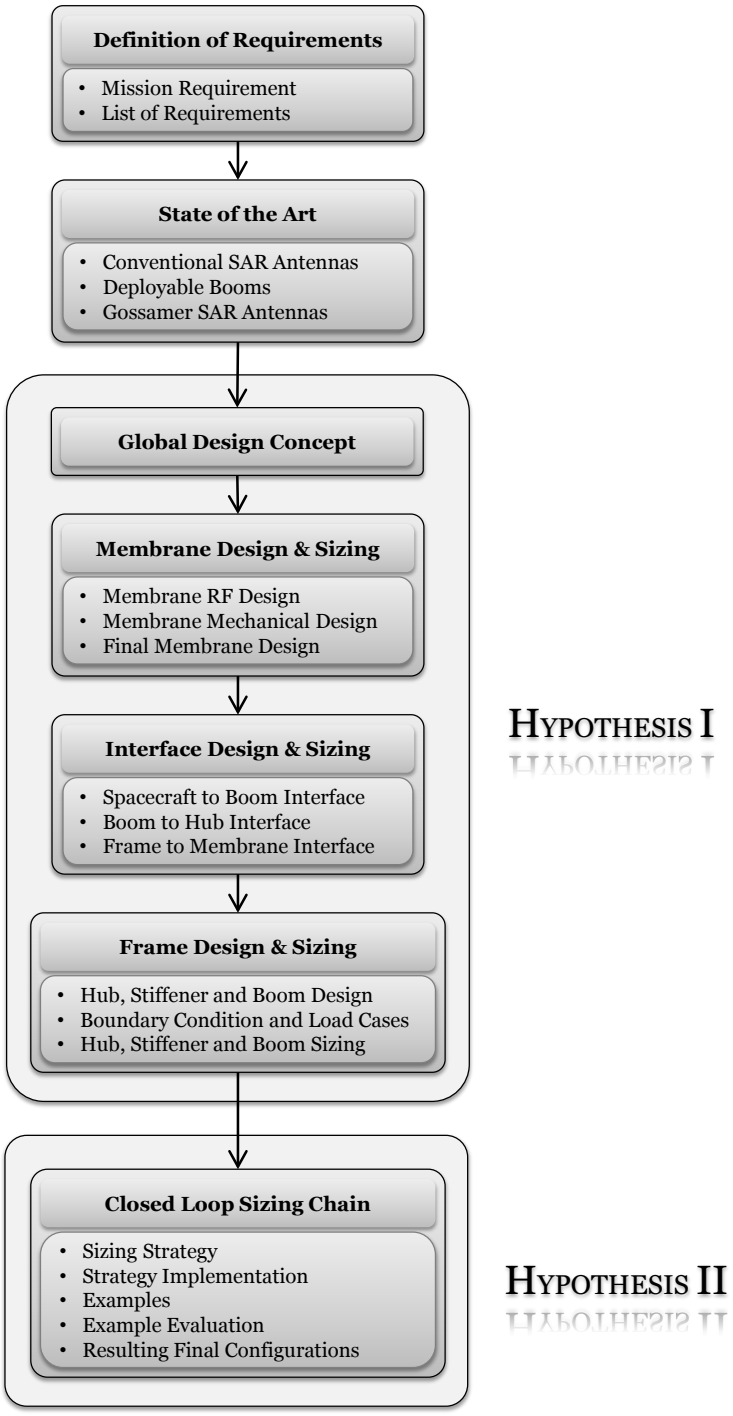

Figure 2.: Thesis structure

4 DEFINITION OF REQUIREMENTS

To provide a foundation for the following chapters, basic mission requirements as well as technical requirements are defined in this chapter.

4.1 MISSION REQUIREMENTS

The envisaged mission of a satellite is the key information to define the overall design of the necessary SAR antenna. The mission profile for the here discussed antenna is the monitoring of *Global Change Indicators*. They can be defined as quantifiable natural physical occurrences that allow conclusions on global or local deviances of the climatic or ecosystematic processes. Exemplary indicators are vegetation distribution, soil moisture, polar caps, glaciers, ocean salinity, or ocean currents.

For the defined mission profile radar frequencies in L- or P-band are preferable. This fact is caused by a given causal dependence between the wavelength and the penetration depth of radar waves in general (see Figure 65 in Annex A.1 on page 143).

Band definition according to IEEE
P-band: 0.23GHz-1GHz,
L-band: 1GHz-2GHz

Furthermore, the wave length is a limiting factor for the maximum spatial resolution of the resulting images. The dependency is hereby linear. So exemplary, the doubled radar frequency is equivalent to the halved wave length and, thereby, to a doubled spatial resolution (see (4.1) and (4.2)).

$$\lambda_{SAR} = \frac{c}{f_{SAR}} \tag{4.1}$$

$$\lambda_{SAR} \propto Res \tag{4.2}$$

where

$\propto$	proportionality operator
c	speed of light in vacuum
f_{SAR}	SAR operation frequency
λ_{SAR}	wavelength of SAR operation frequency
Res	resolution of the radar images (pixel size)

The interaction of penetration depth, SAR frequency and resolution is a classical problem of radar applications. For example the resolution of a high frequency radar satellite for traffic monitoring is exact enough to detect single cars. But, indicated by the low penetration depth, problems to detect the vehicles under leafy trees appear.

For the here given mission objective there is no need to have a high resolution. The radar signals have to partly penetrate the vegetation to monitor it or penetrate it completely for monitoring of global soil properties without dependence to vegetation.

As the mission and RF design is not the objective of this work, a generic mission is defined hereunder that can comply with future needs of large deployable SAR antennas but shall not be understood as a real mission.

Aiming for an application for very light radar antennas, multi-satellite mission scenarios as previously described by Krieger and Moreira [35], Moreira et al. [48], and Zink et al. [78] are an attractive opportunity.

Thereby, Krieger and Moreira describe so called *Multistatic SAR Satellite Formations*[35] whereas Zink et al. name them *Cartwheel Constellations*[78]. Both use multiple receive antennae distributed over multiple satellite platforms in combination with one transmitting antenna. Using the transmitted radar signal and the received data of the entire formation in combination with the exact knowledge of the satellites spatial separation enables the usage of interferometric SAR processing methods. Beside the higher resolution of the gathered data, the interferometric methods generate also 3-dimensional information on the observed object. Thus, highly detailed 3D mapping is possible.

In contrast Moreira et al. [48] present a formation flying of two almost identical SAR satellites. The TanDEM-X formation is an upgrade of the TerraSAR-X mission by a second similar satellite. Both platforms are orbiting each other and the Earth in a double helix like trajectory. At October 2010 [57] the first interferometric operation of both satellites was confirmed. The achieved results as well as the later collected data depicts the huge potential of such formation flying SAR platforms.

In contrast to the described TerraSAR-X/TanDEM-X concept, it can be assessed that future satellite formations will consist of highly differential platforms where the *tranceiving* SAR satellite is much more complex than the receive-only ones. Thereby, an assessment of the capabilities of the two satellites is made hereunder.

TRANSCEIVE: *Combined word of TRANSmit and reCEIVE*

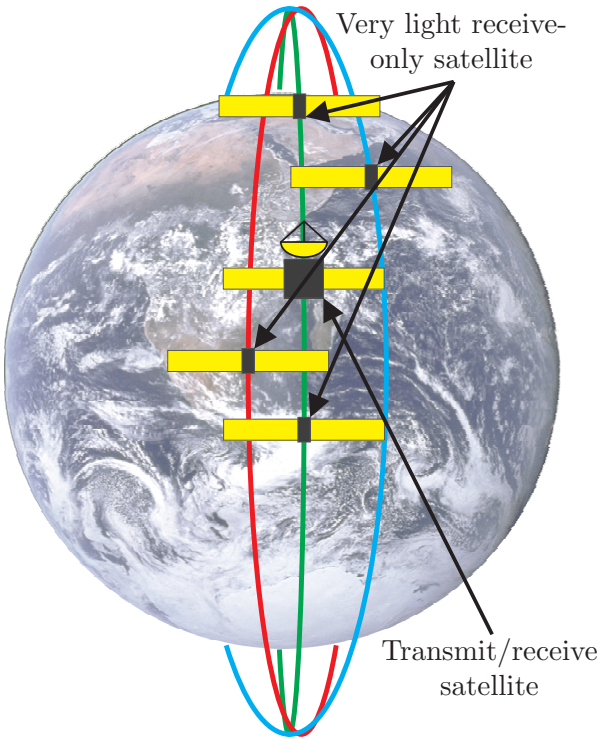

Figure 3.: Proposed mission design

Transmit and receive satellite (transceiver):

- Radar transmit and receive functionality,
- Ground communication for TELEMETRY (TM)/TELECOMMAND (TC) and data down link,
- Inter-satellite communication for TM/TC and data transfer,
- Power system including sufficient solar arrays and batteries to provide energy for above listed capabilities.

TELEMETRY: *Contains data from the satellite like position and orientation, temperature, battery or fuel capacity, etc.*
TELECOMMAND: *Contains commands for the satellite like target orbits, information on upcoming sensing tasks, etc*

Receive-only satellites (receivers):

- Radar receive functionality (low power consuming),
- Inter-satellite communication for TM/TC and data transfer,
- Power system incl. sufficient solar arrays and batteries to provide energy for above listed capabilities.

Driven by the high power consuming SAR transmit functionality and the down link of the gathered data of the entire constellation, it is assessed that the tranceiver satellite will have a considerably

higher need for electric power than the receiver platforms. Thus, the demand for large solar arrays as well as batteries for backup is given at the transceiver which increases the weight of the power sub-system and, thereby, the mass of the entire satellite. Contrary, the receive only satellites do require less energy for their RF tasks and do not have to transfer the data to the ground. This will decrease the mass of the satellite to a minimum. Bus architectures of *SmallSat* level are, therefore, realistic.

Usually, satellites with less than 500kg are considered as SmallSats *but there is no fixed definition*

The proposed mission design is shown in Figure 3. It is characterized by:

- Multi-satellite mission utilizing one transmit/receive- and multiple receive only satellites for interferometric SAR
  - Transmit option uses conventional parabolic antenna
  - Receive option requires only one extreme light and packing efficient antenna per satellite
- Antenna operating in L-band at 1.25GHz
- Use in lower earth orbits
- Beam steering shall be possible

4.2 LIST OF REQUIREMENTS

The basic requirements for the antenna design are listed hereunder and define the basis for all later developments:

1. Operation in *receive-only* mode,
2. Antenna operation frequency of 1.25GHz (L-band),
3. Antenna aperture shape shall be rectangular,
4. Antenna membranes setup:
   - Three antenna membranes (patch-, ground-, and transmission line membranes) made of each 50µm thick Kapton®,
   - One service membrane made of 100µm thick Kapton® (more information on the service membrane is given in section 7.1 on page 35),
   - Spacing between patch and ground membrane of 12.7mm,
   - Spacing between ground and transmission line membrane of 6.35mm,

- Spacing between transmission line and service membrane of 10.0mm,

5. Antenna array size of $A_{AA} = 40m^2$ with a length to width ratio $k_{WL} = \frac{1}{4} \dots \frac{1}{6}$,
6. Maximum specific mass of $1\frac{kg}{m^2}$,
7. Stowed maximum volume of $0.8m^3$,
8. Minimum first structural mode at 0.4Hz,
9. Operation in Low Earth Orbit (LEO),
10. Ability to withstand 20 on-ground stowing and packing processes,
11. Ability to withstand temperatures between $-100°C$ and $+100°C$.

4.3 CONCLUSION

As there is currently no mission planned for the here proposed antenna a generic mission has been assessed that is oriented on current and past SAR sensing missions. Some mission and technical requirements have been explained and, finally, a set of key requirements is given that is occasionally referred in the following chapters.

5 STATE OF THE ART

This chapter gives a brief introduction about existing deployable antennas and deployable booms. Thereby, two categories of antennas are considered: Conventional SAR antennas are described to provide a basic understanding of the dimensions and mass of large space antennas to emphasise the large potential of the gossamer systems. Moreover, the common concepts for gossamer deployable antennas as well as their basic elements, the deployable booms, are introduced.

5.1 CONVENTIONAL SAR ANTENNAS

Figure 4a shows the Canadian radar satellite RADARSAT-2 with its deployable antenna made of four deployable and one rigid panel interconnected by hinges and stabilised by an also deployable strut backbone structure.

RADARSAT-2 was launched at December 14th, 2007 from Baikonur, Kazakhstan by a Soyuz. (source www.radarsat2.info)

The ASAR antenna of the European satellite ENVISAT is shown in Figure 4b. It is also using a deployable panel setup but the panels are not supported by a backbone structure.

ENVISAT was launched at March 1st, 2002 from Kourou, French Guiana by an Ariane-5 (source www.esa.int)

Table 1 enumerates some key parameters of both antennas. It is obvious that those concepts can not be considered gossamer. The antenna of RADARSAT-2 has a specific weight of $36.5\frac{kg}{m^2}$ and ENVISAT's ASAR antenna weights even $57.7\frac{kg}{m^2}$. Here it needs to

(a) Canadian RADARSAT-2 with deployed solar arrays and deployed radar antenna (lower darker panels, Courtesy of CSA)

(b) European ENVISAT with deployed ASAR antenna (Courtesy of ESA)

Figure 4.: Exemplary SAR satellites

PARAMETER	RADARSAT-2	ENVISAT
Satellite size	3.7m x 1.36m	26m x 10m x 5m
Aperture size	15m x 1.37m	10m x 1.3m
Satellite weight	2200kg	8211kg
Aperture weight	750kg	750kg
SAR frequency	5.405GHz	5.331GHz
Resolution	3m	30m

Table 1.: Antenna key parameters of RADARSAT-2[2] and ENVISAT

be emphasised that the operation frequency is four times higher than the one of the here adressed membrane antenna. Thus the requirements on the shape accuracy are also four times stricter. However, it is assumed that these specific masses do not represent the structural optimal solutions and that there is a huge potential for mass saving.

5.2 DEPLOYABLE BOOMS

The backbone structures of huge membrane antennas are usually build of deployable masts or booms. As there is a wide spectrum of available systems, the common systems are reviewed hereunder.

5.2.1 *Tubes*

Tubular booms are defined by a circular cross section and a continuous shell surface.

Open STEMs

The oldest but also most matured concept is pictures in Figure 5a. Open STEMs(STORABLE TUBULAR EXTENDIBLE MEMBERS) have a circular but slit cross section in deployed state. Due to the slit, the cross section can be unfolded and the boom can be rolled for space saving storage. But the slit is decreasing the torsional stiffness of the deployed boom significantly. The right hand concept in Figure 5a shows a so called Interlocking BI-STEM that combines two STEM booms of opposing open cross sections to one circular boom with a closed cross section. The resulting com-

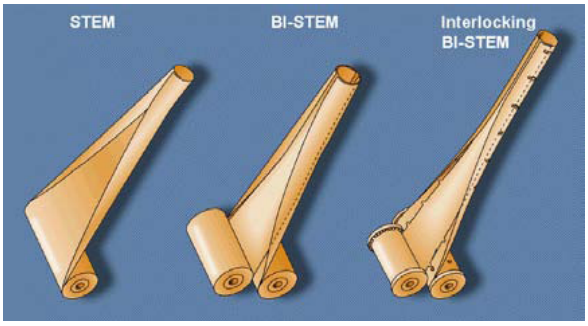

(a) Different STEM concepts (Source: NASA)

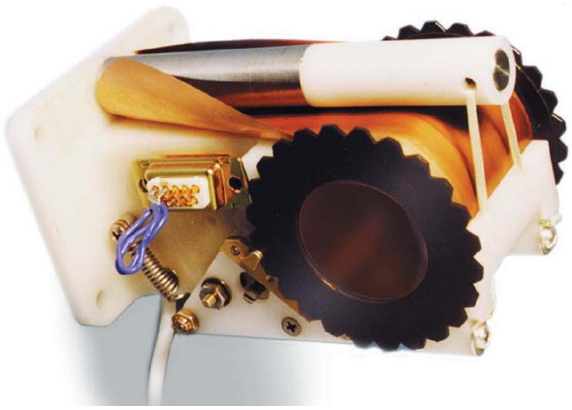

(b) STEM TIP Drum antenna boom by Northrop Grumman [26]

Figure 5.: STEMs with open cross section

bined boom is stiffer but heavier. The most open STEM booms are made of metal alloys but also versions using composites have been investigated [7, 32, 72].

Open STEMs are designed in a way such that they always intended to achieve the deployed state. So a deployment by pure stored elastic strain energy is possible.

Therefore, the self-deployment needs to be controlled by an adequate restraining system. Comparable to a cable winch, this is possible by a motorized drum and a surrounding housing.

Figure 5b shows an alternative concepts that deploys only by strain energy. The white rope at the right hand side can be cut by a pyrotechnic guillotine to release the drum with the coiled boom. The deployment is then performed autonomously [26].

Big advantages of STEMs are their small amount of required stowage volume, their simple manufacturing and high maturity due to decades of use for antennas and instrument booms. Dis-

Structural Efficiency
Soft term for mass depending structural performance like stiffness per mass or strength per mass

advantageous is the low *Structural Efficiency* that is caused by its open cross section [49].

Lenticular Booms (Closed STEMs)

DLR's rollable CFRP boom features a closed cross section but can be flattened (see Figure 6a and 6b) and coiled for volume efficient stowage. As the used material is only 0.1mm thick, the resulting boom weighs only 62g/m [70]. However, this basic concept is no development of DLR but has been investigated before by Boeing (1967), TRW (1969) and Sener (1980-ies) [61].

In contrast to open STEMs, the closed versions are not able to deploy autonomously in a directed manner. Therefore, deployment control principles are necessary to guide the process.

Figure 6c shows one concepts that utilises applied Velcro tape to inhibit self-deployment and an inflatable polymer hose to deploy the boom by applying pressure to it.

Another concept is pictured in Figure 6d. Here, the boom is restrained by a cylindrical cage and deployed by an electric motor. This electric system is more complex than the inflation concept but requires no extra features like Velcro or a hose applied to the boom.

Both deployment control technologies have been successfully tested under artificial weightlessness during a parabolic flight campaign in 2009. Figure 6e shows an exemplary test record of one out of 15 successful inflation driven deployments [68, 70].

Inflatable tubular booms

Figure 7 provides an overview on different inflatable boom concepts. The basic principle is thereby comparable: The boom is made of a flexible layer that can be folded or rolled for space saving storage. The deployment is realized applying an internal pressure to the boom. After deployment, the stiffness of the boom can be maintained by different approaches. The inflatable booms of Bonnefond et al. are designed for short durations and are also used as pushing actuators. Therefore, this boom concept is simply stiffened by maintaining the internal pressure [13] (see Figure 7a). A comparable inflatable boom concepts has been used in a NASA flight experiment that tested an inflatable antenna of L'Garde [73, 22].

However, such an approach is only valid for short duration structures that are only used for some hours or even days. A longer use of inflatable structures by maintaining pressure would

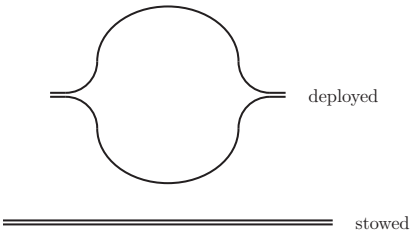

(a) Deployable boom cross section

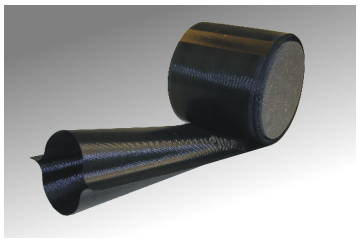

(b) Rollable DLR Boom

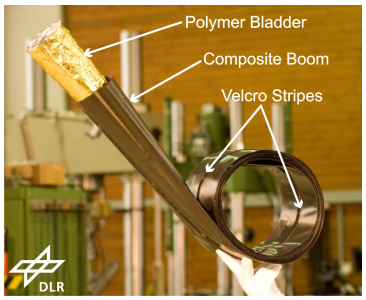

(c) Inflation base deployment control principle

(d) Electric deployment mechanism

(e) Successful inflation driven boom deployment during parabolic flight campaign in 2009

Figure 6.: DLRs CFRP booms

require huge gas reserves to counteract potential leaks from MICROMETEOROIDS AND ORBITAL DEBRIS (MMODs) impacts. Hence, different methods of rigidising or curing have been developed. The most usual way is the utilisation of an uncured composite *prepreq* that is cured after deployment by heat or by ULTRA VIOLET (UV)-radiation from the Sun.

prepreq *Common abbreviation for* ***pre****-im****preg****nated uncured composite material*

Barbet et al. introduce a rigidisation technique that cures carbon composite booms in space by implemented electric heating wires (see Figure 7b) [8, 9]. To guarantee a homogeneous curing in space despite of the unsymmetrical radiation scenario an enclosing Multi Layer Insulation (MLI) is required. In contrast Lefevre et al. present a glass composite that is cured by the Suns UV-light [38].

Such in-space curing of composite materials by heaters or UV-light possess different advantages and drawbacks: Curing by sunlight requires no extra heating elements on the booms and no MLI and is, therefore, not increasing the mass of the boom and the required power for supplying the heaters. But the rigidising requires transparent fibres to illuminate all parts of the resin. So, the use of glass fibres is mandatory and the application of this curing method to the higher performing carbon fibres is not possible.

Despite the transparency of the material, the Sun facing side of the structure will always absorb more energy from the sun light and will consequently cure faster than the shadow side. This unsymmetrical curing condition need to be equalized by rotating the structure. Otherwise it can result in a deformed structure due to the inhomogeneous curing process.

(a) Packed (left) and deployed (right) inflatable tubular boom by EADS-ST [13]

(b) Implemented electric heater applied to a rigidizable inflatable boom by Alcatel Space (extracted from [8])

(c) Opened Aluminum Laminate Boom by JPL (extracted from [41])

Figure 7.: Inflatable boom concepts

A different rigidising concept is discribed by Lou and Feria as followed:

> *"These sandwich laminates are made by bonding thin aluminium foils to polyester films, such as Kapton. While the polyester films provide tear resistance and a gas seal, the aluminium foils are stretched by pressure just above the yield point to provide rigidity of the inflatable structure."*
>
> *[42, p. 4]*

Four years later, Lou and Fang describe an advanced version of such boom that is reinforced with longitudinal metal tapes and circumferential rings [41]. Such boom is displayed in Figure 7c

Two alternative rigidising concepts are introduced by Fang et al. in [21] and by Schwartz in [58].

More information on inflatable space structures is given by Freeland et al. in [23], Cadogan et al. in [16] and Langlois and Roumï¿½as in [36].

5.2.2 *Trusses*

A very common concept for deployable masts is the truss. It consists of *longerons* (aligned with the longitudinal mast direction), longeron connecting circumferential *battens* and further supporting *diagonals*.

Given by the framework structure, the same amount of material achieves a higher radius of gyration for the truss concepts than for STEM concepts. However, this increased radius of gyration does also lead to increased stowed volume and deployed diameter of the trusses.

As shown in Figure 8 trusses can be stowed using different techniques. The Figures 8a and 8b show trusses that are packed by applying torsion to the boom which leads to a flexible deformation of the truss elements. Comparable to some tube concepts mentioned in the previous subsection 5.2.1, this deformation process stores elastic energy in the truss that can be used as driver for the deployment. McEachen states in [46] that ATKs SAILMAST is using this potential. A central rope or lanyard is inhibiting the otherwise fast and uncontrolled deployment of the boom. By slacken the lanyard continuously, the deployment can be controlled (see Figure 8b). Contrary, Figure 8a shows the concept of ATK that uses a rotating nut to deploy the boom in a controlled manner. Thereby, the nut is guiding the boom in its week transition zone. This support enables limited load bearing capabilities

The transition zone *of a deployable boom is a travelling section of a partially deployed boom that is in between the stowed and deployed state*

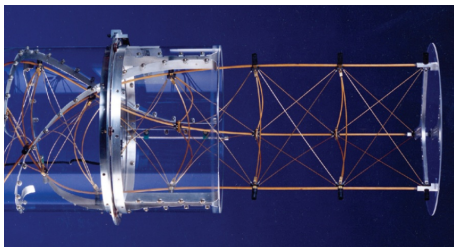

(a) Deploying truss by ATK

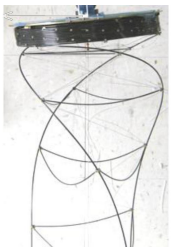

(b) Very light SAILMAST by ATK (extracted from [46])

(c) Deployable FAST mast for ISS by AEC-Able Engineering [72]

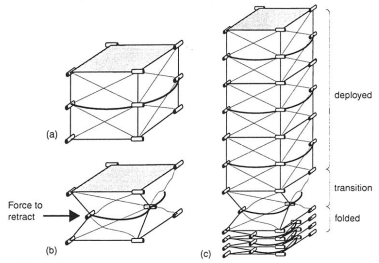

(d) FAST mast folding principle [72]

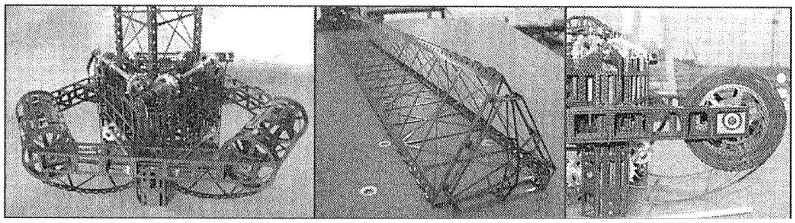

(e) TriLok truss concept by ATK [49]

Figure 8.: Truss concepts

of the partially deployed boom already during deployment. This widens the field of application but this extra feature has to be paid by a more complex and consequently heavier mechanism.

The Figures 8c and 8d show another truss concept [10]. The FAST mast uses joints and particularly bendable battens instead of bendable longerons for stowing (see Figure 8d). Therefore, the boom can be stowed without applying global torsion but requires a relatively complex control mechanism at the deployment transition zone. A comparable system - the ADAM mast [17]- is introduced by Stohlman and Pellegrino in [64].

The next level in kinds of truss deployment concepts is pictured in Figure 8e. ATKs TriLok [56] is deployed by assembling three face layers by a mechanism. As the single face layers have a relatively low bending stiffness, they can be coiled around a

(a) Inflatable Isogrid boom (extracted from [6])

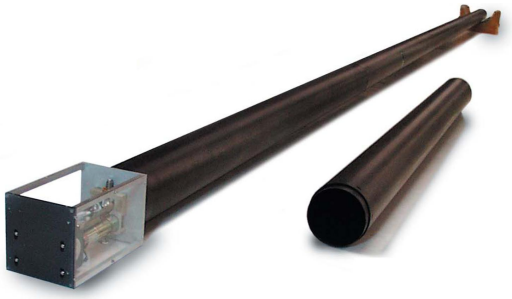

(b) Telescopic Boom by Northrop Grumman (extracted from [51])

(c) Slotted boom hinge by University of Cambridge, UK (extracted from [43])

Figure 9.: Other boom concepts

spool with small diameter and can be, therefore, stowed in a very efficient way. But here the gain in packing efficiency has to be paid by an increased complexity and mass of the deployment mechanism.

5.2.3 *Other Concepts*

Allred et al. propose an inflatable Isogrid boom as shown in Figure 9a [6]. The uncured, Isogrid structure of thin carbon composite rods is deployed by pressurising the internal hose. After full deployment the composite is rigidised using UV-light.

A further developed Isogrid boom is presented by Agnes et al. in [5]. In contrast to Allred et al. the boom of Agnes et al. use graphite shape memory polymer for the rigidisation.

Figure 9b shows a complete other concept. Northrop Grummans Telescopic Boom consists of multiple conical CFRP tubes that latch to each other in deployed configuration. The deployment is driven by an internal STEM boom with open cross section. Due to this deployment method, the telescopic mast can be deployed and retracted multiple times [51].

The last here presented concept for deployable booms uses local hinges in otherwise stiff circular hollow tubes. Mallikarachchi and Pellegrino introduce such concept in [43, 44] (see Figure 9c) where the hinges are not generated by adding special hinge elements but by weakening the circular boom intentionally with slots. Therefore, the manufacturing of such booms is less complex than the one of trusses. The interplanetary probe MARS EXPRESS use a comparable boom for deploying its 40m long MARSIS instrument antenna [45].

MARS EXPRESS was launched at June 2nd, 2003 from Baikonur Cosmodrome, Kazakhstan by an Soyus-Fregat (source www.esa.int)

5.2.4 *Deployable Booms - Conclusion*

The previous pages give a *brief* overview on available concepts for deployable space booms that is by far not all-embracing.

A more complete study on gossamer deployable booms is given by Murphey in [49]. An updated version is recently given by Hillebrandt in [28, 29]. Murphey is thereby introducing performance parameters for different loading schemes that make a comparison of different boom concepts possible.

Hillebrandt uses the same parameters but includes more boom concepts in his study. The result of this study is that truss concepts, and specially the TriLok mast, provide the best structural performance when bending or axial compression (column loading) is considered. The performance of the STEM and Isogrid boom performance is about Two to Three time lower.

However, the choice of an appropriate boom for a deployable structure should not only rely on the mechanical parameters. So factors like space durability, flight heritage, modularity, deployment concepts, reparability, manufacturability as well as robustness against manufacturing uncertainties or even impacts by MMODs need to be respected in relation to the proposed mission and application.

5.3 GOSSAMER SAR ANTENNAS

A lot of work has been already performed on gossamer antennas. The majority of this work was done in the USA but also some European concepts exist.

The here given state of the art will concentrate on deployable array membrane SAR antennas that are defined by a flat antenna surface that carries printed or bonded antenna patches. Other antenna concepts do base on large deployable parabolic reflectors

that are either inflatable [23] or umbrella like mesh antennas [47, 50]. Those concepts will not be part of this section but can be reviewed using the given literature as a starting point.

5.3.1 *Working Principle of Flat Array Antennas*

All flat array antennas require special elements on the membrane to either reflect incoming waves or receive and transmit them. Those elements are called *micro strip antennas* or *patch antennas*.

Figure 10 shows a sketch of such a basic antenna element. It consists of 3 parts: The ground plane metallisation at the bottom, the upper metallization that forms the patch and the supplying micro-strip feed line, and the dielectric isolator between both metallizations. The combination of isolating dielectric and the both conductors acts as a resonator that amplifies transmitted and received waves. In both cases, the RF signals are transferred from and to the patch via the micro strip lines.

The optimal thickness of the dielectric depends on the wavelength of the operated signals. A signal at lower frequencies and thereby longer wave length does require a thicker dielectric of up to a few centimetres.

Normally this would increase the mass of such patch antenna in a very inconvenient way so that a use for gossamer antennas would not be attractive. But the space environment offers a very smart solution: The vacuum itself is a perfect dielectric as well. Therefore, the ground plane and the top plane can be separated and can be e.g. carried by different membrane layers which relative positions are fixed.

To further advance membrane antennas, a third patch membrane can be added for a second polarization direction. The resulting three-layer antenna is capable of horizontal and verti-

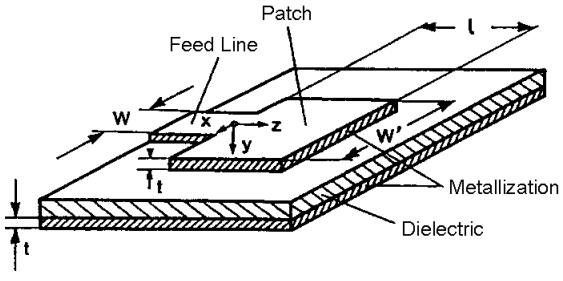

Figure 10.: Basic setup of one micro strip or patch antenna element (extracted from [34])

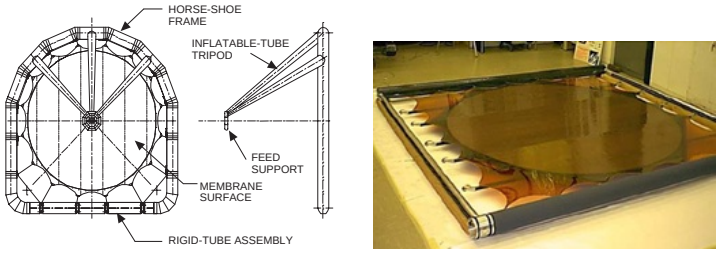

(a) Inflatable antenna (extracted from [21])

(b) US inflatable reflector antenna (extracted from [41])

Figure 11.: Reflectarray antenna concepts

cal polarization which results in more information that can be gathered on the observed object.

Antenna beam *is a common term in RF engineering and refers to the directional radio pattern of the antenna. For the most focused antennas this pattern has the shape of a baseball bat or a* beam

Moreover, the feed lines for the patches are not mandatory to use this elements for transmit and receive. It is also possible to use the patch elements as reflecting unit. Like for conventional parabolic antennas, an array of passive patches on a flat surface can be used to focus the emitted RF signals of a single feed horn. To shape the emitted *antenna beam*, the patch dimensions are not identical at the entire reflector but each patch has a dedicated geometry to generate a defined phase shift for each element. All combined elements lead to the required antenna beam shape by intended interference of all patches. Arrays with this passive beam shaping are called *Reflect Arrays*.

The following pages will give an overview on existing passive *Reflect Arrays* and *Direct Radiating Arrays*.

5.3.2 *Reflect Arrays*

Figure 11a shows an inflatable reflect array antenna designed, build and tested by Fang et al. at NASA JPL. The aperture has a diameter of 3m and is designed for 32GHz (Ka-band) operational radar frequency. It has a mass of only 13.57kg which results in specific mass per aperture area of $1.92\frac{kg}{m^2}$. The horse shoe like shape of the frame was chosen to ease the packing of the antenna. As shown in the figure the lower part of the frame is rigid. During rolling it is used as supporting hub for membranes and the deflated rest of the frame. The inflatable parts of the frame are made of spring tape reinforced aluminium laminate booms [21]. This antenna was also RF-tested and revealed an *"excellent radiation pattern characteristic"* [21, p. 2]. An overview on other comparable systems is given in [39].

More details on aluminium laminate boom type are given in section 5.2 on page 19

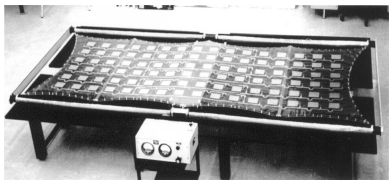

(a) Inflatable membrane antenna done by JPL and L'Garde (extracted from [30])

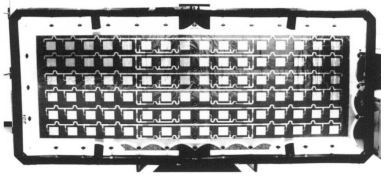

(b) Inflatable membrane antenna done by JPL and ILC-Dover (extracted from [30])

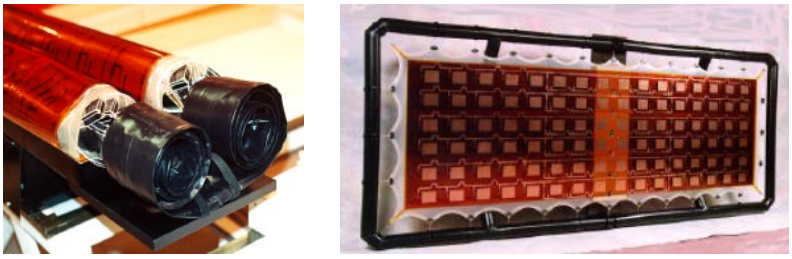

(c) Concepts of JPL and ILC-Dover in stowed (left) and deployed configuration (right) (extracted from [15])

Figure 12.: Deployable gossamer antenna concepts

5.3.3 *Direct Radiating Arrays*

Figure 12 shows two concepts for array antennas of a size of 3.3m x 1m. Both antennas are 1:3 sub scale models. According to Huang et al. in [31] the breadboard shown in Figure 12a is setup by JPL and L'Garde while the one in Figure 12b is done by JPL and ILC-Dover. Figure 12c shows the JPL/ILC Dover concept again in stowed and deployed configuration. The L'Garde concept features a specific mass of $3.3\,\mathrm{kg}\frac{\mathrm{kg}}{\mathrm{m}^2}$ while *"The ILC Dover unit has a slightly higher mass."*[31, p. 3].

Both antennas are supported by a frame of inflatable booms but the L'Garde concepts use the inflatable booms only for the long edges of the frame and use solid elements for the short edges. The JPL/L'Garde concept is again using aluminium laminate booms for rigidisation of the inflated frame. The curing concept for the approach of JPL/ILC Dover is not given but the image of the packed ILC Dover concept in Figure 7c implies that the frame is either made of a not rigidisable polymer material for laboratory tests or of rigidisable carbon composites.

A similar concept is introduced by Cadogan and Grahne in [15] and by Lopez et al. in [40]. Both give a specific mass of only $1.6\frac{\mathrm{kg}}{\mathrm{m}^2}$ for a full scale 9.5m x 3m model. However, Lopez et al. are stating that this value is a theoretical one that demands the use

of so far not used carbon composite materials and *"does not include the transmit-receive (TR) modules (≈ 10kg), antenna electronics equipment (≈ 10kg) and cable harnessing (≈ 7kg)."* [40, p. 8].

Huang gives also more details on the antenna membranes in [30] but this information will be reviewed later in chapter 7 starting on page 33.

Taking a closer look on the deployed configuration of the antenna in Figure 12c one can see two vertical support bars behind the membrane that interconnect the long horizontal deployable booms. Cadogan and Grahne make no statement in [15] on the motivation for those bars but a reasonable explanation for their existence is the support of the long horizontal booms against buckling from bending loads that are introduced by the membrane tensioning forces.

5.4 CONCLUSION

The first review on conventional SAR antennas, in the first section of the chapter, visualises the potential of gossamer antennas. As defined in HYPOTHESIS I, the objective of the present thesis is the design of an antenna with less than $1\frac{kg}{m^2}$. The conventional systems feature specific masses of $36.5\frac{kg}{m^2}$ and more.

The second section on deployable booms gives a brief but wide introduction in available concepts for antenna backbone structures and ended with a recommendation for truss and tube concepts. It also states that there is not *one* optimum concept but the appropriate deployable boom concept needs to be chosen for every application depending on specific mission requirements.

The third and last section introduces some past gossamer antenna concepts and ends with direct radiating array antennas of down to $1.6\frac{kg}{m^2}$ specific mass that does *not include* the RF components. So the gap between the requirement of $1\frac{kg}{m^2}$ for a fully functional membrane antenna (incl. RF components) and the existing concepts is obvious.

Taking the chance to fill this gap was the main endeavour for the here presented work and the resulting thesis.

6 GLOBAL DESIGN CONCEPT

This chapter briefly introduces the global design of the membrane antenna in the final evolutionary step which will be the basis for all following work.

Other previously considered antenna designs are not shown here but can be reviewed in [67].

6.1 DESIGN CONCEPT

Figure 13 gives an impression on the basic design and deployment concept that is inspired by those of Fang et al.[21], Lopez et al.[40] and Huang[30].

It consist of a frame of two deployable booms, two rigid rolling hubs and some transversal frame stiffeners as well as four parallel membranes for the RF functionality. During packing each half antenna - including frame and membranes - is rolled on one hub. This rolling is performed with each hub from both sides and results in a compact stowed antenna where the sensitive booms and membranes are safely wrapped around the rigid hub and are therefore protected from the static and dynamic launch loads.

Photographs of the first breadboard can be reviewed in Annex A.4 on page 148.

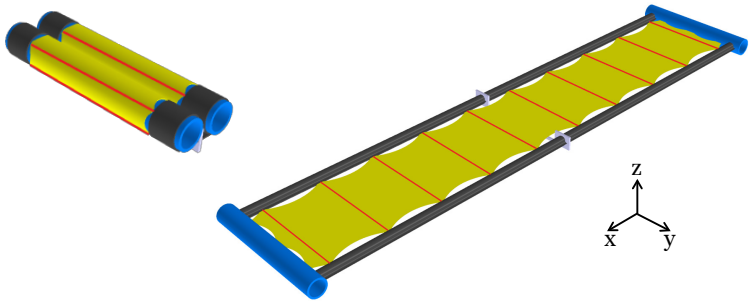

Figure 13.: Basic antenna concept in stowed (left) and deployed configuration (right), the antenna is composed of deployable booms (gray), rolling hubs (blue), membranes (yellow), and transversal stiffeners (red)

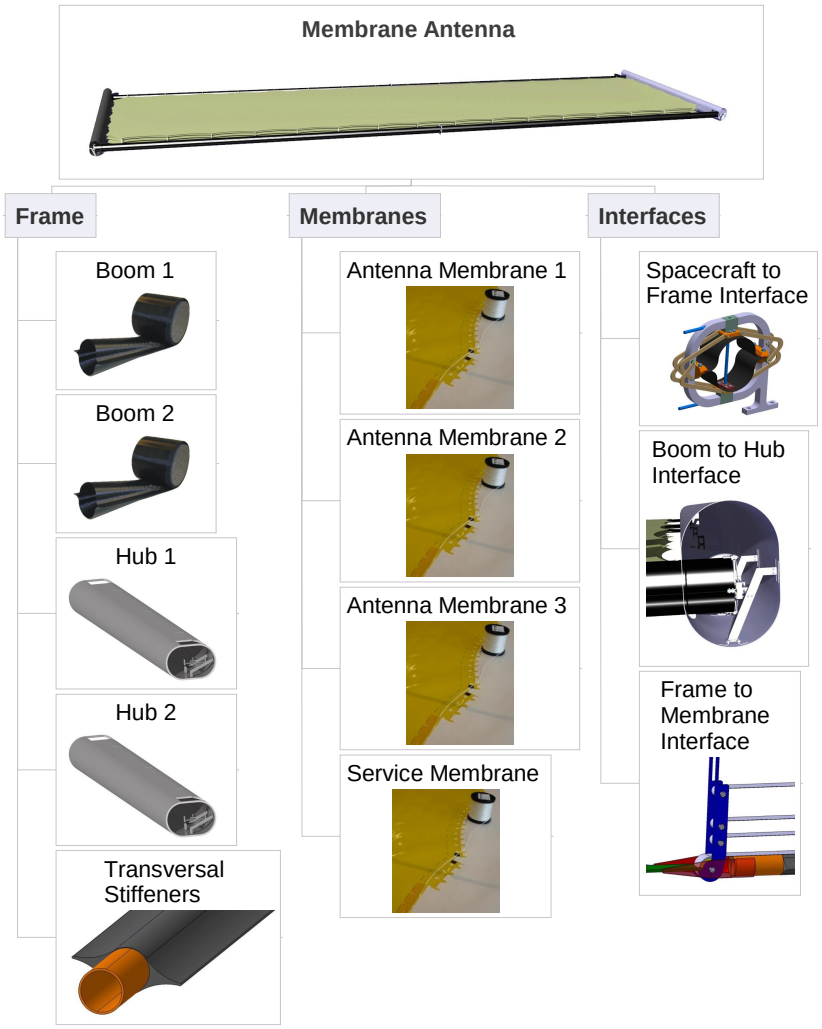

Figure 14.: Membrane antenna product tree

6.2 DETAILED CONCEPT

To provide a general overview on the design and some term definition, a product tree of the antenna is shown in Figure 14. The antenna is subdivided into three assembly groups: the frame, the membranes and the interfaces. These groups are reflected in the following three chapters.

The Figures 15a, 15b and 15c show some overview images from the deployed and stowed final concept.

The antenna functionality is provided by three membranes (yellow) with applied antenna elements (not modelled). A fourth membrane is added to carry the harness and amplifiers for feeding the antenna elements on the other three membranes. Details

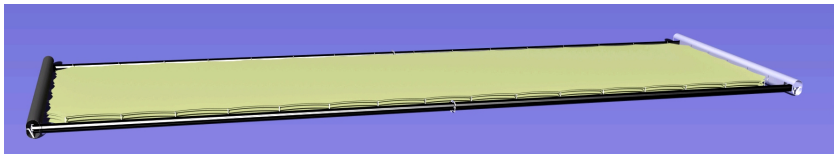

(a) Deployed antenna

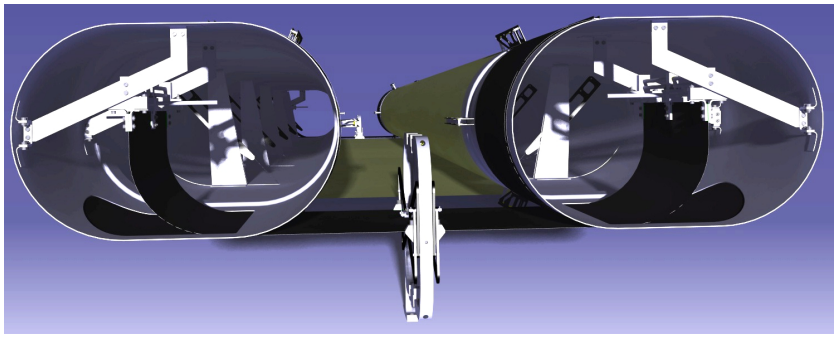

(b) Side view into hubs of stowed antenna

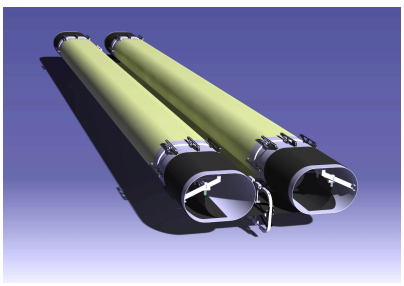

(c) Stowed antenna

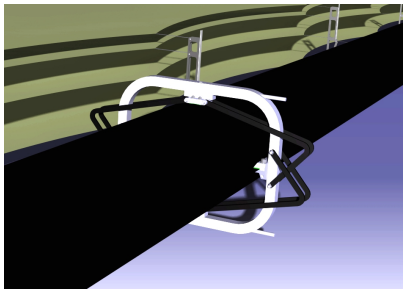

(d) Spacecraft to boom interface

Figure 15.: General membrane antenna design

on design and sizing of the membranes are given in Chapter 7 starting on page 33.

The frame is made of two inflatable booms, two rigid hubs and transversal stiffeners. The used booms are rollable CFRP booms of the inflatable type that are described before in section 5.2.1 on page 14 and shown in Figure 6c. Due to the use of inflatable booms, the entire antenna can be deployed by applying pressure to the inner boom hose and does not require complex mechanisms.

The transversal stiffeners are required to offload the booms from bending and shear loads evolving from the membrane tensioning forces introduced by the boom to membrane interfaces. These loads would otherwise deform the boom cross section which would degrade the boom integrity and lower its perfor-

mance. More details on the frame are provided in Chapter 9 starting on page 67.

The connection between antenna and spacecraft is realized by two interfaces that are mounted at the middle of each boom (see Figure 15d). As the boom is changing its cross section during deployment, the interface also needs to follow this deformation. A comparable interface is required for the connection of the booms and hubs at the four antenna corners (see Figures 16a and 16b). Moreover, there is also a dedicated interface for the connection of the membranes and the frame (see Figures 16d and 16c). So called CONSTANT FORCE SPRINGS(CFS) are used to maintain the required tensioning forces for all thermal scenarios. Details on the design and sizing of the interfaces can be reviewed in chapter 8 starting on page 55.

The images presented in the Figures 15 and 16 derive from a previous antenna version that did not include transversal stiffeners and that used thereby another frame to membrane interface concepts. Details on the latest version of those interfaces and the integration of the stiffeners are also given in Chapter 8.

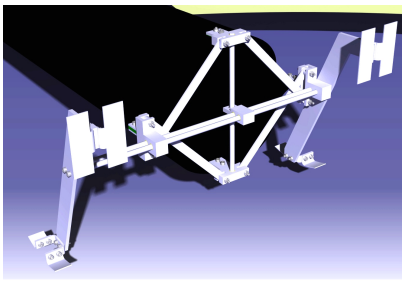

(a) Boom to hub interface (hub is set transparent)

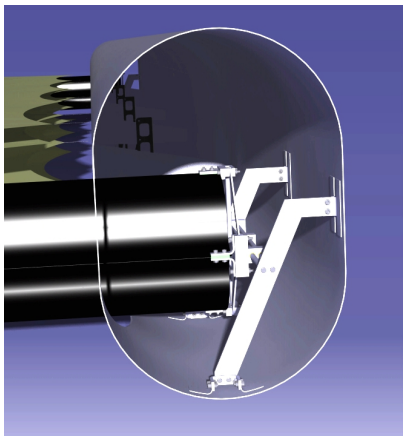

(b) Side view on hub

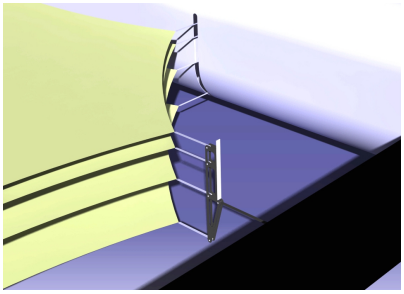

(c) Corner section including deployed frame to membrane interfaces

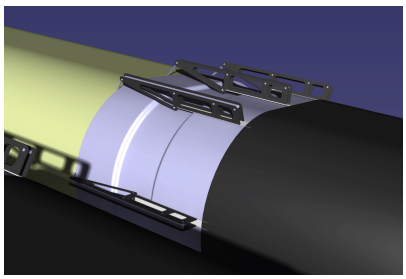

(d) Close look at hub with back flipped frame to membrane interfaces (applies for stowed configuration)

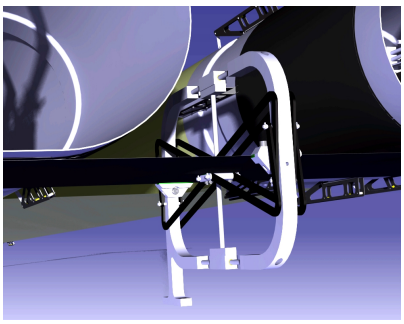

(e) Details on stowed spacecraft to boom interface

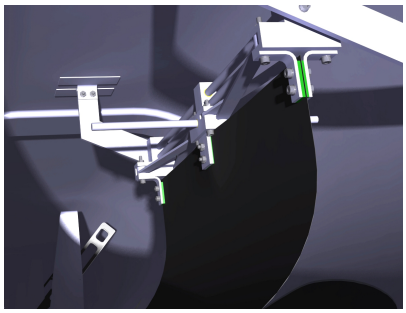

(f) Details on stowed boom to hub interface

Figure 16.: Details of proposed membrane antenna

7 MEMBRANE DESIGN & SIZING

As the antenna functionality is the main driver for the structural design, the definition of the antenna membrane setup, the membrane design and sizing should be the initial steps for the antenna design and sizing.

The following pages will contain information and design guidelines for the membrane design. To visualize the derived equations and methods, the sizing of the considered membrane is done in parallel and resulting properties are given.

7.1 MEMBRANE RF DESIGN

As stated before, the RF design of the antenna membrane is not a part of the given mechanical design task. Nevertheless, a coarse design is required to know the specific mass of the membranes.

Hence, a membrane design is used that is in general identical to the one presented by Huang in [30] (see Figure 17). The presented antenna is designed for a radar operation frequency of 1.25 GHz (L-band). Therefore, this frequency will be also considered for the here discussed antenna.

Huang describes the membrane setup as followed:

> *"The top layer has all the rectangular patches with a set of microstrip power divider lines for generating horizontal polarization. The middle layer is the ground plane with a set of aperture coupling slots. The bottom layer has only the power divider lines that excite the top-layer patches with vertical polarization through the coupling slots in the ground plane layer. [...] The three membrane layers are separated 1.27 cm between the top radiator layer and the middle ground-plane layer and 0.635 cm between the middle layer and the bottom transmission-line layer. [...] The membrane material used is a thin film of 5-micron-thick copper cladding on a 0.13-mm-thick Kapton dielectric material."*
>
> *[30, p. 2]*

However, there are some differences in the membrane design that derive from the in section 4.1 specified mission requirements

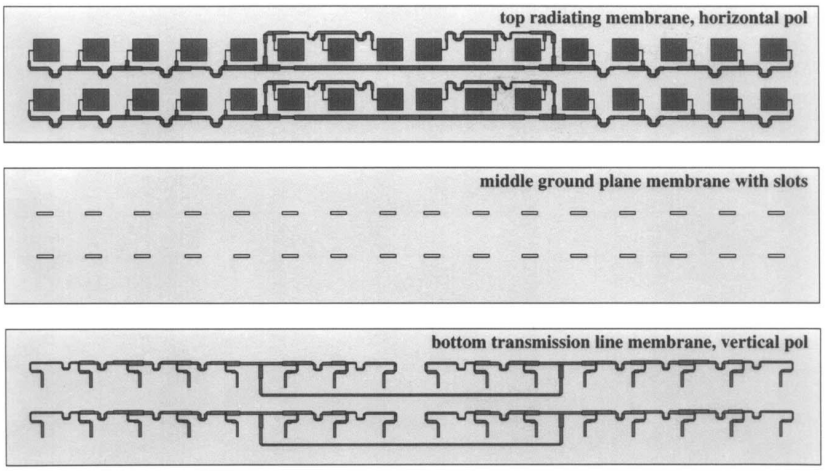

Figure 17.: Antenna membranes layout for dual-polarized micro-strip array as designed by Huang (image extracted from [30])

that demands a two-dimensional electrical steerable antenna. This option is very attractive for antennas as the system can instantly change its angle of observation without performing fast manoeuvres that would load the structure due to inertia reactions. Furthermore, advanced SAR methods like the *spotlight mode* can be used which increases the resolution of the gathered data. So an electrical steerable antenna is more complex in terms of the RF components but can have a lower strength and can be thereby lighter than antennas that have to withstand fast manoeuvres. Moreover, it enables more sophisticated SAR methods and makes the entire antenna more attractive for the science behind the mission.

spotlight mode *describes a method where the satellite is observing the same spot on the celestial body while flying over it. Therefore, the antenna beam needs to be steered constantly. Due to the resulting longer observation time per dedicated spot, the acquired data contains more details and delivers images of higher resolution.*

To implement this capability into a patch antenna a dedicated signal for each patch needs to be provided. By applying phase shifts to the unique patch signals the antenna beam can be pivoted without changing the attitude of the satellite. The phase shifts are thereby depending on the required steering angle and the position of the addressed patch in the array

Taking a closer look on Figure 17 and 18 reveals that all patches of one row are fed by the same micro-strip line. Hence, each line could be provided with a dedicated phase shifted signal that allows a beam steering only in the vertical direction.

To add a steering capability in the horizontal direction the previously mentioned unique signals for each patch are required. Theoretically this could be done by micro-strip lines as well. But a practical problem arises that can be understood by reviewing

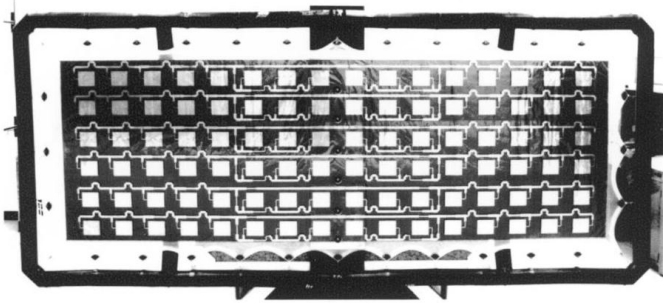

Figure 18.: 1:3 model of an inflatable L-band SAR array developed by JPL/ILC Dover Inc. (image extracted from [30])

Figure 18 again and concerning that the displayed 1:3 model is only scaled in kinds of its overall dimensions and number of patches. Hence, the size of the patches and the thickness of the feed lines are of full scale size. If each patch needs its own signal, the surface in the gaps between the patches would not be sufficient for all required micro-strip lines. This problem further increases when the antenna is brought to full scale which will increase the number of patches by a factor of $3^2 = 9$. It would be possible to increase the gaps to accommodate all lines but this would increase the antenna dimensions without increasing the RF performance and is, therefore, not considered.

To solve this problem the feeding method needs to be changed. So the patches are not fed by micro-strip lines but by Low Noise Amplifiers (LNAs) that are located next to the patches. The LNAs are supplied with power and signals by coaxial cables. One LNA can supply two patches. To assess the number of required LNAs and the amount of harness the number of patches for the proposed 40 m^2 array could be interpolated. The antenna in Figure 18 contains a total number of 96 patches on an area of 3.3m^2. Thus, an array of 40m^2 would require a number of 1164 patches, 582 LNAs and 582 coaxial cables.

The resulting mass of the carrying membrane and its composition is given in Table 2. Details on the contained values are placed in Annex A.2.

It is obvious that a huge amount of the overall weight of the membrane (82.96%) is provided by the harness. To decouple this mass from the antenna membrane and also prevent wrinkling of the membrane due to Coefficient of Thermal Expansion (CTE)-mismatch of membrane, cable and LNA material, a fourth membrane is added to the antenna design concept. This extra membrane is labeled as *service membrane*. The service membrane

ELEMENT	UNITS	MASS PER UNIT	MASS
Substrate	1	3.1200kg	3.12kg
LNAs	582	0.0008kg	0.47kg
Harness	582	0.0300kg	17.46kg
Mass			21.05kg

Table 2.: Mass of a $40m^2$ membrane that carries LNAs and harness

contains harness and LNAs and is located below the three *antenna membranes* to not disturb the signals at the receiving front.

Due to the huge masses that the service membrane has to handle, the thickness of this membrane is set to the double value of the one of the antenna membranes. The resulting masses and specific masses for all four membranes are given in Table 3. These values will be considered as baseline for the following design of the remaining antenna parts.

ELEMENT	ANTENNA MEMBRANES	SERVICE MEMBRANE
Substrate	3.1200kg	6.24kg
LNAs	-	0.47kg
Harness	-	17.46kg
Mass	3.1200kg	24.17kg
Spec. Mass	$0.078\frac{kg}{m^2}$	$0.6041\frac{kg}{m^2}$

Table 3.: Mass and specific mass of the membranes

7.2 MEMBRANE MECHANICAL DESIGN

As the expected external loads for the deployed membranes are very small, the mechanical membrane design is mainly driven by the prevention of membrane wrinkling and the selection of adequate membrane tensioning forces to tune the structural modes to the required values.

7.2.1 *Membrane Modal Sizing*

Due to the lack of significant bending stiffness of the thin polymer material, the prevention of out of plane membrane movement is

only possible by in plane tension of the membrane. Hence, it is essential for the structural modes of the membrane and, due to the huge system mass fracture of the membranes, also important for the overall system stiffness.

According to bullet #8 in the list of requirements on page 11 the systems first mode shall be $f_{1_S} = 0.4\text{Hz}$. To decouple the first mode of the membranes from the first mode of the overall system, the target frequency for the membrane f_{1_M} is set to be 110% of the antenna frequency f_{1_A}.

$$f_{1_A} = f_{1_M} \cdot 1.1 = 0.44\text{Hz} \tag{7.1}$$

It is thereby assumed that the missing damping of an atmosphere as well as the use of the stiff carbon composite booms generate a modal characteristic that is characterised by narrowband resonance peaks. Hence, a variation of only 10% seems to be feasible.

The mode frequencies of the membranes are governed by the membrane tension. To calculate the required membrane tension and, therefore, the membrane attachment force at the edges, two approaches are presented hereafter. The first is based on an analytic equation and the second is using a Finite Element Analysis (FEA) for the calculation.

The results of both methods will be compared afterwards.

Analytic approach

The analytic approach is appropriate for a first study on the required load levels. The following equation can be used to derive the first mode frequency f_{1_M} of a rectangular simply supported membrane with applied in-plane tensioning forces [25, page B44]:

$$f_{1_M} = \frac{\sqrt{\frac{1}{\rho_M \cdot e_M}\left[\frac{u_1}{{l_1}^2} + \frac{u_2}{{l_2}^2}\right]}}{2} \tag{7.2}$$

where

ρ_M	membrane density
e_M	membrane thickness
l_1	length of first edge of a rectangular membrane
l_2	length of second edge of a rectangular membrane
u_1	line load on first edge
u_2	line load on second edge

VARIABLE	VALUE	COMMENT
f_{1_M}	0.44Hz	identical to f_{1_M} (see Equation 7.1)
ρ_M	$1300\frac{kg}{m^3}$	density of Kapton®
e_M	$50 \cdot 10^{-6}$m	thickness of antenna membrane (see bullet #4 on page 10)
l_1	12.65m	$\sqrt{\frac{A_{AA}}{k_{WL}}}$ (see bullet #5 on page 11)
l_2	3.16m	$l_1 \cdot k_{WL}$

Table 4.: Membrane properties for U_{12} calculation

To ease the design process and also limit the cost of the later structures by use of same parts, the assumption is made that each membrane to frame interface will contain the same set of CFSs. Hence, the forces will not vary between the different membrane edges. Furthermore, the geometry of the edge cut-outs shall have the similar length on membranes length and width edges.

membrane length edges *refer to the both membrane edges at the longer membrane side that will be later also denoted as x-direction;*

Hereby it is understood that these assumptions will lead to a sub-optimal concept. But a detailed optimization again requires a detailed antenna membrane RF design and will, therefore, not be part of the here presented work.

Converting the assumption on the equal forces at each edge to an equation leads to

membrane width edges *is, therefore, considering the shorter membrane edges that will be later also denoted as y-direction*

$$U_{12} = U_1 = U_2 \tag{7.3}$$

Thereby, Equation 7.2 can be transformed into

$$f_{1_M} = \frac{\sqrt{\frac{U_{12}}{\rho_M \cdot e_M}\left[\frac{1}{{l_1}^2} + \frac{1}{{l_2}^2}\right]}}{2} \tag{7.4}$$

Solving equation 7.4 for U_{12} and using the exemplary variables of Table 4 U_{12} can be calculated to:

$$U_{12} = \frac{4 \cdot {f_{1_M}}^2 \cdot \rho_M \cdot e_M}{\frac{1}{{l_1}^2} + \frac{1}{{l_2}^2}} \tag{7.5}$$

$$U_{12} \approx 0.474\frac{N}{m}$$

Finite element approach

In contrast to the analytic approach, the required line load for the membrane edges cannot be calculated directly with a FE

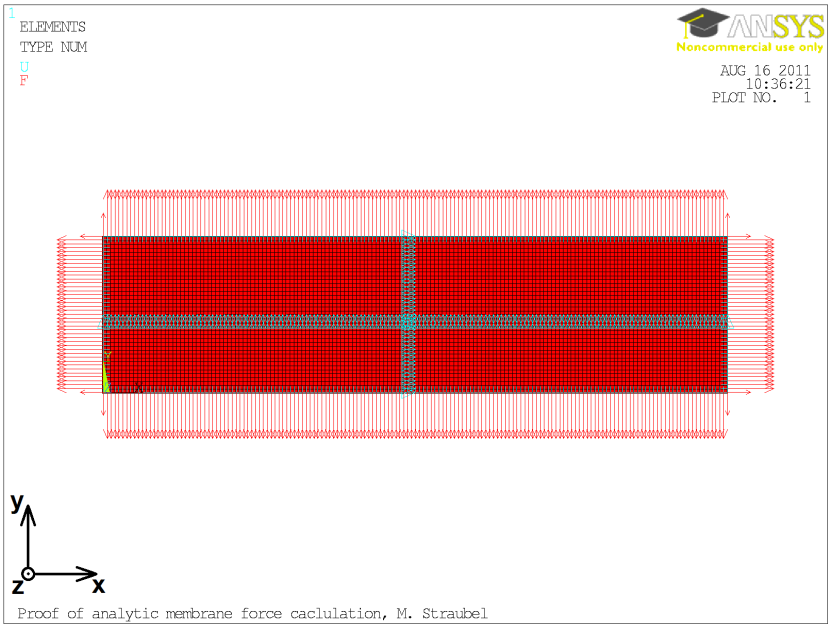

Figure 19.: ANSYS element plot containing line laods and boundary conditions

model. But it is possible to calculate the first mode frequency of a membrane with defined load scheme. Hence, to derive the required line loads for the membrane an iteration needs to be performed.

Such iteration of a more complex membrane concept will be performed in Section 7.3.2 starting on page 50. Here, only one solution is done to finally confirm the results of the analytic approach by using the U_{12} defined in Equation 7.5.

The model used the same geometry and material properties as given in Table 4. It consist of 6400 element of the ANSYS element type `SHELL181`. The bending stiffness of the element was disabled to comply with the boundary conditions of the equation that is proofed here.

`SHELL181` is a 4 node linear shell element with a here not used multi-layer option.

The calculation of the first mode of a tensioned membrane requires two subsequent calculations. The first one computes the tension in the membrane due to applied line loads at the edge. Afterwards the modal analysis can be performed using the previously calculated stresses.

The Figure 19 shows the element plot containing the edge forces and the boundary conditions for the first calculation. The following boundary conditions apply:

- Translation in z-direction (out of plane direction) for each edge node is not allowed
- Translation in y-direction for all nodes on the horizontal symmetry axis of the membrane are not allowed
- Translation in x-direction for all nodes on the vertical symmetry axis of the membrane are not allowed
- All other translation and rotation degrees of freedom are not constraint

The results of this first load step show an equally distributed stress. Finally, Figure 20 shows the out of plane displacement of the first mode of the tensioned membrane. The frequency is given in the upper left corner and has a value of 0.440107Hz.

Conclusion - membrane modal sizing

Both the analytic and the FE approach delivers almost identical results. The difference between the target value for the first mode frequency of $f_{1_p} = 0.44$Hz and the result of the FE calculation is only 0.024%. Hence, it can be assumed that the chosen analytic approach is very appropriate for the definition of the tensioning membrane forces.

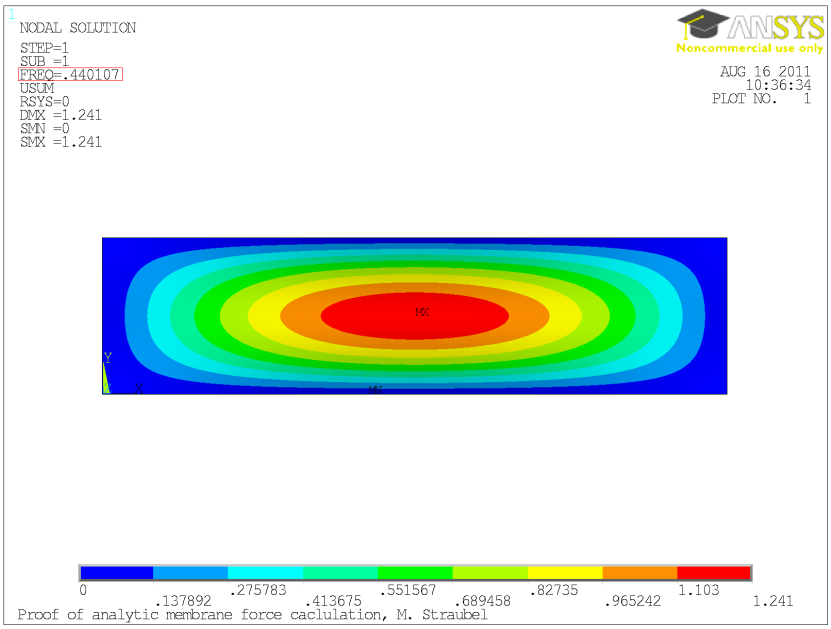

Figure 20.: Result of modal membrane analysis (first mode shape plotted)

7.2.2 *Membrane Wrinkling*

By definition the term *membrane* describes a shell that bending stiffness is that low that even a very small in-plane compression load will cause an immediate buckling of the membrane shell. Therefore, membranes are considered to carry only in-plane tension loads and out of plane loads that converts into in-plane tension loads when the membrane is deflected from its original plane.

However, even by applying only tension loads to membranes, compression loads can evolve due to transversal contraction, unsymmetrical force application, strain differences due to highly loaded main load paths, or even strong thermal gradients. The resulting buckles are denoted as *wrinkles* and the process as *wrinkling*.

Wrinkling generates local distortion and deformation in-plane as well as out-of-plane and can, in case of a membrane antenna, lower the RF performance by violating the shape accuracy requirements for the defined patch antenna design. In contrast to the theoretical considerations in section 7.2.1, the tensioning of a rectangular membrane by constant line loads at the edges is practically hard to realize. Moreover, a force application at multiple points is considered as it is also shown in all sub figures of Figure 12 on page 25.

To investigate the wrinkling of different membrane designs, either tests or simulations need to be performed. For large deployable space membrane structures, reliable testing is only possible for sub scale breadboards. For full scale test the influence of the gravity would be too significant to neglect it. Also own test had shown, that very small air movements in the test room, as they appear due to heating, ventilation and air conditioning, opening or closing of doors and windows, or even breathing persons next to the test setup, will excite vibrations in the membranes that complicate a survey of the membranes shape [67].

Hence, the final approval of the full scale wrinkling behaviour needs to be performed by simulations that algorithms had been previously verified with sub scale model tests.

Wrinkling tests

The basic setup for a wrinkling survey consist of a system that is able to load the membrane in a predefined manner and a system that is able to determine the membranes surface shape.

For force application a systems of ropes, pulleys and masses is often used to apply very well defined forces to the membranes [75].

Due to the low thickness of the membranes, the most surface survey systems rely on contact less measurement to prevent any major physical interaction between the survey system and the specimen. Thereby, the usual measurement tool is a combination of stereo cameras and a photogrammetry software. In addition laser based systems can be used as well but the costs of those laser systems are much higher and, therefore, in the most cases not available.

Although these systems need no direct contact, it is often necessary to threat the membrane surface in any kind to generate a diffuse reflecting surface. As antenna membranes are often made from nearly transparent Kapton® and equipped with metallic and thereby specular reflecting patches, a treatment of membranes prior to surface surveys is in the most cases mandatory.

Different surface preparations are possible that depend again on the used method. For *photogrammetry* the 2-dimensional images of two cameras are combined by software to a 3-dimensional image of the observed object. An applied irregular pattern of paint is required to give the software a high number of unique points and deliver a high density of measurement points on one shot. But the irregular pattern requires two layers of paint (e.g. a basic plain white background with black speckle pattern) that can easily double the areal mass of a thin membrane. Even worse is the effect that the applied paint shrinks during the drying process which will lead to a bending pretension of the membrane.

Another possibility is the application of adhesive retro reflective targets to the specimen. These targets are tracked by the stereo cameras and allow very precise information on their position. Depending on the used membrane, the targets could again influence the specimen by adding local mass and stiffness to the membrane. Moreover, this system can only derive information on the targets. Thus, the resolution is not as high as for the photogrammetry.

To avoid the effect of the targets or paint on the membrane it is moreover possible to project targets or patterns to the membrane [11, 52]. However, even for this process a surface treatment is required to achieve a diffuse reflecting surface. The density of measurement points could be easily increased by performing multiple measurements with slightly repositioned projected pattern and combining the data of all measurements.

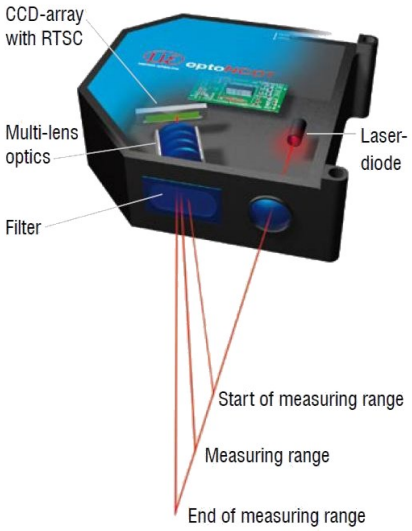

Figure 21.: Schematic of a laser distance sensor based on triangulation (source www.micro-epsilon.de)

But for this method the user should to be aware of the following effect: Due to the projection, the targets or the pattern has no fixed in-plane position on the membrane. Consequently, only out-of-plane deflections can be monitored [52].

The laser based systems are using a triangulation based (see Figure 21) or transit time measurement technique to validate the distance of a measured object in relation to the sensor. In contrast to the stereo cameras, one measurement does only generate data on one point. So to range an entire surface the whole sensor needs to be moved or tilted, or the laser beam needs to be redirected by movable mirrors. As this is not possible in an instantaneous manner, laser measurement method is only valid for static or quasi-static measurements.

During the work on the here presented antenna, membrane wrinkling tests were also performed. Figure 22 show the survey of a rectangular membrane. The used setup includes:

- Stiff aluminium frame with system of ropes, pulleys and masses for load application
- Transparent housing to prevent membrane vibration by air currents
- Modified winding machine for guiding of a triangulation laser sensor

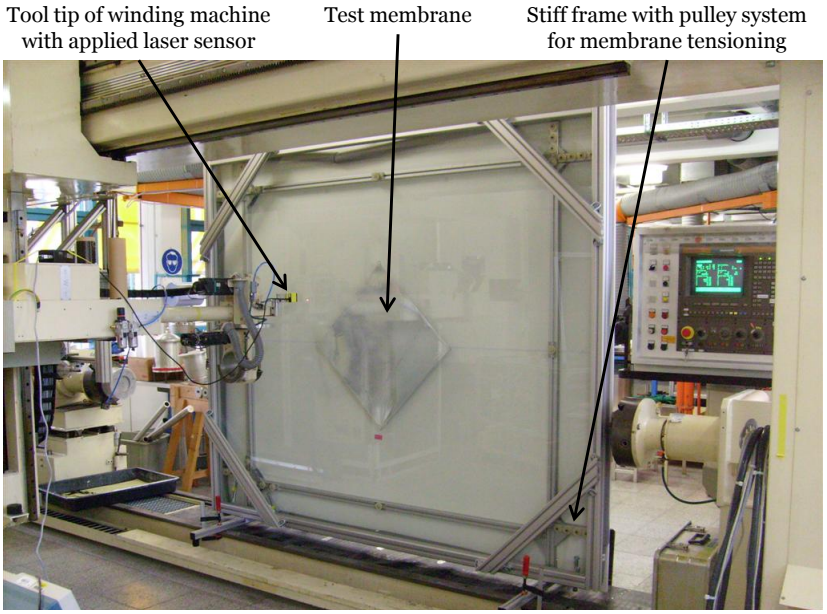

Figure 22.: Test setup for membrane wrinkling survey

- Positioning of pulleys and processing of data supported by MATLAB

For more information on the used test setup please refer to Annex A.3 on page 146 and the references [66, 79].

Wrinkling simulation

Figure 23 shows the result of a wrinkling simulation and illustrates the potentials of FE models for wrinkling prediction. In this work, performed by Wong et al.[77], a membrane with a dimension of 500mm x 500mm was simulated. The forces are applied to the short edges visible at all four membrane corners. They act parallel to the membrane diagonals and within the membrane plane. Furthermore, the forces of the opposing corners are of the same value and the forces in the lower right and the upper left corner are four times higher than the ones in the lower left and the upper right corner. The membrane is not modelled as a classical membrane but as a very thin shell with residual bending stiffness and limited compression loading capabilities.

This example is very sophisticated but for the most practical cases of large membrane structures to detailed and required therefore a huge amount of calculation time. A more appropriate approach for a huge membrane is a FE model that uses shell elements with an enabled *membrane option* as it is available for

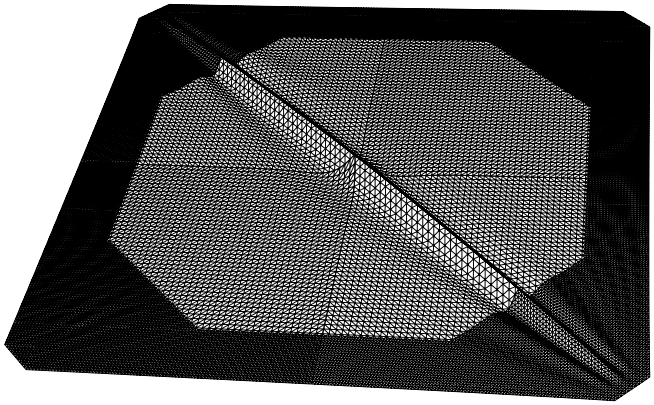

Figure 23.: Example for wrinkling simulation as performed by Wong et al. (image extracted from [77])

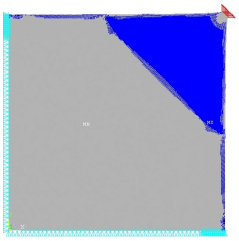

(a) Simulation results of rectangular antenna membrane

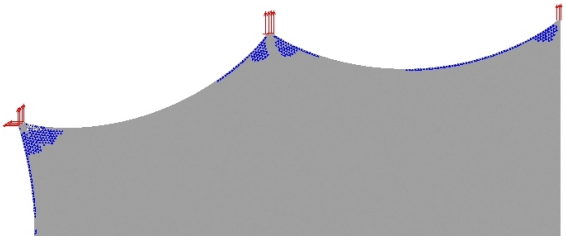

(b) Simulation results of oval antenna membrane

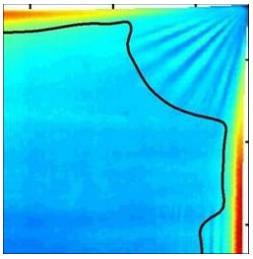

(c) Test results of rectangular antenna membrane

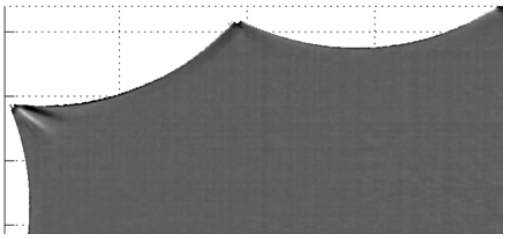

(d) Test results of oval antenna membrane

Figure 24.: Comparison between wrinkling simulation and test (Figures extracted from [79])

ANSYS's `Shell41` element type. With this activated membrane option ANSYS calculates the stress state of each element and checks the 2nd principal strain for negative (compression) values. If compression is observed in any direction, the stiffness of the element in this direction is disabled.

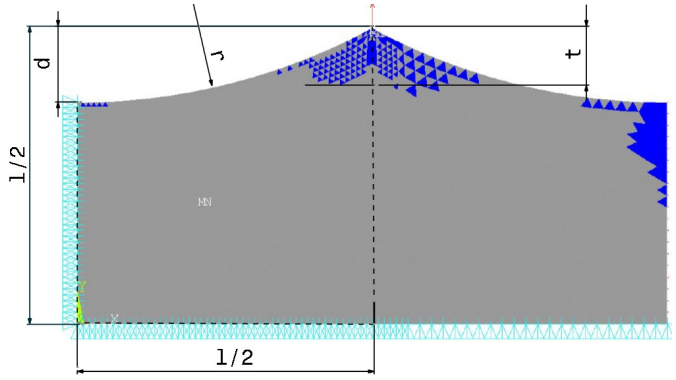

Figure 25.: Proposed antenna membrane edge geometry (Figure extracted from[80])

After calculation, the FE post processor is able to show a plot of all elements and mark the ones thats stiffness has been manipulated to not carry compression loads. Hence, this method is ideal to identify the potential regions for wrinkling but cannot predict the amplitude and the wavelength of the wrinkles. However, this calculation required very less computation time. A more detailed simulation with information on amplitude and wavelength is only necessary if the observed potential wrinkling regions are located in critical regions.

Wrinkling verification approach for the here given concept

Many researchers have considered the problem of membrane wrinkling before. Thereby, both test and simulation have been used to further understand and predict the ongoing processes [74, 76, 77, 4, 79, 80].

For the here considered antenna design Straubel et al. and Zï¿½rnig put a lot of effort on wrinkling simulation and test of comparable membrane breadboards[67, 79]. Zï¿½rnig also applies the developed methods to the full scale antenna membrane design and defined some design rules for the membrane edge geometry[80] that are considered as baseline for the further design.

The Figure 24 compares the results between performed simulations and tests [79]. As obvious, the wrinkled areas measured in the tests could be very well predicted using the simulation with ANSYS's simple `Shell41` element.

Therefore, this type of wrinkling simulation has been assumed to be sufficient for the further progress. A study on the membrane edge geometry has been performed by Zï¿½rnig in [80]. A unity

cell of the basic edge concept is shown in Figure 25. Between the force attachment points, circular segments are cut-out to prevent compression loaded membrane regions.

Zï¿½rnig states that an appropriate value for the quotient between length l and depth d of the cut-out is $k_{CutOutLD} = \frac{d}{l} = \frac{1}{10}$.

This factor will be the baseline for the further design. It is understood, that this kind of edge sizing is a coarse approach but as long as the membrane RF design is not fixed, it is a reasonable assumption for the further design of the membrane supporting frame.

7.3 FINAL MEMBRANE DESIGN

With the results of the previous section the shape of the membranes can be specified. In combination with the specific mass per membrane, the required membrane tensioning forces can be derived to deliver an input for the later discussed frame to membrane interfaces.

7.3.1 *Membrane Geometry*

A non true-to-scale sketch of the proposed membranes is shown in Figure 26. In this figure the number of force attachment points is not realistic but have been decreased to a number that is appropriate to be displayed. This outer geometry is thereby identical for all four membranes. To comply with the later introduced closed loop sizing chain algorithm, the design is parameterized.

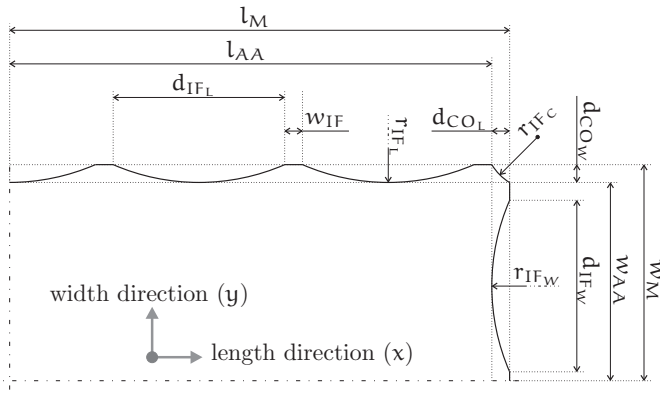

Figure 26.: Membrane geometry and notation (representative quarter)

Its parameters can be calculated by basic geometrical equations. Therefore, the following input parameters are required:

- Area of the antenna array A_{AA}
- Array length to width ratio k_{LW}
- Target value for distance between the membrane interface points d_{IF}
- Width of the membrane interface area w_{IF}

Out of these values, the following parameters can be calculated:

- Length of array l_{AA} and width of array w_{AA}
- Length of membrane l_M and width of membrane w_M
- Number of membrane interfaces at the edge in membrane length direction N_{IF_L} and in membrane width direction N_{IF_W}
- Length of cut-outs between the membrane interface points at the edge in membrane length direction d_{IF_L} and in membrane width direction d_{IF_W}
- Radius of cut-outs at the edge in membrane length direction r_{IF_L} and in membrane width direction r_{IF_W}
- Depth of cut-outs at the edge in membrane length direction d_{CO_L} and in membrane width direction d_{CO_W}
- Radius of cut-outs at the membrane corners r_{IF_C}
- Area of the resulting antenna membrane A_M

The number of attachment points per edge in length direction is thereby limited to even values to not locate a frame to membrane interface at the same position as the space craft to boom interface.

Figure 27 shows the results of two exemplary membrane designs of a $40m^2$ array with a target distance between the membrane interface points $d_{IF} = 1m$ and the width of the membrane interface area $w_{IF} = 20mm$. The both figures contain each a design for the upper and the lower boundary of the allowed value for k_{LW}.

Table 5 contains the detailed values for some of the before listed variables. Obviously the different values for k_{LW} did only change the number of attachment points in length direction. Therefore,

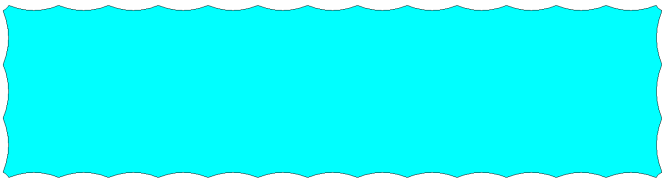

(a) $k_{LW} = \frac{1}{4}$

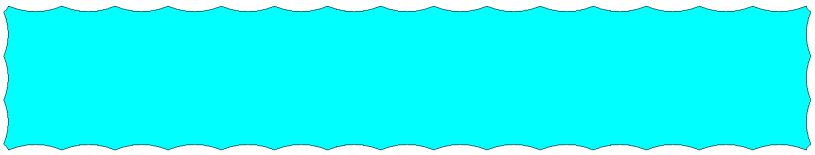

(b) $k_{LW} = \frac{1}{6}$

Figure 27.: Exemplary membrane geometries for different array length to width ratios k_{LW}

the cut-out length in width direction needs do be increased for the $k_{LW} = \frac{1}{4}$ case. From pure membrane mass, this version is also the most efficient one as its membrane area is is slightly less (0.4%) than the one of $k_{LW} = \frac{1}{6}$. Furthermore, this wider but shorter membrane uses only 14 instead of 16 interfaces per length edge which saves 4 interfaces per membrane.

So from theoretical side, the $k_{LW} = \frac{1}{4}$ version in a bit more efficient than the $k_{LW} = \frac{1}{6}$ configuration but practically the differences in mass are too small to make a significant difference.

The in section 8.3.1 introduced frame to membrane interfaces weigh only about 5.1 gram per piece.

PARAMETER	$k_{lw} = \frac{1}{4}$	$k_{lw} = \frac{1}{6}$
l_{AA}	12.649m	15.659m
w_{AA}	3.162m	2.784m
l_M	12.855m	15.492m
w_M	3.353m	2.582m
N_{IF_L}	14	16
N_{IF_W}	4	4
d_{IF_L}	0.952m	1.012m
d_{IF_W}	1.027m	0.834m
A_M	$41.064m^2$	$41.234m^2$

Table 5.: Resulting dimension parameters of the membrane geometries displayed in Figure 27

To ease the understanding of the further steps, the $k_{LW} = \frac{1}{4}$ configuration will be the baseline for the further design.

7.3.2 *Membrane Tensioning*

Here a method for the calculation of the required membrane tensioning force is introduced. Thereby, the different masses of the antenna and service membranes do not require dedicated calculations. Moreover, it is assumed that, according to Equation 7.5 on page 38, a linear dependency between the required tensioning force and the specific mass of a membrane applies. Therefore, the following considerations concentrate only on the antenna membrane. The tensioning forces for the service membrane can be calculated by multiplying the result of the antenna membrane by the quotient of the both specific masses.

As the defined membrane geometry and the force application scheme of the previous subsection differs from the ideal approach in sub subsection 7.2.1, the introduced analytic approach is not fully applicable. However, Equation 7.5 is useful to generate reasonable start values for the later FEA based optimization.

Analytic design

For the above introduced $k_{LW} = \frac{1}{4}$ membrane configuration, Equation 7.5 results in an unified line load U_{12} of

$$U_{12} = \frac{4 \cdot {f_1}_M{}^2 \cdot \rho_M \cdot e_M}{\frac{1}{{l_M}^2} + \frac{1}{{w_M}^2}} = 0.64 \frac{N}{m}. \tag{7.6}$$

where

${f_1}_M$	first mode frequency of the membrane, here 0.44Hz
ρ_M	membrane material density, here $1560 \frac{kg}{m^3}$ for Kapton® including 20% margin
e_M	membrane material thickness, here $50 \mu m$
l_M,w_M	as defined in Table 5

With the given dimensions of the membrane and the number of frame to membrane interface points, values for the interfaces

forces at the length edge F_L and width edge F_W can be calculated to

$$F_L = \frac{U_{12} \cdot l_M}{N_{IF_L}} = 0.584N, \tag{7.7}$$

$$F_W = \frac{U_{12} \cdot w_M}{N_{IF_W}} = 0.533N. \tag{7.8}$$

These values can be used as start values for the following FEA. In contrast to those results, the further design will not consider different force levels for the length and width edges but only use the mean value of both. This assumption is made to ease the design and sizing of the antenna. However, it is understood that the result is not optimal and might be reconsidered for a later detailed design.

FEA supported optimization

To calculate the final membrane interface forces for the antenna membranes F_{MA}, an ANSYS FE model is used. As already stated on page 38, such model can not calculate the required forces but it can predict an exemplary first mode frequency of an antenna membrane $f_{1_{MA}}$ for a specified force F_{MA}. Hence, an iteration based optimization of the force value needs to be performed to find a global optimum. To perform an iteration it is necessary to have a basic understanding of the relation between the optimized input variable and the target parameter to not find a local instead of global optimum.

Here the input variable is the membrane interface force and the target parameter is the membranes frequency. Using Equation 7.6 and assuming that all antenna dimensions and material definitions remain constant and the force attachment points are equidistantly distributed along the edges, Equation 7.6 can be transformed to

$$U_{12} = {f_{1_M}}^2 \cdot \frac{4 \cdot \rho_{MA} \cdot e_{MA}}{\frac{1}{{l_M}^2} + \frac{1}{{w_M}^2}} \tag{7.9}$$

$$F_{MA} = f_{1_{MA}}^2 \cdot k. \tag{7.10}$$

Thus, the relation between force and frequency is a simple quadratic one. Therefore, it would be an usual approach to calculated three sample results, fit a quadratic equation in this scatter, and solve the quadratic equation for the required force value

F_{MA}. The quadratic dependency is also nullifying the risk of finding a local instead of a global optimum.

Including a final verification simulation of the derived value this process requires a total of $3+1=4$ simulations to find a result. As the here introduced optimization is later used for a closed loop sizing chain, the simulation time is also of interest.

One calculation requires about 50 *seconds on a* 2.4GHz *dual core processor with* 3.5GB *RAM*

Therefore, another more efficient way is considered. It uses the in Equation 7.10 observed quadratic dependency between F_{MA} and $f1_{MA}$ to simply calculate the force value for the next calculation $F_{MA_{(i+1)}}$ out of the results of the previous simulation ($F_{MA_{(i)}}$ and $f1_{MA(i)}$).

Recalling the assumption that the k variable in Equation 7.10 is a constant, the following claim can be formulated:

$$\frac{F_{MA_{(i)}}}{f1^2_{MA(i)}} = \frac{F_{MA_{(i+1)}}}{f1^2_{MA(i+1)}} \tag{7.11}$$

$$F_{MA_{(i+1)}} = \left(\frac{f1_{MA(i+1)}}{f1_{MA(i)}}\right)^2 \cdot F_{MA_{(i)}} \tag{7.12}$$

Table 6 shows the results of an exemplary iteration that uses the in Equation 7.12 described approach. Each line in the table represents one FEA calculation. As start value for $F_{MA_{(i)}}$ the mean value of the in Equation 7.7 and 7.8 calculated forces F_L and F_W is used. The third column gives the percentage of difference between the calculated first mode $f1_{MA(i)}$ and the target frequency $f1_M$. As obvious, almost after the second iteration a sufficient accuracy is achieved. An optional third iteration meets the frequency target value perfectly.

Figure 28 shows the first mode shape of the membrane as it results from the third calculation. By using this response surface optimisation, the calculation time can be accelerated by a factor of two.

However, the necessity of the second calculation shows that the analytically motivated claim in Equation 7.12 is not fully

ITERATION i	$F_{MA_{(i)}}$	$f1_{MA(i)}$	$\frac{\lvert f1_{MA(i)} - f1_M \rvert}{f1_M}$
1	0.55823N	0.40642Hz	7.632%
2	0.65429N	0.43994Hz	0.014%
3	0.65448N	0.44000Hz	0.000%

Table 6.: Membrane force iteration results

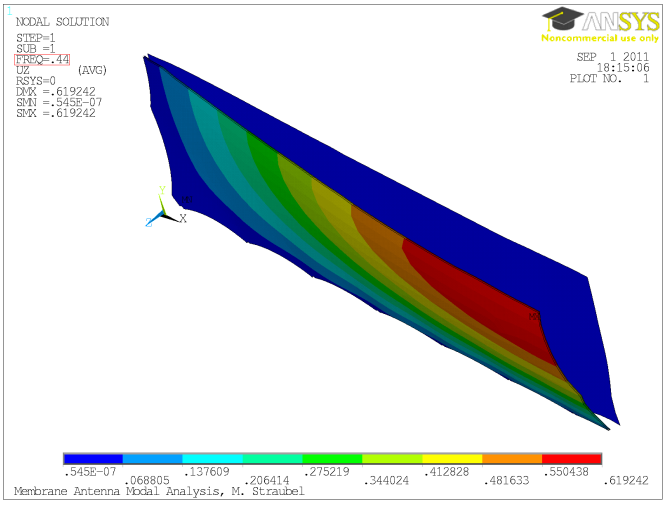

Figure 28.: First mode of antenna membrane

applicable to the more complex FE model. It is assumed that this inaccuracy arise from the different membrane edge geometries, the different force application (discrete and continuous application) as well as the additional impact of the springs length in the FE model that virtually increases the size of the vibrating membrane.

As stated before, the resulting F_{MA} is only true for the antenna membrane. The force for the service membrane F_{MS} can be calculated using the following equation:

Please refer to Equation 7.6 to see the linear dependency between the membrane specific mass per area($\rho_M \cdot e_M$) and the tensioning force

$$\begin{aligned} F_{MS} &= F_{MA} \cdot \frac{\mu_{MS}}{\mu_{MA}} = F_{MA} \cdot 7.7454 \\ &= 5.0692\text{N} \end{aligned} \tag{7.13}$$

where

F_{MA}	frame to membrane interface force, here 0.654N
μ_{MS}	specific mass of service membrane, here $0.6041\,\frac{kg}{m^2}$
μ_{MA}	specific mass of antenna membrane, here $0.078\,\frac{kg}{m^2}$

A verifying FEA for the service membrane with this force value results in a first mode frequency of 0.440175Hz which means a percentaged difference to the target frequency f_{M_T} of 0.04%.

Therefore, the in Equation 7.13 postulated approach is assessed to be very applicable.

7.4 CONCLUSION

The objective of this chapter was a sizing of the required membranes to deliver input on the antenna frame design. Therefore, a exemplary set of RF-requirements was chosen that result into a first assessment of the membrane layer design and their mass.

From the first mass assessment the decision was made to add a fourth service membrane to accommodate the huge amount of harness without violating the flatness accuracy of the three antenna membranes by CTE mismatch of RF-components and substrate.

After fixing the required membrane number and the layer design, the edge shape and the required tensioning forces for the membrane have been tailored.

Thereby, the edge shape is mainly important for prevention of wrinkles that could affect the antenna performance by local distortion of membrane regions. Some test and simulation approaches for wrinkling have been presented that result in a simple design rule for the outer shape geometry.

In contrast, the membrane tensioning forces have been sized using criteria for the first mode frequency of the membranes. Therefore, an analytic approach for first assessments as well as a FEA based iteration have been specified to determine appropriate forces.

Finally, the here presented membrane design bases on a literature based RF design and is, therefore, applicable for the further mechanical antenna design. It does not claim to be optimised for the need of the addressed mission. However, the used sizing methods and the discussed thoughts are also applicable to other membrane concepts and can be used as mechanical sizing guideline for various other RF concepts.

8

INTERFACE DESIGN & SIZING

The chosen deployment approach requires different interfaces between spacecraft, booms, hubs and membranes. A total number of three interface types and two sub-types is required:

1. Spacecraft to boom interface
2. Boom to hub interface
3. Frame to membrane interface
    a) Boom to membrane interface (including the transversal stiffeners)
    b) Hub to membrane interface

Figure 29 shows the position of some exemplary interfaces.

Caused by the changing cross section of a deploying boom, the CTE mismatch of frame and membrane material, and the rolling of parallel membranes this task is not trivial. The following subsections will, therefore, introduce the dedicated requirements as well as the chosen designs.

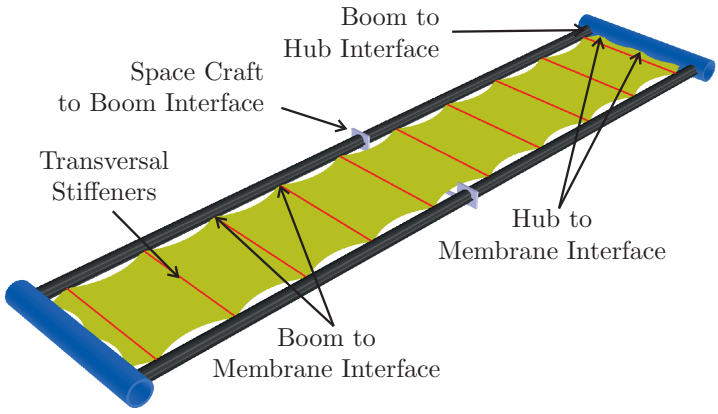

Figure 29.: Interface locations at deployed antenna

8.1 SPACECRAFT TO BOOM INTERFACE DESIGN

The interface between spacecraft and boom has to fulfil the following requirements:

1. Follow the changing cross section of the boom during deployment,
2. Provide stiff connection between spacecraft and boom during deployment,
3. Provide stiff connection between spacecraft and boom after deployment,
4. Provide a possibility to transfer pressurized gas to the inside of the boom to inflate it.

Figure 30 shows the difference between the both boom cross sections and the regions that are attractive to be used for clamping. The areas are chosen because of their ideal locations to transfer bending loads from the interface to the boom and the low deformation of those regions during deployment. Thereby, the cross section part at the flange will perform no deformation while at the upper and lower clamping location a deformation of the boom is theoretically necessary but the change in curvature is small.

Photographs of an already manufactured interface can be reviewed in annex A.4 on page 148 in Figure 68c.

The result of the design is shown in Figure 31a. The mechanism is basically made of aluminium. The sliders are equipped with POLYTETRAFLUOROETHYLENE (PTFE) and are sliding on aluminium (vertical) or stainless steel (horizontal) bars. All four clamping brackets are made of two parts that are bolted together to apply perpendicular pressure on the boom surfaces. Thereby, the

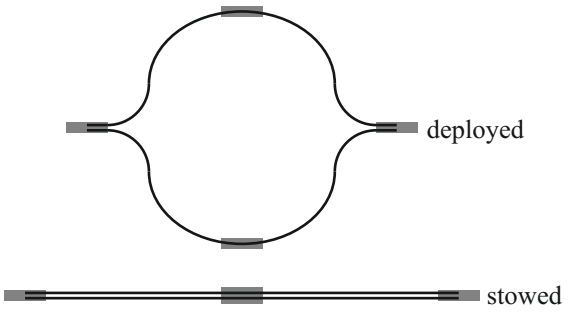

Figure 30.: Boom cross section in deployed and stowed configuration (with grey marked regions for clamping)

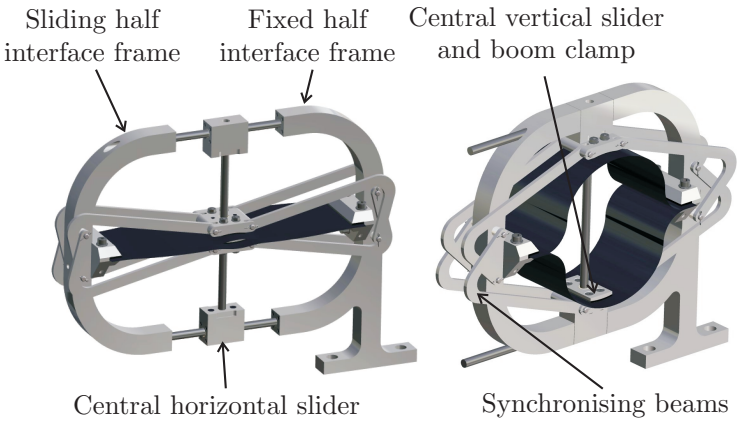

(a) Interface in stowed (left) and deployed (right) configuration

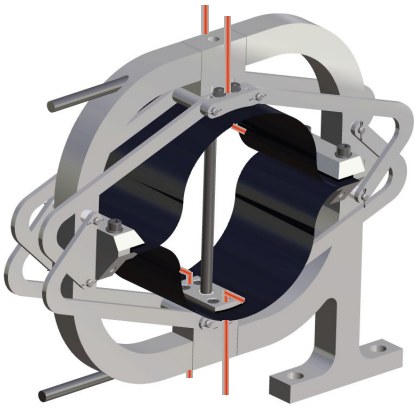

(b) Interface with red marked location for the gas inlets

Figure 31.: Spacecraft to boom interface

boom's CFRP has no direct contact with the bracket's aluminium but is protected by a layer of elastomer foam of 1 mm thickness.

The mechanism is able to follow the deforming boom cross section during deployment by repositioning of the clamping points. The upper and lower clamping parts are rigid so that they cannot follow the curvature change in the boom cross section in this region. This results in an unnatural deformation of the boom in the stowed state but also in a good load transfer in the deployed configuration. However, for this design it has been considered that a load transfer from interface to boom, in stowed state, is not meaningful and thus not required. Test on two prototypes had shown that the boom is not damaged by this enforced deformation.

Figure 31b shows the foreseen implementation of the gas inlets for the boom inflation. The vertical sliders can be used to integrate

such feature. The red marked gas pipes can be supplied by flexible tubes that are attached to the synchronising beams.

Despite of the general positive behaviour of the prototypes, some issues have been observed: The mass of one mechanism is 0.8kg which is considered to be still too much for a gossamer structure interface. Moreover the local stiffness at the clamping brackets is also too high. A large stiffness gradient applies when the forces from the very thin boom shell are transferred to the massive aluminium brackets. Although the use of the elastomer layers between CFPR and Aluminium, tests show that the failure of a boom due to too high bending loads will always occur close to the brackets. It is, therefore, recommended to reinforce the boom laminate around the clamps foot points by additional layers to decrease the gradients and generate a smoother stiffness gradient. Moreover, the mechanism is so far not designed to work in the harsh space environment but is only a functional demonstrator. However, the outlook in Chapter 12 will show an alternative, much lighter concept that is currently under investigation at DLR.

More details on this mechanism can be reviewed in [80].

Although some aspects need to be improved, the prototype interfaces were used for the first breadboards and mass calculations in this thesis. It is assumed that a final flight model will have lighter spacecraft to boom interfaces but the prototype is some kind of a worst case interface and is, therefore, baseline for this work.

8.2 BOOM TO HUB INTERFACE DESIGN

The mechanisms for the boom to hub interface are similar to the ones of the spacecraft to hub interface. But as the boom is

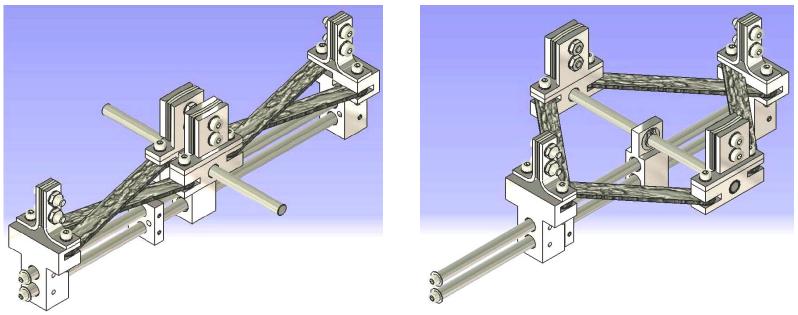

(a) opened configuration (for stowed boom)

(b) closed configuration (for deployed boom)

Figure 32.: Boom to hub interface

clamped at the end and not in the center, a surrounding interface frame is not required. Figure 32 shows some details on the boom to hub interface. The application to the hub in the final antenna concepts is displayed in Figure 16b and 16a on page 31. The mass of one boom to hub interface including the base construction that is bonded to the hub (see Figure 16b) is 0.4kg.

The design of the hub and the boom to hub mechanism are well documented in the report of Sommerwerk [63].

8.3 FRAME TO MEMBRANE INTERFACE DESIGN

The main task of the frame to membrane interfaces is to establish a mechanical connection between the antenna frame and the four membranes during all mission phases. As the frame consists of booms and hubs, two different interface types have been designed.

Thereby the *boom to membrane interfaces* and the *hub to membrane interfaces* have to fulfil a common set of requirements as well as each some dedicated ones.

Common requirements are:

- The interfaces needs to support the membrane in stowed, deploying and deployed configuration.
- While in deployed configuration, the interfaces have to ensure that all membranes are in the defined parallel distance to each other.
- While in stowed configuration, the interfaces have to ensure that the distances between the membranes need to be close to zero to coil them on the same hub without risking in-plane travelling of the different layers due to different rolling radii.
- The interface needs to compensate CTE related deformation differences between the CFRP frame and the polymer membrane without significant changes in membrane interface forces or membrane spacing.
- The transition of the interface from stowed to the deployed configuration is done automatically.

To quantify the CTE related relative deformations of frame and membranes a short verification of this effect is done here. The CTE of Kapton® is about 40 times higher than the one of the used

Figure 33.: Different CONSTANT FORCE SPRINGSS (source www.lispring.com)

CFRP boom material in in-plane direction. However, space structures in general have to sustain high temperature gradients. The compensation of the expected thermal deformations is, therefore, an usual issue one has to deal with when designing gossamer structures of materials with highly different CTEs for the harsh space environment.

The elongation difference in the longer dimension of the antenna Δl is calculated:

$$\Delta l = l_A \cdot \Delta T \cdot (\alpha_K - \alpha_B) = 58.5mm \tag{8.1}$$

where

l_A	antenna length, here 15m
ΔT	temperature difference, here 200K (see requirements 11 on page 11)
α_K	CTE of Kapton®, here $20 \cdot 10^{-6} \frac{1}{K}$ [18]
α_B	CTE of the deployable booms, here $0.5 \cdot 10^{-6} \frac{1}{K}$ [61, p. 50]

Consequently, each of the two short membrane edges is changing its distance to its connected hub by 29.25mm. This deformation is the worst case value for the further calculations.

One option for compensation is the use of the already introduced CONSTANT FORCE SPRINGS (CFS) (see Figure 33). CFSs are made of thin tapes of metal that are coiled to a cylindric shape. Actually, there are a special type of STEM booms as they are previously introduced in section 5.2.1 on page 14. But in contrast to the STEM booms the state of minimum elastic energy of the CFS is reached the stowed configuration.

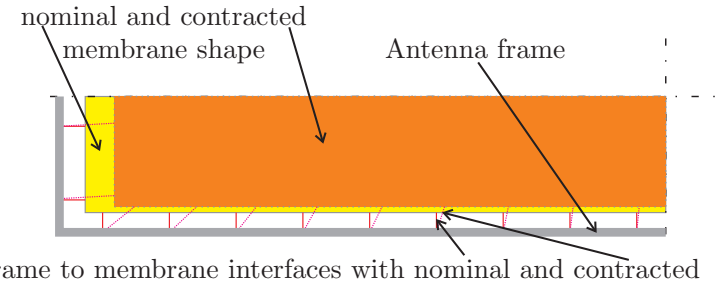

Figure 34.: Sketch of thermal membrane deformation (not true to scale, frame deformation neglected, representative quarter displayed)

Hence, the springs always intend to achieve the coiled state while STEM booms are trying to reach the deployed state. In contrast to classical springs, the force over deformation characteristic in these springs working range is almost horizontal (see Annex A.5 on page 149).

Of the shelf CFSs with a operation force F_{CFS} of 1N have an operation deflection Δl_{CFS} of $\leqslant$ 70mm (See again Annex A.5). Hence, from practical side a compensation of this relatively small length deflection is unproblematic.

However, there is also a shear effect that applies to all interfaces but is most significant for the interfaces at the booms next to its tips. Figure 34 visualizes this problem by using a simplified and not true to scale sketch. This shear problematic could be counteracted by frame to membrane interfaces that are able to pivot within the antenna plane. But this will change the force attachment angles between all membranes and the frame which could generate wrinkles in the membranes and also a modified frame loading. The pivoting angle can be minimized by increasing the length of the interface elements but this will also result in an increased antenna dimension without increasing array area and would, therefore, decrease the structural efficiency of the antenna structure.

Although this shear problematic has been noticed, it will not be further respected in this thesis. This is done due to the following reasons: To respect this effect, simulations and tests on membrane wrinkling with respect to changing force attachment angles are necessary to define acceptable angle margins. Therefore, again a detailed design of the membranes, including patches, LNAs, and harness, is required that is so far not available.

Moreover, the effect is also driven by the CTE-mismatch between frame and membrane material. Currently Kapton® is considered for the membrane substrate because it is a usual membrane material for space. However, as the membrane RF design is not done the substrate is not fixed and could be substituted in a later detailed design.

Concluding this shear problematic one can state: It has been noticed and understood but it is the conviction of the author that this problem is solvable and that it does *not* have the potential to be a concept show stopper.

8.3.1 *Boom to Membrane Interface*

In addition to the general requirements for the frame to membrane interfaces, the boom to membrane interfaces have to include the transversal stiffeners to transfer the membrane tensioning forces to the stiffener and transfer the combined - mainly inertia based - loads from this stiffener-membrane package to the booms. More details on the necessity of the stiffeners will be given in chapter 9.

As the CFSs solved the CTE-problematic, the design of a interface mechanism is possible. It is assumed that each membrane requires a dedicated CFS at each frame to membrane interface to respect the fact that one outer membrane will almost always shadows the other three ones and, thereby, the membranes will have different temperatures during space operation.

Figure 35 shows the basic design of the regarding interface. In addition, some figures of the mechanism deployment are given in Annex A.6 on page 152.

All figures use the same colours for marking the different interface and antenna components:

1. Boom connection plate (green),
2. Fixed side plates (red),
3. Movable side plates (blue),
4. CFSs (light grey),
5. Dry lubricated PTFE bearings for CFS support (not shown),
6. Screws and nuts (light grey)
7. Deploying boom (orange, on the left hand side),

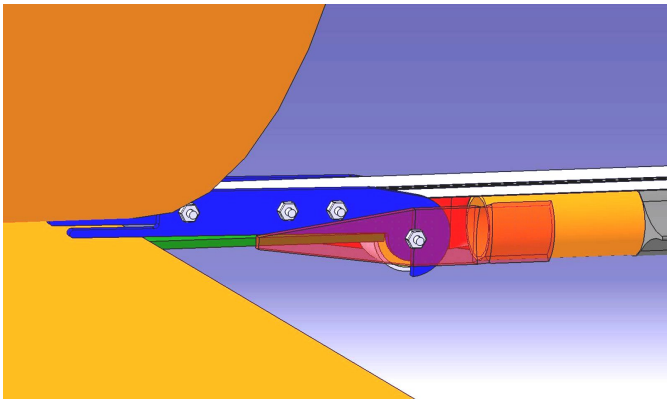

(a) stowed configuration

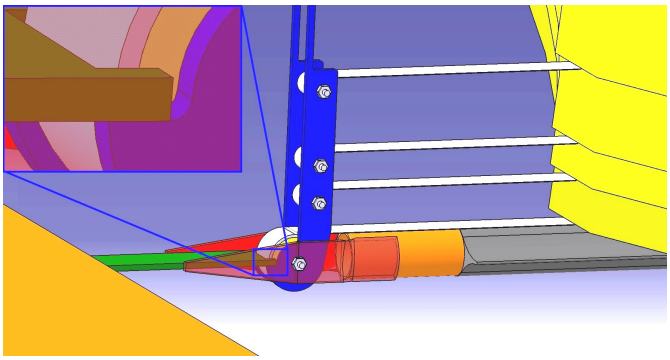

(b) deployed configuration

Figure 35.: Boom to membrane interface

8. Antenna (light yellow) and service (dark yellow) membranes,

9. Transversal stiffeners (orange rod) with membrane protective cover (dark grey).

Obviously, the interface consists of a fixed and a moveable part. The fixed part is connecting the boom flange with the service membrane CFS and the transversal stiffeners. The movable part carries the other three springs for the antenna membranes and is connected to the fixed part by a bolt.

The movable parts of the interfaces can be tilted by 90° for the antenna stowing process to decrease the distances between the membrane layers to zero. The flexibility of the CFS is thereby ensuring that only a minimal in-plane travelling of the membranes occurs.

To prevent an interface deployment in stowed antenna configuration, the movable parts are equipped with each a small

extension that locks itself under the flange of the previous boom layer (see Figure 35a).

Once unlocked, the deployment of the interface is driven by the CFSs. These forces are always aligned to the plane of the regarding membranes which is never on the same level as the rotation axis of the movable part (see again Figure 35a for details). This offset between axis and forces generates a torque that is always acting such as the movable part tries to flip up to the upright position and lock into an end stop. This stop is established between the boom connection plate and the movable side plates. It is visible in the magnified part of Figure 35b.

Caused by the small required distances between the membranes, the overall dimensions of this mechanism are very tiny. The movable side plates are only 45mm long, M1.0 screws and nuts are used for assembly and the overall mass of one interface is about 5.1 grams without margins. This value includes the first six components of the above given listing.

Hence, this relatively simple setup fulfils all requirements previously defined in the list on page 59.

8.3.2 *Hub to Membrane Interface*

Figure 36 presents the design of the hub to membrane interfaces. As obvious, the concept is less complex than the one of the boom to membrane interface. This is caused by the enclosed position of the interface inside the hub and the thereby missing necessity of movable parts. So the four CFSs are just located inside of the hub cut-out to not interfere with the membranes in stowed configuration. The springs are free to rotate using the

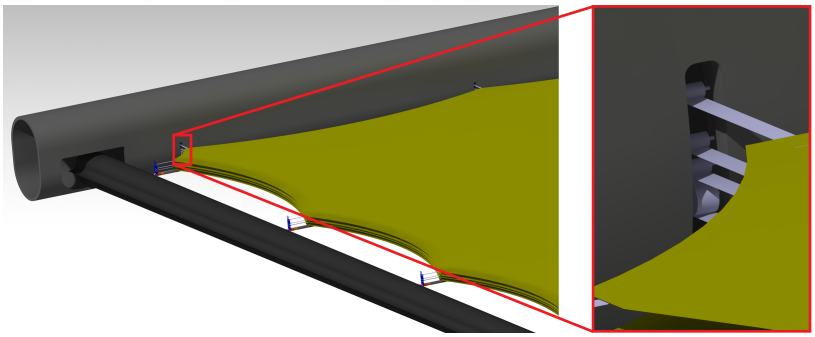

Figure 36.: Position in the overall design (left) and setup (right) of an exemplary hub to membrane interface

same combination of screws, nuts and bearings that is used for the boom to membrane interfaces.

Both frame to membrane interface types are also displayed in Figure 74 in Annex A.6.

8.4 INTERFACE SIZING

So far this chapter has mainly focussed on the design of the interfaces but it does not be very specific on the sizing of the different parts. This is caused by the different levels of maturity of the interfaces.

At least all interfaces are so far designed on engineering model level and need to be further improved for a detailed design.

The design of the spacecraft to boom interface has been checked only on the sinusoidal VEGA launch loads and passed these simulations (please refer again to [80] for details).

In contrast, the boom to hub interface and the frame to membrane interfaces are mainly sized to the required functions, manageable handling and assembly. This has been done because all mechanisms are relatively small and light. Hence it is assumed that they are able to stand the launch and operation loads in the current or a slightly modified version.

However, this is a state that can be considered sufficient for a basic design concept but the interfaces need to be further designed and optimized for a final concept.

8.5 CONCLUSION

This chapter gave methods for the design of the three required interfaces for connection of spacecraft, booms, hubs, transversal stiffeners, and membranes.

Thereby, the design and sizing is mainly driven by functional requirements to generate meaningful but not flight-designed concepts for the general antenna design.

9 FRAME DESIGN & SIZING

Finalizing the design and sizing of the membranes and the interfaces, the design and sizing of the main structural part - the antenna frame - can be performed. The frame has to facilitate the following features:

- It shall be stowable/deployable,
- Establish a mechanical connection between the membranes and the spacecraft,
- Provide sufficient stiffness in stowed and deployed configuration with respect to the expected loads,
- Provide membrane tension by carrying the frame to membrane interfaces.

Figure 37 shows again the basic concept of the antenna. The frame consists of the deployable booms, the coiling hubs, the transversal stiffeners and the boom to hub interfaces. This chapter will elaborate a design and an appropriate sizing of three of these frame parts: The booms, the hubs and the stiffeners.

Hence, the design of these three components, the boundary conditions and expected load cases are introduced. A sizing strategy is presented and the sizing methods for those parts are described.

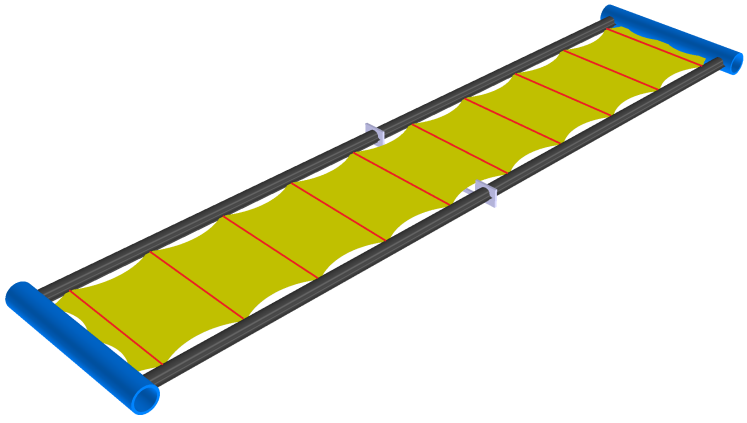

Figure 37.: Deployed antenna

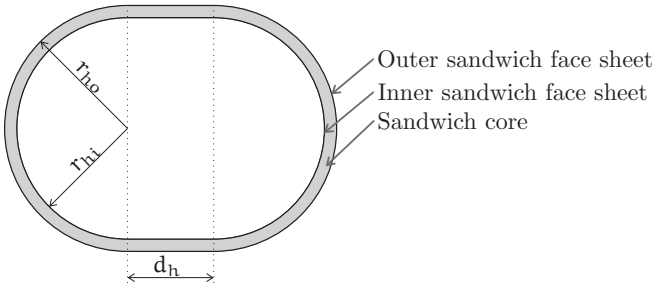

Figure 38.: Hub cross section definition

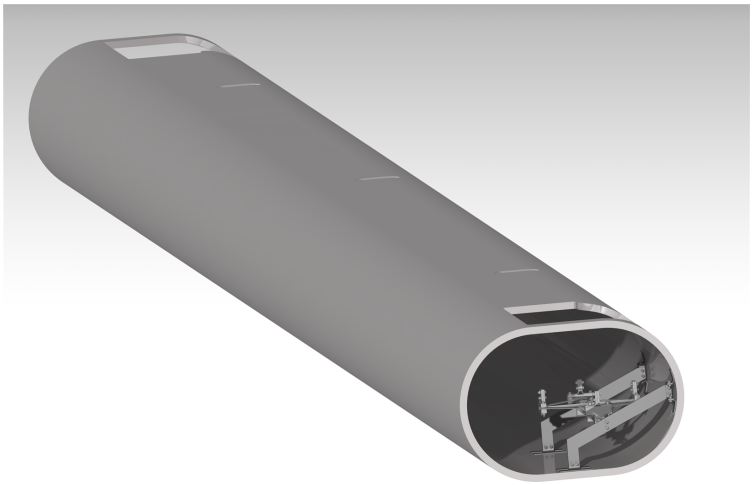

Figure 39.: Basic hub design

9.1 HUB DESIGN

Figure 38 shows a sketch of the basic hub cross section design. The outer cross section is defined by two half circles of $r_{ho} = 100mm$ radius that are connected by two $d_h = 70mm$ long straight elements. Thereby, the radius of the half circles derives from the recommended minimum coiling diameter of the used CFRP booms. The straight part between both half circles is necessary to guarantee the coiling diameter also for the last quarter winding of the boom (see Figure 15b on page 29).

Figure 39 shows the entire hub its final design. Previous hub concepts can be reviewed in [69] and [63]. Obviously, there are two large and three smaller cut-outs in the hub shell. The larger ones are for the feed-through of the deployable booms and the smaller ones are for the CFS of the hub to membrane interfaces. Consequently, the number of boom related cut-outs remains constant but their geometry needs to be updated when the boom

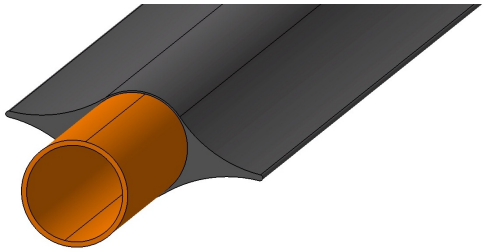

Figure 40.: Transversal stiffener concept with its CFRP member (orange) and the membrane protection cover (dark gray)

cross section is changed. Contrary, the three cut-outs for the CFSs are related to the membrane design and can vary in amount and position but not in their geometry.

To guarantee high global and local hub stiffness with a minimum of mass, a sandwich composite has been chosen for the hub shell material. The hubs ends are reinforced with metallic rings that help to transfer the loads from the launch interface blocks to the hub shell. The use of a metal for this design has mainly pragmatic reasons: The loads introduced in this section are an inconvenient combination of in-plane, out-of-plane and shear loads. Using an isotropic material is much easier and more robust for sizing because the *von Mises* stress criteria can be used to make accurate failure statements. It is the conviction of the author that a final design should contain composite instead of metallic reinforcements but for the current development phase, the effort for the implementation of composite stiffeners is unreasonably high.

More details on the sandwich will be given in section 9.6.

The material properties of the used hub materials are given in Annex A.9.

9.2 STIFFENER DESIGN

Figure 40 shows the very basic concept of the transversal stiffeners. It consists of a stiffness providing central CFRP tube and a protective cover that should minimize the deformation of the membranes during coiling and stowed period.

For the tube material the T800 carbon fibre is used. The protective cover has so far no defined material but it should be appropriate to use very light, space qualified foam.

9.3 BOOM DESIGN

As previously summarised in the conclusion of the boom state-of-the-art sub section (section 5.2.4 on page 22), a decision about an appropriate boom concept for a deployable structures is not a trivial thing.

For the membrane antenna, the boom concepts previously introduced as inflatable CFRP boom concept has been chosen. The following reasons lead to this decision:

The inflatable concepts is described on page 16 and pictured in Figure 6c on page 17

1. The knowledge of design and the tools for manufacturing of such booms is still present at DLR. Therefore, it is less complicated to adapt the current concept instead of generating a new one.

2. Both the booms and the membranes need to be stowed by rolling. Thus, both parts can be coiled around the same cylinder.

3. A comparably stiff truss would have a larger cross section and would thereby increase the stowed and deployed antenna volume.

4. The boom concept is monolithic and does not need to rigidise in space. Thus, the shape accuracy is very high and the option to test the deployed flight hardware prior to launch is given.

5. Deploying the boom by a combination of Velcro and inflation bladder adds additional mass to the boom but again everything is monolithic and does not contain any conventional hinges or bearings.

The cross section geometry of *the nominal boom design* is given in Figure 41. Except of the material thickness, this figure is true to scale to the boom design used for the past DLR/ESA Solar Sail study (see [61] for details). The geometry parameters of this past concept are selected as initial values for the later performed adaption of the cross section to the given loading. The initial values are defined to:

- $r_{b1} = 20mm$,
- $e_{b1} = 70mm$,
- $e_{b2} = 90mm$,

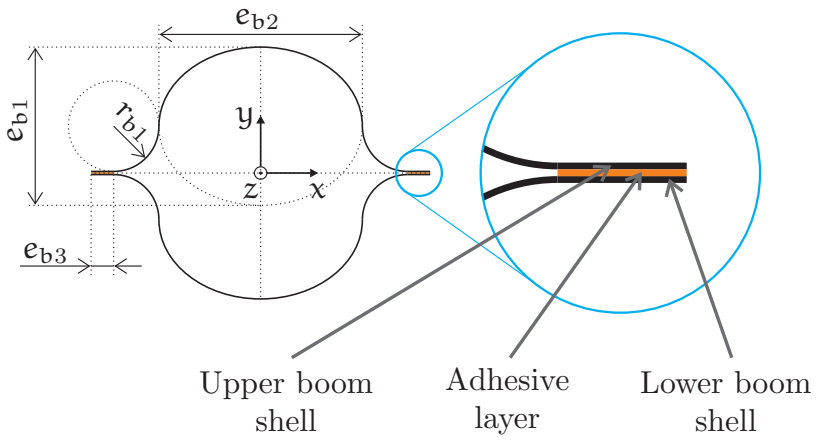

Figure 41.: Boom cross section and *local* boom coordinate system definition

- $e_{b3} = 10mm$,
- Boom shell thickness $e_{bs} = 0.1mm$,
- Boom adhesive thickness $e_{ba} = 0.03mm$.
- Resulting deployed size (width/height) of $150mm/110mm$
- Resulting stowed size (width/height) of $209mm/0.23mm$
- Resulting specific mass of $0.068\frac{kg}{m}$ (incl. 20% margin)

9.4 BOUNDARY CONDITIONS

A special challenge with deployable structures is that the sizing of the structure will include a bunch of different hardware configurations. Thereby, not only the positions of parts change but also their function in the structure.

For example, in the given concepts the deployable boom is an important component for the stiffness of the deployed antenna but in stowed configuration it is just a passive mass that has to be carried by the hubs.

So for both deployed and stowed configuration, load cases and boundary conditions need to be defined.

9.4.1 *Stowed Configuration*

A detailed view on one end of a stowed antenna is shown in Figure 42. In contrast to the previously displayed figures here

the proposed launch lock concept is given. Both hubs rest on two support blocks at each hub end. Tensioned belts (red) are added in order to fix the hubs on the blocks. The combination of blocks and belts inhibits all translative and some rotatory DEGREE OF FREEDOM (DOF). For deployment the belts are cut at one side and retracted at the other to not interfere with the deployment process.

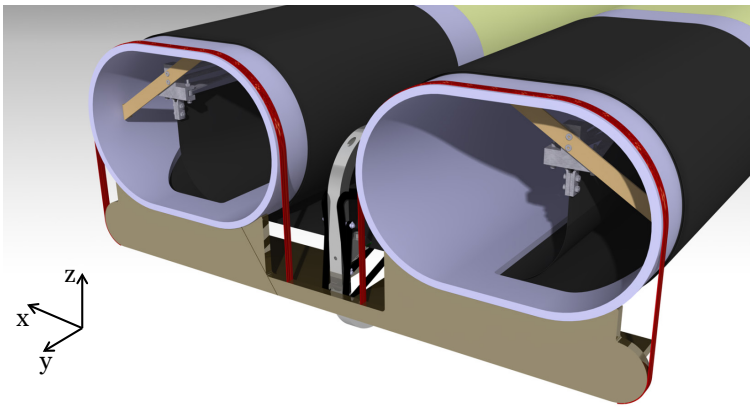

Figure 42.: Detailed view on launch lock concepts

Here it needs to be mentioned that this belt is only one possible approach. Another concept could use bolts for connection of hubs and support blocks that are cut by pyrotechnical bold cutters before deployment. However, the boundary conditions for the stowed structure will remain comparable. Therefore, for the discussed sizing of the stowed structure the DOF of the hubs and support blocks will be coupled at the contact surfaces. In addition, the locally introduced forces of the stabilising belt are respected by applying an appropriate pressure to the contact regions of belt and hub.

In stowed configuration one hub has to carry its own mass plus the passive mass of the following parts:

- Three half antenna membranes,
- One half service membrane,
- Two half booms,
- Two boom to hub interfaces,
- The half of all frame to membrane interfaces,
- The half of all transversal stiffeners.

9.4.2 *Deployed Configuration*

In the deployed configuration, the only mechanical connection between the spacecraft and the antenna is established by the two spacecraft to boom interfaces. As the used interfaces are very massive, the connection between spacecraft and booms can be considered to be of ideal stiffness. The boom to hub interfaces are also considered to be ideally stiff.

In case of any loading, the deployed booms have to support their own mass plus the following parts:

- Three antenna membranes,
- One service membrane,
- Two hubs,
- Four boom to hub interfaces,
- All frame to membrane interfaces,
- All transversal stiffeners.

9.5 LOAD CASES

Comparable to the changing boundary conditions, the load cases differ for each mission phase. For the given concepts the following sizing load cases should be respected:

1. Stowed configuration
    a) Steady state pressure of the launch lock belt that fixes the hubs on the support blocks
    b) Steady state acceleration loads during launch,
    c) Random acceleration loads or acoustic loads during launch,
    d) Minimum first mode frequency needs to be above a defined limit.
2. Deployed configuration
    a) Membrane tensioning forces,
    b) Steady state acceleration loads due to manoeuvres,
    c) Minimum first mode frequency needs to be above a defined limit.

LOAD CASE	VALUE TO TRACK	DESCRIPTION
launch lock belt loads	varying according to mass of all components	required pressure to fix hubs on their support blocks
steady state acceleration	$a_{long} \leqslant 9.375g$ $a_{lat} \leqslant 9.375g$	expected steady state accelerations during launch
random vibration	$a_{3\sigma GRMS} \leqslant 33.36g$	the antenna shall be able to stand this random vibration equivalent load
first mode	$f_{1_{SA}} \geqslant 25Hz$	the first mode of the stowed antenna shall be above this value

Table 7.: Loads and requirements for the stowed antenna configuration

LOAD CASE	VALUE TO TRACK	DESCRIPTION
membrane tensioning loads	36 interfaces with each 9.709N force	only an example for one possible membrane configuration
first mode	$f_{1_{DA}} \geqslant 0.4Hz$	the first mode of the deployed antenna shall be above this value

Table 8.: Loads and requirements for the deployed antenna configuration

The values for the dedicated loads are given in the Tables 7 and 8. Details on the chosen numbers are discussed in Annex A.7 on page 154 for the stowed antenna and in Annex A.8 on page 161 for the deployed antenna.

For the stowed configuration the steady state acceleration is always covered by the random vibration equivalent $a_{3\sigma GRMS}$ value. Therefore, dedicated steady state simulations will not be performed.

9.6 HUB SIZING

As mentioned before, the different parts of the antenna are of different importance for the deployed or stowed configuration. The hubs contribute a significant stiffness to the stowed and deployed antenna but the expected loads for both configurations are very different. So in stowed configuration they have to carry all other antenna parts and stand the launch loads with this additional mass. In contrast, in deployed configuration the hubs have to stand the relatively low membrane tensioning forces and contribute their part to the global frame stiffness to match the target mode frequency of only 0.4Hz. Consequently, the hub will be sized on basis of the stowed configuration. It is assumed and later proven that the strength of a hub that is sized for the launch loads is by far enough to stand all loads expected for the deployed configuration. Moreover, in deployed configuration the hub is more acting as a tip mass for a cantilever-like configuration. Thus, it is more an additional loading factor than a supporting structure.

Using the introduced hub design, the sizing concentrates on the composition of the sandwich laminate. To have a starting point for first calculations, a reasonable setup is created. It uses a classical sandwich layup where the core material is enclosed by two face sheets. The core is represented by an aluminium honeycomb layer with a nominal thickness of 10mm. The face sheets are again composed of three CFRP layers where two UNI DIRECTIONAL (UD) layers with fibres oriented in hub length direction (0°) enclose one UD layer with fibres oriented in hub circumferential direction (90°):

- Layer 1: CFRP-UD , 0°
- Layer 2: CFRP-UD , 90°
- Layer 3: CFRP-UD , 0°
- Layer 4: Aluminium Honeycomb , 0°
- Layer 5: CFRP-UD , 0°
- Layer 6: CFRP-UD , 90°
- Layer 7: CFRP-UD , 0°

With a nominal UD layer thickness of 0.15mm, the thickness of the entire hub shell material adds up to 10.9mm. This single

layer thickness is considered to be still easy to handle during manufacturing and integration. However, current of the shelf UD layers can be ordered down to 0.04mm but their handling is more sophisticated. Thus, the here presented sizing of the hub will at first concentrate on this initial uncomplicated layup. In case of an unsatisfying calculation result, the stiffness can be increased by adding more UD layers to the face sheets or vary the thickness of the core material. Later results will also show the effects of further decreased single layer thickness.

9.6.1 *FE model*

Figure 43 shows the detailed ANSYS FE-model that contains all cut-outs for booms and CFSs. Due to symmetry, only a half hub is modelled.

Figure 44 gives a detailed view on the hub end that is connected to the launch support block. The red marked elements indicate the regions that are loaded with the belt equivalent pressure defined in Annex A.7.4.

The support block is modelled using ANSYS's `solid92` 10-node tetrahedral volume element while the hub shell is modelled using the `SHELL281` 8-node quadrilateral layered shell element that is degenerated to a triangular shape to match to the tetrahedral solid element. The *layered* option of the `SHELL281` is thereby used to model the hubs sandwich layer by layer. This more sophisticated element type requires more calculation time and generates larger result files but enables the engineer to extract material stresses for each layer. The decision has been made that this gain in information on the composite is worth the extra calculation time.

It is assumed that the tensioned launch lock belt does never allow the hub to lose the contact with its support blocks. Therefore, it is a valid approach to not model complex contact definitions but couple the contact surfaces of hub and support blocks by sharing common nodes. To model the boundary conditions between the spacecraft and the stowed antenna, the bottom nodes of the support block are fixed for all DOFs.

As usual, the general element size is relatively large to limit the simulation time but next to critical regions it is refined locally to give detailed results for those regions. In case of the here presented configuration this is particularly true for the contact region between hub and support block, one part of the boom feed trough edge and the CFS cut-outs (see Figure 44).

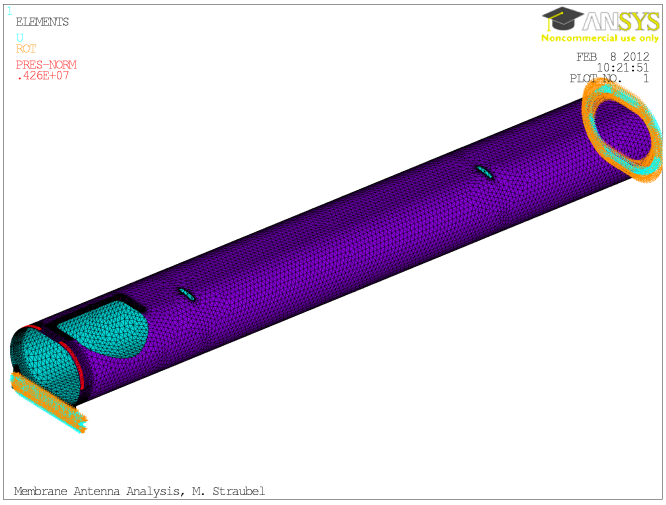

Figure 43.: Meshed half hub with boundary conditions

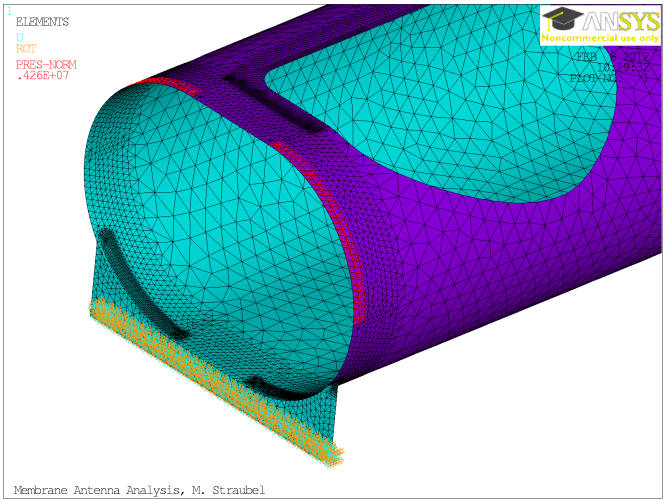

Figure 44.: Detailed view on hub end with refined mesh

Moreover, it has been noticed that the CFS cut-outs are very critical to the laminate in some load cases. Thus the edges of the cut-outs have been reinforced with beam elements. Those reinforcements are again made of aluminium and have a rectangular cross section. Figure 45 shows these stiffening elements in a view where the hub is sliced through the cut-out and where ANSYS's `\eshape` option is activated. The reinforcement cross section is highlighted in light green.

`\eshape` displays beam and shell elements not only as 1 or 2-dimensional elements but use the definitions on beam cross section and shell layup to generate a 3-dimensional view

The Figures 43 till 45 may imply that the model does only contain the hub shell and the aluminium stiffeners, but the mass of the other antenna parts that are wrapped around in launch configuration are respected as well. They are included by an

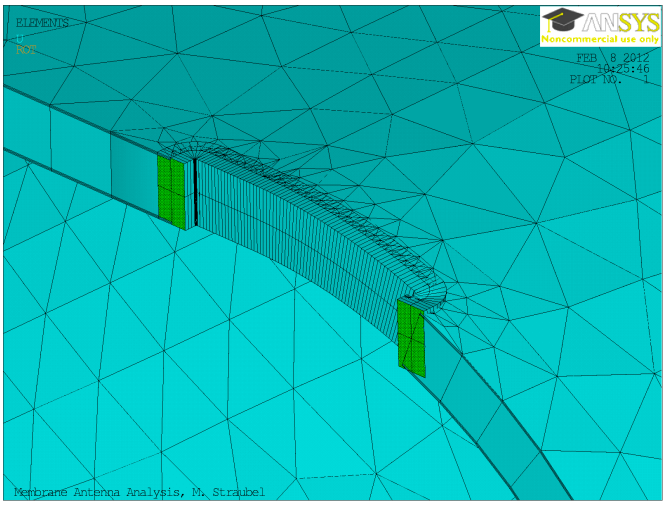

Figure 45.: Detailed view on stiffened CFS cut-out region (elements left on the cut-out central line are hidden)

increased density of the sandwich core material of the hub shell by an appropriate amount.

9.6.2 *Failure Criteria*

The sub-sections below will present results of different finite element analysis of the hub. To assess how critical the resulting deformations and stresses are, one has to define criteria that specify when material failure occur.

Aluminium

Aluminium is used for the hub support blocks and the stiffening rings at the hub ends as well as the CFS cut-out stiffeners. As usual for isotropic metal, the equivalent *van Mises Stress* is used to assess the probability of a failure. The aluminium is considered as broken if the van Mises stress exceeds the maximum allowed stress $\sigma_{\mathrm{Alu}_{max}}$ defined in Table 38 in Annex A.9.

Composite sandwich

A failure assessment for non-isotropic composite sandwich materials is a much more sophisticated task as it is for the isotropic aluminium.

As indicated above, the used FE model is able to give resulting stress values for each layer of the sandwich. Thus, the sandwich can be evaluated layer by layer. Consequently, separate failure

criteria for the UD carbon composite layers of the face sheets as well as the honeycomb sandwich core need to be defined. For the honeycomb, the following criteria will be used:

- The out-of-plane compression shall not exceed the maximum allowed stress $\sigma_{Corecz_{max}}$ defined in Table 36 in Annex A.9
- The shear stress shall not exceed the maximum allowed values $\tau_{Corexz_{max}}$ and $\tau_{Coreyz_{max}}$ defined in Table 36 in Annex A.9

For the CFRP UD layers, no single maximum stress values apply. Instead, composite failure criteria are used to assess the risk of failure. As there is still no definitive consensus on the most reliable criterion[62], a bunch of criteria will be used to be on the safe side. It is understood, that this can result in too conservative results. The following criteria will be respected:

- Puck fiber failure criterion
- Puck inter-fibre (matrix) failure criterion
- Tsai-Wu Strength Index
- Inverse of Tsai-Wu strength ratio index
- Hashin fibre failure criterion
- Hashin matrix failure criterion

ANSYS is using inverse safety factor $k_{S_{inv}} = 1/k_S$ to indicate how critical a stress state is:

- $k_{S_{inv}} < 1.0 \Rightarrow$ no damage/failure applies
- $k_{S_{inv}} \geqslant 1.0 \Rightarrow$ damage/failure applies

Those inverse safety factors are automatically calculated by ANSYS for all six above defined criteria, using the material data defined in Table 34 in Annex A.9. The user has to decide if he wants to see the inverse safety factor of only one of those criteria or the worst (highest value) of all criteria. The last option will be the baseline for all following examinations.

The use of an additional safety factor is not meaningful in this case. This decision has been made because the following facts:

1. The CFRP plies are evaluated using a bundle of failure criteria which is in this combination very conservative,

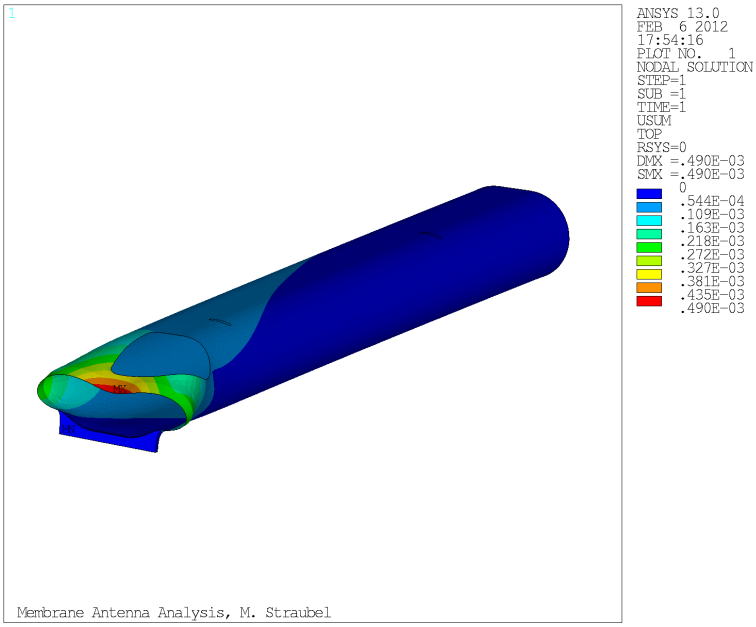

Figure 46.: Scaled deformation of hub under pure belt loading (deformation scaling factor of 200)

2. As the later results will show, the highest loads will occur in edge and cut-out regions which could be easily reinforced in a later detailed design study.

9.6.3 *Launch Lock Belt Tension*

Figure 46 shows the scaled deformation of the hub that is loaded only by the belt force equivalent pressures. A maximum deformations of up to 0.49mm has been calculated.

The reinforcements have been unselected for the plot because their loading is very uncritical - van Mises stress below $1.40 \cdot 10^6 \frac{N}{m^2}$

To assess how critical this is to the aluminium parts of the hub and its support block, Figure 47 shows the van Mises stress plot of all aluminium parts except the CFS cut-out reinforcements. The figure indicates that the highest load applies in the support block next to two *spikes* at both block sides. Due to the scaled deformation in the figure, it is obvious that this maximum in stress is related to the strong laterally bending of these spikes.

Comparing the maximum value of the plot to the in Annex A.9 defined maximum stress results in a safety factor $k_{S_{Alu1}}$ of:

$$k_{S_{Alu1}} = \frac{\sigma_{Alu_{max}}}{\sigma_{vM_{Alu}}} = \frac{510.0 \cdot 10^6 \frac{N}{m^2}}{103 \cdot 10^6 \frac{N}{m^2}} = 4.95 \tag{9.1}$$

So this pure belt loading is uncritical for the aluminium parts.

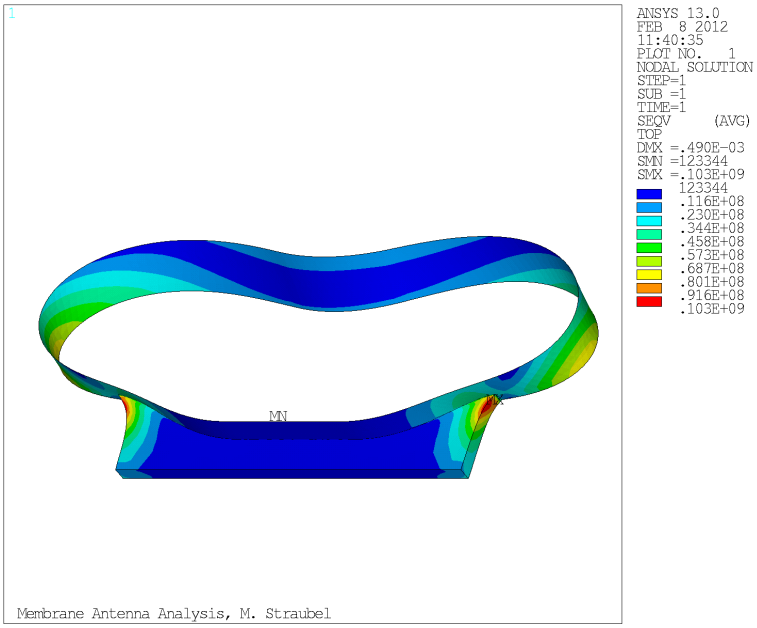

Figure 47.: Van Mises stress in aluminium ring and support block (deformation scaling factor of 200)

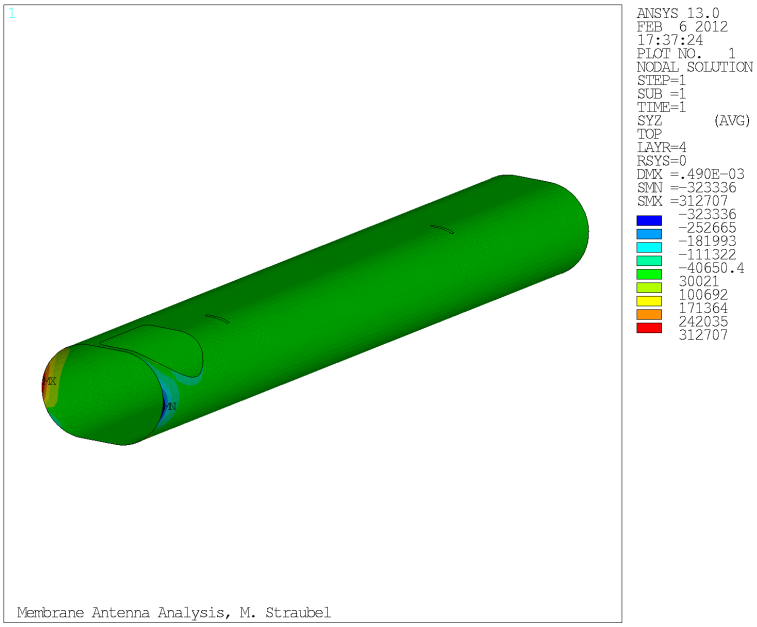

Figure 48.: Shear stress in yz direction for honey comb core material (hub layer #4) under pure belt loading

The evaluation of the sandwich part is more complex. Table 9 gives all results of interest for all layers as well as safety factors that refer to the maximum allowed values specified in Annex A.9.

CRITERION	LAYER #	ORIENT.	VALUE	k_s
Combined Criteria	1	0°	0.142	7.05
Combined Criteria	2	90°	0.112	8.95
Combined Criteria	3	0°	0.135	7.43
Out of Plane Compression σ_{Corecz} in $\frac{kN}{m^2}$	4	0°	−45.966	37.51
Shear Stress τ_{Corexz} in $\frac{kN}{m^2}$	4	0°	220.693	6.25
Shear Stress τ_{Coreyz} in $\frac{kN}{m^2}$	4	0°	323.336	**2.56**
Combined Criteria	5	0°	0.207	4.83
Combined Criteria	6	90°	0.141	7.11
Combined Criteria	7	0°	0.210	4.75

Table 9.: Layer based results of the hub loaded only by the belt loads

Obviously, the sandwich core shear stress in yz direction is the most critical parameter. Figure 48 plots this parameter of the core layer and indicates where the maximum values apply. Comparing this figure to Figure 46 gives an explanation for the locations of the maxima: The bending deformation of the shell in this part of the hub is very high. Moreover, the bending around the axial-directed axis is more significant than any shell bending around a circumferential axis. Thus, the location of the τ_{Coreyz} maximum as well as the fact that the maximum τ_{Coreyz} is larger than the maximum τ_{Corexz} are plausible.

With a minimum safety factor of $k_s = 2.56$ all layers of the hub composite are safe and the final result of the pure belt loading load case can be concluded with a clear statement that no parts of the hub and its support blocks will fail.

9.6.4 *Modal Requirement*

As defined in Table 7 on page 74, the stowed antenna has to fulfil the following requirement: $f_{1_{SA}} \geqslant 25Hz$.

The analysis is performed using the Block Lanczos *mode-extraction method in ANSYS*

The above introduced FE-model is used but the element size has been enlarged by a factor of two and the refinements at the hub ends are removed. This has been made to speed up the calculation for the later presented closed loop sizing chain. The

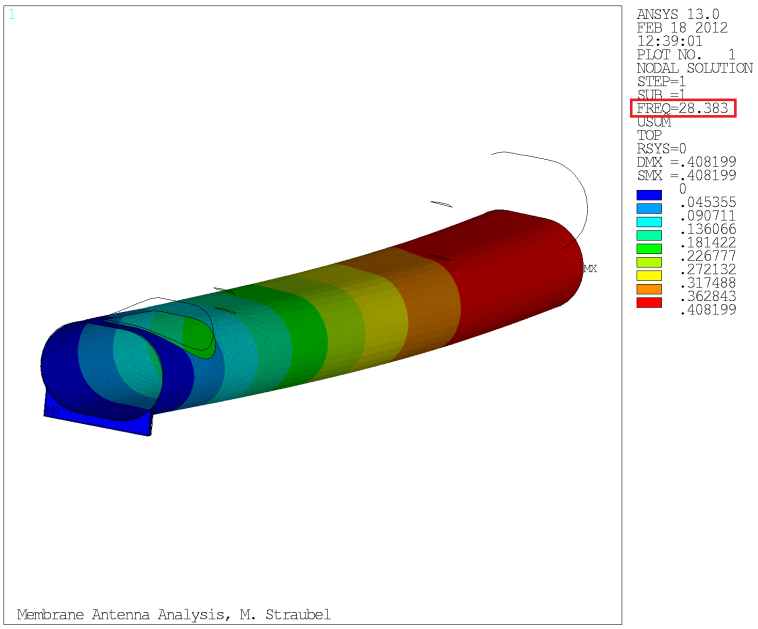

Figure 49.: First mode of stowed hub incl. other applied antenna parts

hub is pre-tensioned by the equivalent pressure of the launch lock belt and a modal analysis is performed. The result of the computation is shown in Figure 49. The achieved first mode frequency of $f_{1_{SA}} = 28.383\text{Hz}$ is also marked in the plot.

Hence, it is obvious that the modal behaviour of this first hub design is sufficient for the here discussed basic configuration. So a modification of the hub shell is not necessary. The pure weight of the shell of one hub is 6.62kg. Thereby, the sandwich shell contributes 5.72kg and the aluminium rings 0.9kg to this value.

9.6.5 *Random Vibration*

For random vibration load related sizing, the equivalent static g_{RMS} load will be used. According to Table 7 in Section 9.5 this load will reach a maximum value of $a_{3\sigma GRMS} = 33.36g$.

This load can apply to all spatial directions. However, this maximum acceleration value will be only applied to the antennas x- and z-direction. This is done because of a acceleration loading in one of those two directions will result in a bending of the hub. It is assumed, that such bending loading is the most severe load case for the hub. The two considered load directions are moreover bidirectional. Thus four possible load cases arise:

- *LC1*: $a_x = +a_{3\sigma GRMS}$, $a_z = 0$

CRITERION	LAYER #	ORIENT.	VALUE	k_s
van Mises Stress in Aluminium Parts in $\frac{kN}{m^2}$			244.298	2.09
Combined Criteria	1	0°	0.42243	2.37
Combined Criteria	2	90°	0.52466	1.90
Combined Criteria	3	0°	0.42733	2.34
Out of Plane Compression σ_{Corecz} in $\frac{kN}{m^2}$	4	0°	161.790	10.66
Shear Stress τ_{Corexz} in $\frac{kN}{m^2}$	4	0°	912.070	1.51
Shear Stress τ_{Coreyz} in $\frac{kN}{m^2}$	4	0°	494.000	2.79
Combined Criteria	5	0°	0.59036	1.69
Combined Criteria	6	90°	0.70381	**1.42**
Combined Criteria	7	0°	0.59514	1.68

Table 10.: Layer based results of the hub loaded by a random vibration equivalent static load in global negative z-direction (LC1)

- *LC2*: $a_x = -a_{3\sigma GRMS}$, $a_z = 0$
- *LC3*: $a_x = 0$, $a_z = +a_{3\sigma GRMS}$
- *LC4*: $a_x = 0$, $a_z = -a_{3\sigma GRMS}$

In addition, the fixation belt equivalent pressure is also applied to the structure for all load cases.

see previous Section 9.6.3 starting on page 80 for further details on failure criteria

For this sizing step the strength instead of the stiffness of the hub is of high interest. Therefore, the strength of the aluminium parts is again evaluated using the *van Mises* stress criteria while the CFRP strength is again evaluated using the above introduces failure criteria.

Table 10 presents the safety factors for each layer of the composite material as well as the aluminium parts for the most severe load case. Here it is a loading in global positive x-direction (LC1).

More detailed, Figure 50 shows the combined failure criteria for the most critical composite layer #6.

The location of the highest value is marked in the plot by white MX letters. They indicate that the critical spot is at the edge of the boom feed through cut-out which is considered as an usual result.

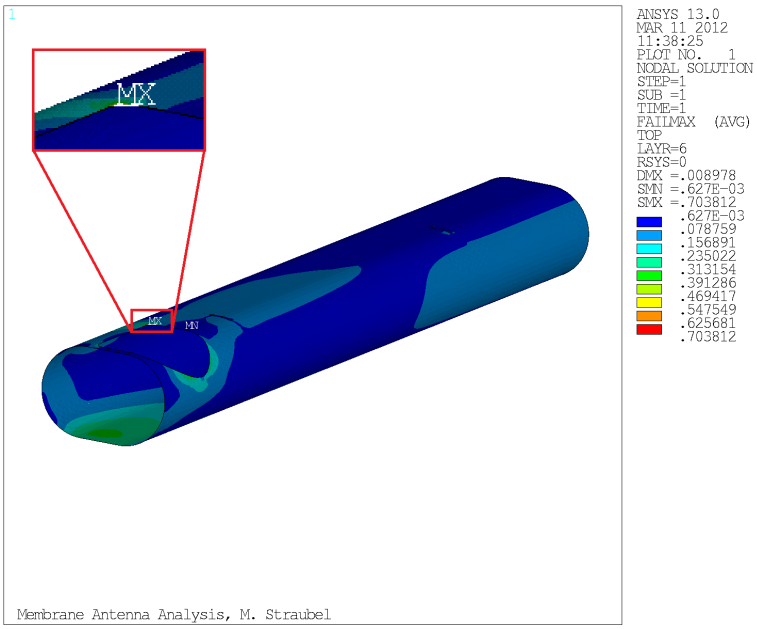

Figure 50.: Combined failure criteria for most critical layer #6 during g_{RMS} loading

As obvious the combined loading is more critical than the one by pure belt pressure but all safety factors are still above the defined limit of 1.0.

9.7 STIFFENER SIZING

The sizing of the frame stiffeners is uncomplicated as the stiffeners have the very regular geometry of a hollow rod which allows sizing them with basic analytic equations.

During the launch, the stiffeners are supported by the hub and the wrapped around membranes. Thus, it is assumed that the launch loads are uncritical to the stiffeners.

In contrast, once the antenna deploys, the stiffeners are no longer supported by hub and membranes but only connected to the booms at both ends. There, the ends are connected to the boom to membrane interfaces. Those interfaces transfer the membrane tensioning forces into the stiffeners and load them by compression in longitudinal direction.

please refer to Figure 35 on page 63 for insight in the here discussed connection between stiffeners and booms

For such long and slender rods under axial loading, global column buckling is the most probable failure scenario. So the rod can be sized using Euler's equation on column buckling:

$$F_{crit} = \frac{\pi^2 \cdot E \cdot I}{(k_E \cdot l)^2} \tag{9.2}$$

where

F_{crit}	critical axial force
E	elastic modulus of column
I	geometrical moment of inertia of column
k_E	Euler's length factor
l	column length

As usual for Euler's equation one has to choose the correct Euler's length factor k_E to adapt the formula to different column boundary conditions. For the frame stiffeners, the boundary conditions are comparable to column with pinned ends on both sides because of the low bending stiffness of the boom flanges. Thus, Euler's length factor can be defined to $k_E = 1.0$.

$$F_{crit} = \frac{\pi^2 \cdot E \cdot I}{l^2} \tag{9.3}$$

Equation 9.3 is, therefore, the baseline for the sizing of the stiffeners. Taking a closer look on this formula reveals that for the stiffeners only the variable I is unknown. The length of the stiffeners is given by the overall geometry of the antenna, while the E is already fixed by the decision to use pultruded CFRP members out of T800 fibres. F_{crit} can be assumed to be nearly equal to the sum of all four membrane tensioning forces at one boom to membrane interface.

The foreseen stiffener cross section is tubular. The general equation for I of a tube is defined to:

$$I = \frac{\pi}{4}\left(r_o^4 - r_i^4\right) \tag{9.4}$$

where

r_o	outer tube radius
r_i	inner tube radius

Inserting Equation 9.4 in Equation 9.3 would result in a equation that depends from the two radius variables which will generate a need to solve the equation for two unknowns. To prevent this, a linear dependency between both radii is defined by using a constant factor. This dependency is then applied to Equation 9.4:

$$r_i = r_o \cdot k_r \qquad \text{for } k_r \in \mathbb{R} \text{ and } 0 < k_r < 1 \tag{9.5}$$

$$I = \frac{\pi}{4}\left(r_o^4 - r_o^4 \cdot k_r^4\right) \tag{9.6}$$

$$I = \frac{\pi}{4} \cdot r_o^4 \left(1 - k_r^4\right) \tag{9.7}$$

where

k_r	radius factor

Inserting Equation 9.7 in Equation 9.3 results in:

$$F_{crit} = \frac{\pi^3 \cdot E}{4 \cdot l^2} \cdot r_o^4 \left(1 - k_r^4\right) \tag{9.8}$$

Solving this equation for r_o gives the required formula for the calculation of the stiffener radii:

$$r_o = \sqrt[4]{\frac{F_{crit} \cdot 4 \cdot l^2}{\pi^3 \cdot E \cdot (1 - k_r^4)}} \tag{9.9}$$

Filling Equation 9.9 with values from the nominal antenna design and multiplying the critical load F_{crit} with a safety factor of 1.5 and setting k_r to 0.9, results into an outer radius of $r_o = 4.075\text{mm}$. The inner radius can be calculated to $r_i = 3.668\text{mm}$ using Equation 9.5.

The first mode frequency of the pre stressed stiffeners is at 2.10Hz and, thereby, in sufficient distance to the required 0.4Hz for the overall structure

9.8 BOOM SIZING

In contrast to the previously sized hubs, the booms are only of interest for the deployed antenna configuration. They are wrapped around the hubs when in stowed setup.

During the deployed life time of the antenna the booms have to stand the loads and fulfil the requirements defined in Table 8 on page 74.

9.8.1 *FE Model*

For the calculation of the frame static and dynamic behaviour, the FE model that was previously used for the calculation of the mem-

brane attachment forces has been extended with a surrounding frame. Due to the symmetry of the structure the model represents only a quarter of the entire structures. Previous simulations with a full model but of reduced complexity (boom modelled from beam instead off shell elements) confirmed that the first mode of the antenna is indeed a symmetric out-of-plane bending mode.

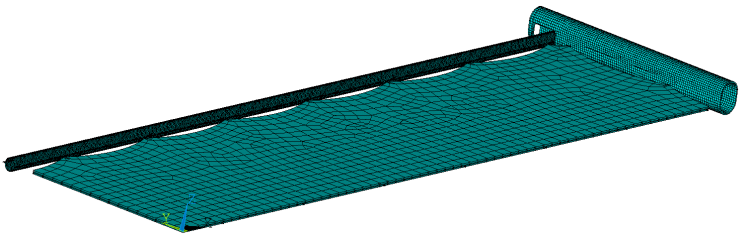

(a) Antenna FE model for deployed configuration (representative quarter)

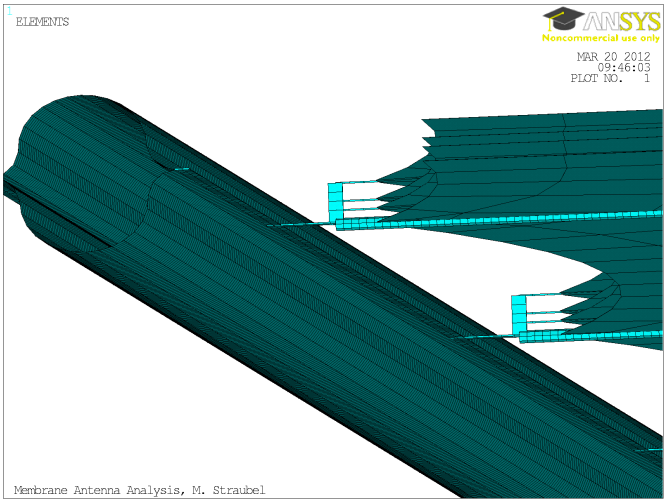

(b) Detailed view

Figure 51.: Membrane antenna FE model

Figure 51a shows the resulting model from an overview perspective while Figure 51b gives a closer look at some details.

This updated model is very detailed, it contains:

- One half detailed boom with parameterised cross section modelled with shell elements,
- One half hub with all cut-outs and aluminium stiffening elements also modelled using layered shells,
- Frame to membrane interfaces using beam elements,
- Transversal stiffeners using beam elements,

- Three quarter antenna membranes and one quarter service membrane modelled with shells.

9.8.2 *Static Antenna Deformation*

The static deformation of the antenna is only driven by the CFSs that tension the membranes. To simulate the pure static deformation of the frame and the membranes, the CFSs can be easily substituted by pairs of opposing forces but the later shown modal sizing requires frame and membranes in a pre-stressed but also mechanically connected configuration. Thus, a connecting element between frame and membranes is required that performs like a CFS.

Some exemplary deformation results are given in Annex A.10.

The realistic modelling of these springs is very challenging using conventional FE element types. Despite of the large ANSYS element type library, an element was not found that generates strain independent mechanical stress and that can be used for modal analyses. Hence, a two-step work around is used to simulate the strain independent force of these components.

The first calculation uses the same FE-model as introduced before but without the beam elements that represent the constant force springs. Instead of the connecting springs between frame and membrane, each CFS is represented by two forces of equal value but opposite direction and this forces are applied to the original spring attachment points at frame and membrane. The forces have thereby the same absolute values as the foreseen springs.

The CFS representing beam elements are visible in Figure 51b as horizontal thin lines connection the vertical spring holder elements to the membranes

The frame is fixed at its interface point in the middle of the boom and the membranes are clamped within both symmetry planes. From solving this model, information on the deformation of the frame and membranes derives that are equivalent to deformation due to CFS.

The basic idea of the second step is to substitute the former used force pairs by beam elements that are shrunk thermally to a level at which they generate the required forces and the resulting deformations of frame and membrane as the separate forces do in the previous simulation.

Therefore, an analytical approach is used, that starts with the results of the first FE-solution. The sketches in Figure 52 visualize the concept. The springs c_1 and c_2 represents the stiffness of the frame and the membrane. The force pairs in Figure 52a and the shrunken beam in Figure 52b represent the CFS.

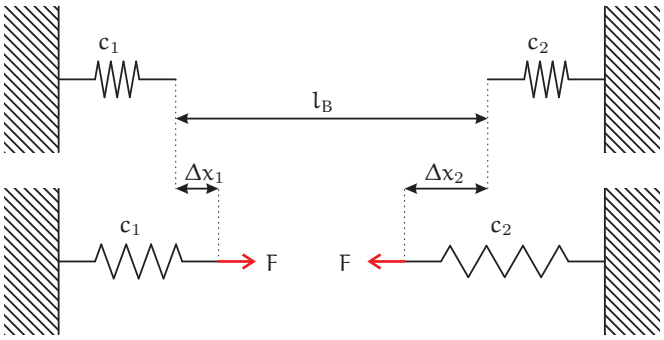

(a) system tensioning by an equivalent force pair

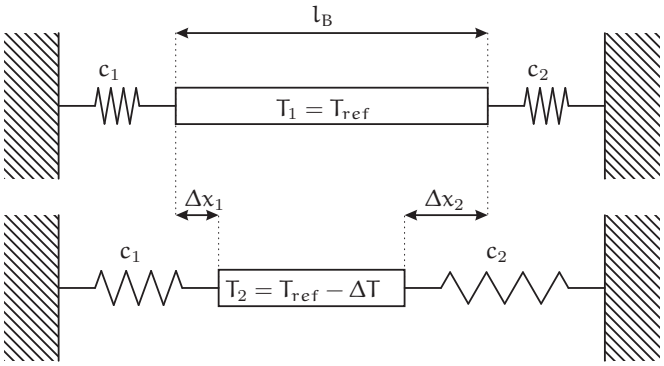

(b) system tensioning by thermal shrinking of a beam

Figure 52.: Schematic system pre tensioning approach

The beam in the thermal load case will be thermally shrunk by a negative temperature difference. The following calculations will show how this temperature difference can be calculated.

The overall strain ϵ_B of the beam is defined to be:

$$\epsilon_B = \frac{\Delta x_1 + \Delta x_2}{l_B} \tag{9.10}$$

where

Δx_1	Displacement of spring c_1
Δx_2	Displacement of spring c_2
l_B	length of CFS equivalent beam

For the thermo-mechanical load case, this strain derives from a summation of the thermal induced strain ϵ_{B_T} and the mechanical induced strain ϵ_{B_M}.

$$\epsilon_B = \epsilon_{B_T} + \epsilon_{B_M} \tag{9.11}$$

Thereby ϵ_{B_T} and ϵ_{B_M} are defined to:

$$\epsilon_{B_T} = \alpha_B \cdot \Delta T \tag{9.12}$$

$$\epsilon_{B_M} = \frac{\sigma_M}{E_B} = \frac{F}{E_B \cdot A_B} \tag{9.13}$$

where

α_B	CTE of the beam material
ΔT	Temperature difference applied to beam for shrinking
σ_M	Mechanical stress
F	Force of equivalent CFS
E_B	Elastic modulus of beam material
A_B	Cross section area of the beam

Although the Equation 9.11 implies an addition of thermal and mechanical strain, one needs to be aware of the fact that the thermal strain is a negative number due to the negative temperature difference.

The E_M is thereby chosen in a way that the spring constant of the beam element in the FE model is identical to the spring constant of the nearly linear part of the CFS characteristic shown in Annex A.5 starting on page 149. This is done again to generate a realistic structural behaviour during the modal analysis. However, this model is not able to respect the non-linear, friction affected hysteresis of the real CFSs.

By inserting the Equations 9.10, 9.12 and 9.13 in equation 9.11 the following evolves:

$$\frac{\Delta x_1 + \Delta x_2}{l_B} = \alpha_B \cdot \Delta T + \frac{F}{E_B \cdot A_B} \tag{9.14}$$

Solving the equation for ΔT leads to:

$$\Delta T = \frac{\frac{\Delta x_1 + \Delta x_2}{l_B} - \frac{F}{E_B \cdot A_B}}{\alpha_B} \tag{9.15}$$

After a first FE-solution that uses force pairs instead of constant force springs, this equation can be used to calculate the resulting temperature differences for each CFS. Using matrices and loops in ANSYS Parametric Design Language (APDL) this can be done fully automated. For the here presented nominal configuration of the antenna this calculation is performed for $36 \cdot 4 = 144$ CFSs.

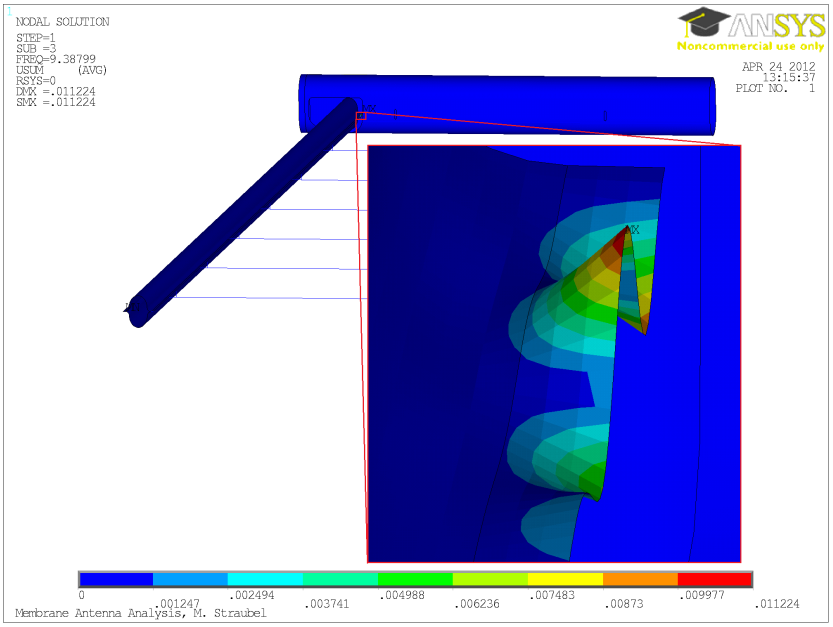

Figure 53.: First antenna buckling mode by boom flange buckling

For the next calculation step the beam elements for the thermal shrinking are added to the FE model, the calculated individual temperatures are applied to the destined beams and a new static solution is performed.

The results of this thermal calculation are very exact. A comparison of the achieved deflections of the force attachment points from this thermal solution with the previous one using force pairs shows a maximum variance of 0.005%. Hence, it is assumed that this approach is valid and it will be the baseline for all later calculations.

9.8.3 *Global & Local Buckling*

A very common failure mode for lightweight structures is a buckling of shells or beams. Considering the given antenna design buckling can occur due to the pre tensioning of the frame by the membrane tensioning forces. Moreover, a buckling due to AOCS related manoeuvre loads is possible as well.

As manoeuvre related acceleration loads are not defined so far, the buckling analysis will concentrate on the pre-stressing of the frame.

Thereby, again the before introduced FE model is used to perform a linear buckling analysis with ANSYS. As the frame parts

are the only parts of interest, the membrane is not used - respectively not meshed - for this calculation. Instead only the equivalent forces of the constant force springs are used to load the frame in a realistic way.

Without modification of the model the first buckling mode applies at a load factor of 1.45 and shows a classical Euler buckling of the transversal stiffeners. This is not surprising because the sizing of the stiffeners in Section 9.7 is done with a safety factor of 1.5 (see page 87). The difference between the theoretical and FEA based safety factor could result from the real boundary conditions for the stiffeners that are loaded by compression by forces that are not aligned with the stiffeners central axis. This offset generates torques at each stiffener tip that reduce the buckling load of the beam.

Beside the stiffeners, the next critical component of the frame should be the booms. To get buckling results of this boom parts the radii of transversal stiffeners are increased by a factor of 3.

After this modification the first structure buckling occurs at a load factor of 9.38. Figure 53 shows this result with an magnified view on the interesting region.

Interpreting this first buckling mode is invalid without taking a look on the other buckling shapes and loads factors: Indeed, the load factors of the following 17 other buckling case are ranging between 9.38 and 12.34. All buckling regions are located at the boom flange but starting from the sixth mode at a load factor of 12.10 the buckling regions are sometimes located at the outer boom flange.

All mode shapes show a boom flange forming sine-like buckles. This behaviour is typical for the flange of such boom when it is loaded in compression. Here the flange compression is arising from the two membrane to hub interfaces at the half hub that pull the hub in negative x-direction. The nominal load of the CFSs for both interfaces adds up to 13.5N. Multiplying this value with the load factor of the first buckling modes results in a critical accumulated axial force of $13.5\text{N} \cdot 9.38 = 126.63\text{N}$.

The fact that the pattern of the first modes is located to the inner boom flange shows that the hub is also bending inwards. This effect is also visible in the deformation plot shown in Figure 54. Hence, a compression force and a bending moment are applied to the boom tip. Both combined loads result in a higher compression of the inner flange.

Reminding the fact that a linear buckling analysis has been used to obtain those results one has to ask how the results would

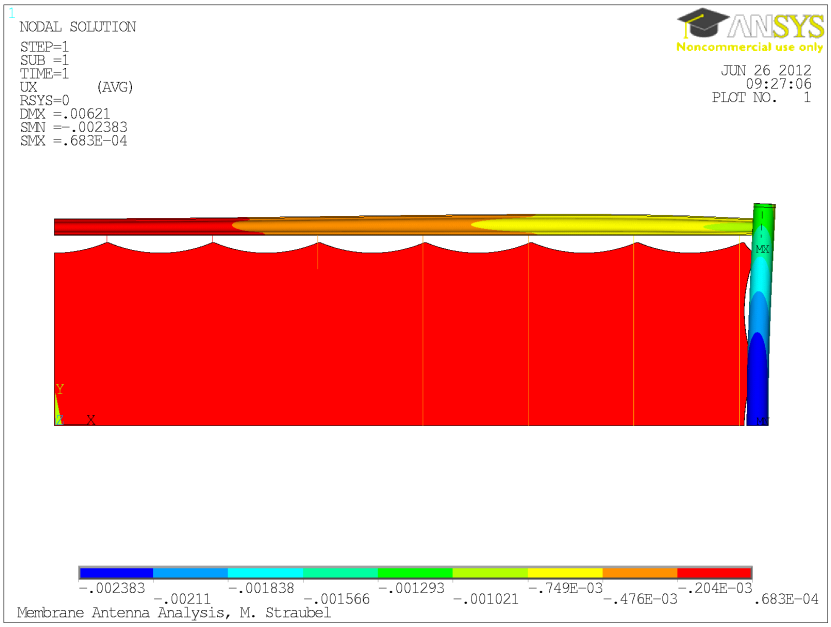

Figure 54.: Statically deformed antenna with a load factor of 12.1 (deformations are given in Meter in x-direction only and the drawing is scaled with a factor of 50)

change using a more sophisticated non-linear buckling analysis with applied imperfections. Both methods have been used before to calculate a pure boom under lateral tip force. Thereby, the linear model was always performing 5% to 10% better than the non-linear ones. So the linear model predicts a more robust structure. However, even for the used pure boom model the linear analyses required about five minutes of calculation time while the non-linear computation needed up to two hours.

The calculations were performed on a notebook PC with an Intel i7 2.2 GHz quad-core processor and 8 GB of RAM

As the observed differences between linear and non-linear calculation are small and repeatable and the linear simulation for the here presented antenna model requires already three hours of processing time, an attempt to do a non-linear calculation was not made.

Concluding this buckling analysis it can be stated, that the buckling of the booms under nominal loads will not apply. However, more realistically modelled interfaces between boom and hub could further decrease the safety factor but the calculated 9.38 seems to provide a comfortable margin.

9.8.4 *Modal Requirement*

The exact sizing of the boom stiffness according to the modal requirement of $f_1 = 0.4\text{Hz}$ requires a complex FE computation. Nevertheless, a coarse approximation can be performed using a basic analytic equation.

Both procedures are introduced below.

Analytic Approach

As defined in Chapter 7 the first mode of the tensioned membranes is 10% above the global target frequency. Hence, for a basic analytic approach it should be valid to substitute the membranes of the deployed antenna by passive masses that are applied to the frame.

The result of this simplification is a frame consisting of four beams with even distributed mass over beam length. Thereby, the bending stiffness of the hubs is some order of magnitude higher than the one of the booms. Moreover, the bending stiffness of the booms in antenna in plane direction is about 1.5 times higher than the bending stiffness in antenna out of plane direction.

Reminder: The hub has a first bending frequency of 28.4Hz *while the antenna shall be tuned to* 0.4Hz

Having these statements in mind, one can easily see that the first mode of such a frame is an out-of-plane cantilever bending mode of the whole antenna. This antenna mode is symmetric to the yz and xz planes and does therefore allow to use a quarter of the structure to build an equivalent model that consist only of one clamped cantilever beam with equally distributed mass and a tip mass.

For this basic mechanical setup, the first bending mode f_{1ana} can be calculated by the following analytic equation [55]:

$$f_{1ana} = \frac{1}{2 \cdot \pi} \sqrt{\frac{3E_b \cdot I_b}{l_b^3 (m_T + 0.23 m_B)}} \tag{9.16}$$

where

E_B	beam elastic modulus
I_B	beam geometrical moment of inertia
l_B	beam length
m_T	mass of tip mass
m_B	beam mass

Using the so far defined boom geometry and available material data (see Section 9.3) the theoretical bending stiffness and mass of the boom can be calculated using analytic equations. Thereby, E_B is defined by the boom laminate stiffness in boom length direction (here 67GPa) and the I_B is equal to the analytically calculated geometrical moment of inertia of the boom with respect to bending around the booms x-axis (I_{xx}).

Bending tests on real specimen [27] had shown that these analytically obtained stiffness values are overestimating the real structure performance by a factor of 1.4. In order to account for these results, the analytically calculated bending stiffness $E_B \cdot I_{B_{xx}}$ will later on be divided by an analysis safety factor k_{ana}:

$$k_{ana} = 1.4 \tag{9.17}$$

$$E_B \cdot I_B = \frac{E_B \cdot I_{B_{xx}}}{k_{ana}} \tag{9.18}$$

Hence, Equation 9.16 modifies as followed:

$$f_{1ana} = \frac{1}{2 \cdot \pi} \sqrt{\frac{3 E_B \cdot I_{B_{xx}}}{k_{ana} \cdot l_B^3 (m_T + 0.23 m_B)}} \tag{9.19}$$

For the distribution of the membrane mass over hubs and booms one needs to specify the mass fractures for both frame component. Therefore, the assumption is made that the mass of each membrane is concentrated along its edge These concentrated masses are then transferred to the hub or boom that it supporting this membrane edge. Thereby, the fraction of mass per edge is proportional to the length of the membrane edge. So a membrane with a k_{LW} of 1/4 will distribute its mass with a fraction of 1 to 4 to its short and long edges. So 1/5 is distributed to the short edge while 4/5 is distributed to the long edge. So, for the quarter antenna the following masses for the representative tip mass m_T apply:

$$\begin{aligned} m_T &= \frac{1}{4} \cdot \left(m_h + \frac{1}{1 + \frac{1}{k_{LW}}} \cdot (3 \cdot m_{MA} + m_{MS}) \right) \\ &= \frac{1}{4} \cdot \left(15.7\text{kg} + \frac{1}{5} \cdot (3 \cdot 3.2\text{kg} + 24.8\text{kg}) \right) \\ &= 5.64\text{kg} \end{aligned} \tag{9.20}$$

where

k_{LW}	antenna length to width ratio

m_h	combined mass of both hubs including interfaces and stiffeners
m_{MA}	mass of one antenna membrane
m_{MS}	mass of the service membrane

For the representative beam mass m_B the following equation is used:

$$\begin{aligned} m_B &= \frac{1}{4} \cdot \left(m_{boom} + m_{st} + \frac{\frac{1}{k_{LW}}}{1 + \frac{1}{k_{LW}}} \cdot (3 \cdot m_{MA} + m_{MS}) \right) \\ &= \frac{1}{4} \cdot \left(1.79\text{kg} + 0.72 + \frac{4}{5} \cdot (3 \cdot 3.2\text{kg} + 24.8\text{kg}) \right) \\ &= 7.49\text{kg} \end{aligned} \tag{9.21}$$

where

m_{boom}	combined mass of both booms
m_{st}	combined mass of all 14 transversal stiffeners

Using this input, the first mode of the antenna can be calculated to:

$$f_{1ana} = 0.299\text{Hz}$$

In order to do a real sizing and tune the first mode to the required value one need to change the geometry of the boom or the used material. The use of other material is not part of the further sizing as there is so far no sufficient experience for the use of high modulus and ultra high modulus fibres for booms at DLR. Hence, a cross section variation is considered that will change the geometrical moments of inertia as well as the mass of the boom and will, therefore, change the result of Equation 9.19.

Before changing the boom cross section, one has to understand its design: An ideal, not deployable shell boom - of high structural efficiency and equal requirements for the bending stiffness around all possible bending axes - would have a circular cross section with a possibly high radius and a possibly low wall thickness. But such a boom could not be flattened for later rolling without damaging the shell material by the strong creases that would form during flattening.

Therefore, the current boom design is a kind of a compromise between this circular ideal cross section and the avoidance of

The boom cross section has been defined before in Figure 41 on page 71

damaging creases during folding. The booms are assembled out of two half shells and co-bonded at a common flange that is e_{b3} wide and that is directly connected to a quarter circle of the radius r_{b1}. The main part of the cross section is then represented by the half elliptic parts defined by e_{b1} and e_{b2}. The circular parts of the boom cross section is acting as a flexure hinge that avoids the unwanted creases.

Moreover, the minimum shell thickness is given by the currently available of the shelf CFRP prepreq. The considered $0.1mm$ is a value that can be achieved using available plain weaves or UD-setups composed of up to three layers.

Please refer to Figure 41 on page 71 for definition of the local boom coordinate system

For the antenna setup, the bending stiffness around the booms x-axis is the most critical. When sizing the bending stiffness around this axis the flange and the circular part are relatively uninteresting. Because of their close location to the bending axis they contribute only 2.24% to the overall geometric moment of inertia (for the nominal boom setup).

In contrast, the half elliptic parts have a high distance from the x-axis and therefore the both ellipse sizing parameters have a higher impact on the bending stiffness around the boom x-axis. Furthermore, the value e_{b1} has the highest impact on the geometric moment of inertia than e_{b2} as it impacts also on the distance of the centre of area of the half elliptic from the bending axis.

Due to this understanding of the cross section and the relatively small difference between the target antenna frequency of 0.4Hz and the on page 97 analytically calculated value of 0.299Hz the

$k_{eb1}[]$	$\mu_b \left[\frac{kg}{m}\right]$	$I_{xx} \left[m^4\right]$	$I_{yy} \left[m^4\right]$	$f_{1ana}[Hz]$
0.5	0.056	$22.78 \cdot 10^{-9}$	$69.97 \cdot 10^{-9}$	0.200
1.0	0.065	$51.02 \cdot 10^{-9}$	$78.33 \cdot 10^{-9}$	0.299
1.3	0.070	$74.93 \cdot 10^{-9}$	$83.35 \cdot 10^{-9}$	0.362
1.4	0.071	$84.17 \cdot 10^{-9}$	$85.03 \cdot 10^{-9}$	0.383
1.5	0.073	$94.10 \cdot 10^{-9}$	$86.70 \cdot 10^{-9}$	0.405
1.6	0.075	$104.71 \cdot 10^{-9}$	$88.38 \cdot 10^{-9}$	0.427
1.7	0.078	$116.04 \cdot 10^{-9}$	$90.05 \cdot 10^{-9}$	0.450
2.0	0.082	$154.52 \cdot 10^{-9}$	$95.07 \cdot 10^{-9}$	0.519

Table 11.: Results of parameter variation for k_{eb1} based on analytical calculations

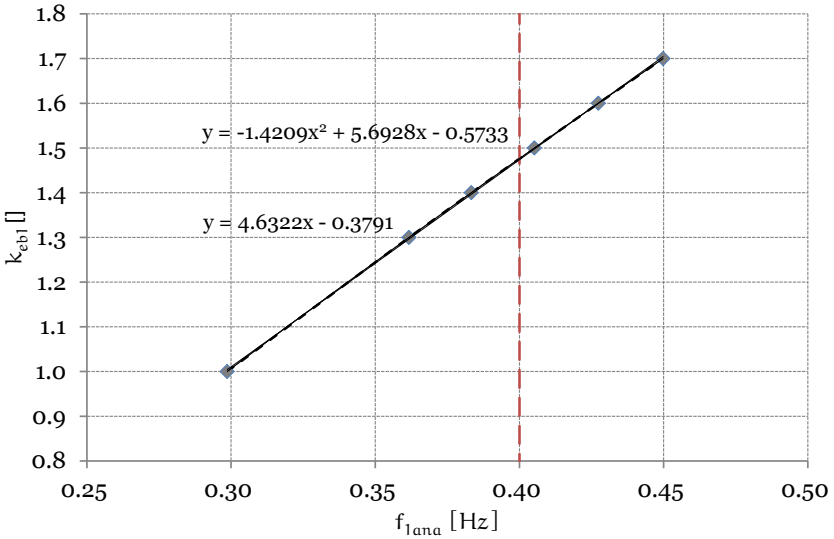

Figure 55.: Result of parameter variation for k_{eb1} including a fitted linear curve and a fitted 2nd-order polynomial

following sizing will only consider a change of the booms cross section variable e_{b1} by a non-dimensional scaling parameter k_{eb1} to result in a scaled parameter $e_{b1_{sc}}$:

$$e_{b1_{sc}} = e_{b1} \cdot k_{eb1} \tag{9.22}$$

Table 11 shows the result of such a k_{eb1} variation on the specific mass of the boom μ_B, the geometrical moments of inertia I_{xx} and I_{yy} of the boom, and the resulting first antenna mode frequency.

As predicted, the scaling of the e_{b1} has a strong impact on the geometrical moment of inertia and, thereby, mainly on I_{xx}. A curve of different complexity can be fitted into this scatter to calculate the required k_{eb1} for a f_{1ana} of 0.4Hz.

Figure 55 indicates that the relation between both parameters is relatively linear. Hence, only a linear curve and a 2nd-order polynomial are fitted into this data cloud.

Thereby the linear fitting leads to an optimal $k_{eb1_{lin}}$ of:

$$k_{eb1_{lin}} = 1.47376$$

Performing the analytic calculation again using this value leads to a antenna first mode that varies by -0.1421% from the target value of 0.4Hz.

The quadratic fitting leads to a optimal $k_{eb1_{quad}}$ of:

$$k_{eb1_{quad}} = 1.47644$$

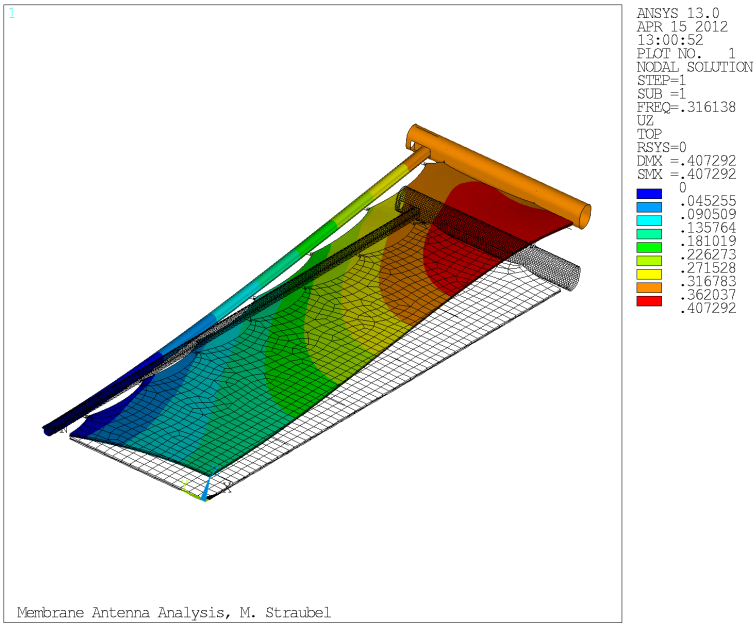

Figure 56.: First antenna mode using booms with the nominal cross section geometry

This results in an analytical obtained first antenna mode that varies by only +0.0048% from the envisaged frequency.

Concluding these results, it is obvious that a pure analytical sizing of the boom geometry seems to be applicable but at least, the next part on the simulation results will show how accurate these analytic, simplified results are.

Simulation

For the simulation of the antenna modal behaviour the pre-stressed FE-model, introduced in section 9.8.2, is used to perform a modal analysis.

As done for the analytic approach before, the bending stiffness of the booms is reduced by a factor of 1.4 to respect test results. Here this is practically done by dividing all elastic moduli and shear moduli of the boom material data by this value.

For the nominal boom geometry the first mode of the antenna is at $f_{1FEM} = 0.31614$Hz (see Figure 56). The analytically obtained value on page 97 is only 5.5% below the numerically calculated which is surprisingly close having the highly different levels of complexity in mind.

As done for the analytic approach before, a sizing of the boom is done by scaling the e_{b1} parameter of the boom cross section by an appropriate value. While the determination of this optimum value for the analytic approach is done using a conventional Microsoft Excel sheet, the optimization here is done again using MATLAB.

The following sequence is thereby used:

1. MATLAB starts a modal analysis for the nominal boom design ($k_{eb1} = 1$) in ANSYS
2. MATLAB calculates the k_{eb1} for the second run by multiplying the k_{eb1} from the first run with the squared quotient of the target antenna frequency divided by the obtained frequency of the first run
3. MATLAB starts a second modal analysis for the previously calculated k_{eb1} in ANSYS
4. MATLAB calculates the k_{eb1} for the third run by multiplying the k_{eb1} from the second run with the squared quotient of the target antenna frequency divided by the obtained frequency of the second run
5. MATLAB starts a third modal analysis for the previously calculated k_{eb1} in ANSYS
6. MATLAB uses the now available three values for the boom scaling parameter and the antenna frequency to fit a 2^{nd} order polynomial into this scatter and calculates a new value for k_{eb1} using this polynomial
7. MATLAB starts a fourth modal analysis for the previously calculated k_{eb1} in ANSYS
8. MATLAB uses the *latest three values* for the boom scaling parameter and the antenna frequency to fit again a 2^{nd} order polynomial into this scatter and calculates a new value for k_{eb1} and initiates the next ANSYS calculation

The calculation method for k_{eb1} used in step 2 and 4 is an empirical approach. The motivation for the first 5 steps is the generation of three data points close to the target frequency value to allow an efficient iteration. The empirical approach fulfils this need.

MATLAB repeats step #8 as often as necessary to reach the defined accuracy. If the required accuracy is achieved on an earlier step, the optimisation is aborted as well. Table 12 shows the result of such an automated sizing with a required accuracy of 0.01% while Figure 57 shows the mode shape of the last iteration given in the table.

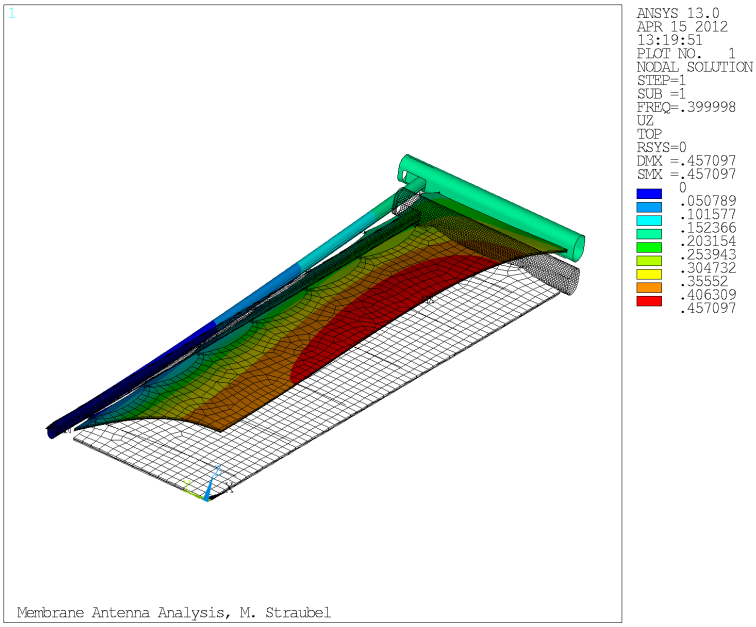

Figure 57.: First antenna mode using booms with the optimised cross section geometry

Analytic Approach vs. Simulation

After solving the problem with two approaches a comparison of both paths is done here.

Figure 58 shows three calculated FE value sets as well as the analytic solution results. The different graphs derive thereby from the following methods and input parameter:

- Analytic results: The same data as shown before in Table 11

RUN #	k_{eb1}[]	f_{1FEM}[Hz]	ACCURACY
1	1.0000	0.3161380	20.96500%
2	1.6009	0.3914204	2.14500%
3	1.6718	0.3968920	0.77750%
4	1.7138	0.3997892	0.05250%
5	1.7170	0.3999983	0.00040%

Table 12.: Result of parameter variation for k_{eb1} based on FE calculations

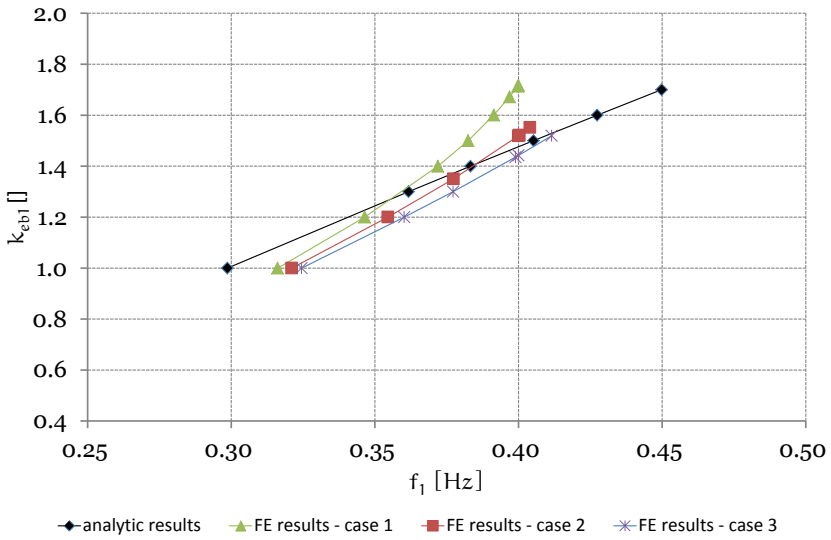

Figure 58.: Comparison of analytic and FE results for boom cross section sizing

- FE results - case 1: The same data as shown before in Table 12 but with three manually added points between 0.31Hz and 0.39Hz
- FE results - case 2: Simulation results calculated with the same procedure as for case 1 but with increased membrane attachment forces that tune the first mode of the pure membranes to 0.48Hz instead of 0.44Hz for case 1
- FE results - case 3: Simulation results calculated with same procedure as for case 1 but with increased membrane attachment forces that tune the first mode of the pure membranes to 0.52Hz instead of 0.44Hz for case 1

The manually added points for case 1 have been added after the automated sizing to have a sufficient distribution of the scatter over the interesting parameter range. For the added point the k_{eb1} have been chosen manually whereas the f_1 is a result of a regarding ANSYS run.

Please review Table 12 again to see how locally concentrated the results for the automated sizing are

At first, the result of the basic case 1 FE solution and the analytic values will be compared: Both solutions are located in the same area but the FE characteristic has a higher slope than the analytic one. Therefore, for small k_{eb1} the analytic approach generates lower first mode frequencies than the numeric one. For higher k_{eb1} values the opposite statement applies.

Due to the complexity of the FE model and the simplicity of the analytic approach it would be reasonable to assume that the

FE model generates more accurate results than the analytic. Thus, it would be very likely that the assumptions and simplifications for the analytic approach are not correct or at least too optimistic.

Indeed, when comparing the Figures 56 and 57 one can see that the mode shape of the antenna is changing for higher frequencies. Figure 56 shows the mode where the bending of the frame is dominating the deformation and the membrane is following the frames deflection in a relatively passive way.

Please refer to Chapter 7 starting on page 33 for more details on the previously performed membrane sizing

In contrast Figure 57 shows a more dominant deflection of the membrane than of the frame. This leads to the assumption that the difference of 10% between the pure membrane first mode frequency and the frequency of the entire antenna is not enough to decouple the modes.

This observation leads to the two additional FE cases with higher target values for the pure membrane first mode frequencies.

As shown in Figure 58 the increased membrane mode frequency decreases the slope and the curvature of the FE solution characteristic. Thus, with a rising membrane frequency the FE solution is more behaving like the analytic solution. This is the reason why the assumption made for the decoupling of membrane and global mode in the analytic modal approach, became more applicable.

But besides the more academic need to achieve comparable results for analytic and numeric results, this result generates another interesting outcome: The boom stiffness that is required to tune the overall frequency to the target value of $f_1 = 0.4\text{Hz}$ is decreasing for increasing first mode frequencies of the pure membrane. This will lead to booms with smaller cross section that are lighter but also narrower when in stowed configuration. The reduced width will again result in shorter hubs and thereby a reduced width of the stowed antenna. More detailed, a change from case 1 to case 3 will result in the following changes for the entire antenna:

1. A boom mass reduction of 0.13kg or 6.4%
2. A hub mass reduction of 0.34kg or 2.2%
3. A stiffener mass gain of 0.13kg or 18.2%
4. A resulting antenna mass reduction of 0.4kg or 0.8%
5. A antenna width reduction of 31mm or 0.8%

So the increased membrane mode frequency results in heavier stiffeners but reduces the mass of the booms and the hubs. The consequence is a loss of nearly a half kilogram of mass. Thus, the case 3 seems to be more recommendable.

Comparing the results of analytic and FE methods it can be stated that the FE model is expected to be more accurate than the analytic model because the FE model is based on less simplifications.

However, such a statement would normally require a verifying test to see *the real* structure behaviour. But - as it always is for gossamer structures - a verifying test is very complicated because it requires the absence of the atmosphere and the gravity. Both could be achieved by using a combination of a huge vacuum chamber and a gravity compensation system but the cost for the involvement of such a facility was far away from the available project budget.

In addition, gravity compensation systems do always interfere with the structure so that also such a test would probably not give an exact result. This is particularly true for all non-quasi-static measurements like a modal structure evaluation.

Nevertheless, tests on part level help to improve the FE results. The first mode of this cantilever configuration is mainly depending on the stiffness of the booms and the mass distribution over the deployed structure. The mass distribution is relatively easy to verify and test on boom stiffness are already respected in the above made calculation. One uncertainty that needs to be quantified in the future is the stiffness of the spacecraft to boom interface. So far it is considered as ideal stiff. Tests need to show if this simplification is valid.

When dealing with the available test data, the FE result is considered to be the best result and the difference towards the analytic result is relatively low (around 5%). The calculation time required to solve the analytic or the FE approach varies by some oders of magnitude. The simulation of one iteration step with ANSYS requires about 60 seconds on a standard PC. The analytic calculation of the same configuration takes far below one second.

So, for a first approach the analytic approach is highly recommended but the FE solution shall remain as last verification.

9.8.5 *Thermal Loads*

The thermal deformation of the antenna due to the asymmetric radiation condition in space is determined in this sub-section in order to understand and quantify the effects.

It is thereby assumed that the deformation of the antenna is significantly driven by a thermally introduced bending deformation of the booms and that the membranes are following this deformation.

The general design of the used deployable booms features excellent thermo-mechanical behaviour as their CTE can be tailored close to Zero. However, the CTE is also temperature depending so that a minimum but existing thermally indicated deformation will appear when the boom is exposed to an asymmetric radiation environment.

Thereby, the shell design of the booms is a drawback. The very low material thickness of the boom leads to a huge ratio between material volume ($0.0000417\,m^3/m$) and outer surface area ($0.417\,m^2/m$). The black CFRP material is characterised by high absorptivity and emissivity. Although the high thermal conductivity of CFRP material (in fibre length direction), the low material thickness limits the amount of thermal energy that can be transported from the hot to the cool side by thermal conduction. In addition, the closed shell surface of the *hot* side shadows the shell of the *cold* side.

The combination of high absorptivity and emissivity and geometry driven, low thermal conductivity leads to relatively high static temperature gradients that deform the booms and, therefore, the antenna. This effect is reduced by radiation transfer that happens between the inner walls of the booms and transports thermal energy from the *hot* side to the *cold* side.

Sickinger did a very intensive investigation on different thermo-mechanical aspects of the boom. The following results are a short conclusion of the results published in [61].

As expected, the static temperature gradients of such boom within a asymmetric radiation condition in space, are relatively high. Sickinger calculated results with respect to different boom orientations, orbit parameters (the Sun shadowed by the Earth or not) and an optional outer reflective layer. Thereby, maximum temperature differences between two boom sides of up to 88.6°C have been identified for the boom with the uncoated CFRP surface. The application of a reflective layer made of aluminised Kapton® reduces the temperature difference by about 20°C to 68.9°C. For

the following examinations, the regular CFRP boom will be considered to make a kind of a worst case thermo-mechanical estimation for the membrane antenna concept.

Sickinger also made a probabilistic thermo-mechanical analysis for a 35m boom within a 350 km Earth orbit. The probabilistic simulation part respects manufacturing errors of the boom by defining standard deviations for ply angle and ply thickness.

The resulting worst case tip deflection u_{max} out of 4000 sample was calculated to be:

$$u_{max} = 717mm$$

This maximum value was measured in boom y-direction which is identical with the out of plane direction of the membrane antenna. Interestingly, this maximum deformation does not apply for the hot case that includes Sun's radiation, Earth's albedo and Earth's inherent infra-red radiation. It applies for the cold case where the structure is shadowed from the Sun by the Earth and only loaded by Earth's inherent infra-red radiation.

Earth's Albedo Radiation *is the Sun's radiation that is reflected by the Earth's surface*

But, given by the stochastic distribution of the huge amount of samples, the above defined value for u_{max} is a very improbable one. Dissolving the worst 1% of the scatter results in a worst case deflection u_{max99} of the remaining 99%:

$$u_{max99} = 568mm$$

This value will be used as baseline for the following calculations. To transfer the results of Sickinger to the antenna one needs to calculate the deflected shape of the antenna with respect to the boom results. Therefore, the following assumptions are made:

1. The boom deformation is the most decisive thermal effect for the antenna. Hub, membrane and interface deformations are neglected.

2. The calculated boom tip deflection evolves from a temperature profile that is characterised by high gradients across the cross section but constant values along the boom length. This profile generates a bending of the boom with constant curvature. Thus, the boom deformation line is represented by a segment of a circle.

To calculate the antenna deformation one has to find an arithmetic function for the deformation line of the 35m long boom. The function $u(z)$ shall thereby define the local deflection of

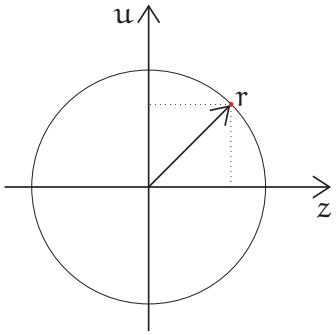

Figure 59.: Circle equation

the boom in boom x-direction u depending on the boom length position z.

The general approach for this equation is the common formula for a circle (see Figure 59):

$$r^2 = u^2 + z^2 \tag{9.23}$$

Solving the equation for u results in:

$$u^2 = r^2 - z^2 \tag{9.24}$$

$$u_{1/2}(z, r) = \pm\sqrt{r^2 - z^2} \tag{9.25}$$

For the following calculations only the negative version of Equation 9.25 will be used. To transfer the intersection point of the curve and the u-axis to $u = 0$ the radius r is simply added to the equation:

$$u(z, r) = -\sqrt{r^2 - z^2} + r \tag{9.26}$$

To complete this equation, one needs to determine the radius of the circle. Solving Equation 9.26 for r results in:

$$r = \frac{u^2 + z^2}{2u} \tag{9.27}$$

Inserting the value of u_{max99} from the previous page for u and the length of the original boom of 35m for z results in:

$$r = 1078.6\text{m} \tag{9.28}$$

Thus, despite of the huge temperature gradients across the booms cross section the bending radius is more than one kilometre wide. This underlines again the outstanding thermo-mechanical performance of this mast concept.

With the fixed value for r a formula for the deformation line is found:

$$u(z) = -\sqrt{r^2 - z^2} + r \tag{9.29}$$

Using this equation one can calculate the worst case deflection of the antenna hubs by inserting the half length of the antenna booms for z:

$$u(z = l_B/2) = 19.9\text{mm}$$

where

| l_B boom length (here 13.104m)

However, this value is just mentioned to give a better impression of the resulting deformation. As there is now a formulation of the booms deflection line available, one can easily calculate the ROOT MEAN SQUARE (RMS) value of the antenna deflection.

$$y_{RMS} = \sqrt{\frac{1}{x_2 - x_1} \int_{x_1}^{x_2} [y(x)]^2 \, dx} \tag{9.30}$$

To find the minimum RMS value of a continuous function in a defined interval one needs to move the entire function along the y axis by the mean value of the function $\widehat{y}$:

The RMS value is a common indicator for the contour accuracy of an antenna aperture which is of high interest for the RF performance.

$$\widehat{y} = \frac{1}{x_2 - x_1} \int_{x_1}^{x_2} y(x), dx \tag{9.31}$$

The resulting minimum RMS value $y_{RMS_{min}}$ is:

$$y_{RMS_{min}} = \sqrt{\frac{1}{x_2 - x_1} \int_{x_1}^{x_2} [y(x) - \widehat{y}]^2 \, dx} \tag{9.32}$$

Applying this general formulation to the deformation line leads to:

$$u_{RMS} = \sqrt{\frac{1}{\frac{l_{AA}}{2}} \int_0^{\frac{l_{AA}}{2}} \left[u(z) - \left(\frac{1}{\frac{l_{AA}}{2}} \int_0^{\frac{l_{AA}}{2}} u(z), dz \right) \right]^2 dz} \tag{9.33}$$

$$= 5.53\text{mm}$$

where

| l_{AA} antenna array length (here 12.649m)

Concluding this calculation it shall be stated that even though manufacturing uncertainties have been respected, the given gossamer design is able to reach very good shape accuracy in the harsh space environment. However, this achieved values cannot be checked against a valid requirement as such a requirement would be the result of a - so far not existing - detailed RF concept.

9.9 CONCLUSION

In this chapter all important frame parts of the antenna are sized. This concludes the sizing of the antenna and results in a final design with the following key parameters:

- Aperture size: $40\mathrm{m}^2$
- Antenna mass: 52.7kg
- Antenna specific mass: $1.32\frac{\mathrm{kg}}{\mathrm{m}^2}$
- Stowed outer dimensions: 0.65m x 4.08m x 0.23m
- Stowed volume: approx. $0.61\mathrm{m}^3$
- Deployed outer dimensions: approx. 13.3m x 4.08m x 0.3m

Hence, the addressed specific mass target of $1.0\frac{\mathrm{kg}}{\mathrm{m}^2}$ could not been met with the nominal configuration.

However, the next chapter will show which parameters need to be changed to reach this ambitious target value.

10

CLOSED LOOP SIZING CHAIN

In Subsection 9.8.4 of the previous chapter, the influence of the first membrane mode requirement on the optimal boom cross section and, thereby, on the stowed width of the antenna, shows how sensitive the overall design reacts on changed requirements.

Moreover, some of the requirements defined in the *List of Requirements* on page 10 are just reasonable assessments that arise from literature studies of similar but not identical antennas or missions. Others are just made with respect to personal experience or expert interviews.

Thus, a real mission design could, for instance, result the following changes:

- The first mode frequency of the deployed antenna could change after defining a satellite and getting new requirements from the AOCS team,
- The first mode frequency of the stowed antenna could change after defining a dedicated satellite structure or changing the launcher,
- The required aperture size, the membrane thicknesses, materials or even the harness mass, could change after a detailed RF study,
- The RF concept could be shifted to reflect-array antenna configuration which will make the heavy service membrane unnecessary.

Combining this relatively low precision in the requirements with the before noticed high sensitivity of the design towards changing requirements results in the conclusion that the before achieved antenna configuration is just one possible setup out of a very wide bunch of configurations.

To understand how changed requirements impact the overall design and to react rapidly on changing RF concepts, material preferences or updated launch loads, a *chain* of significant *closed loop sizing* tasks has been developed that is able to size new antenna configurations of the given basic design within a time frame of seven to eighteen minutes.

The regarding strategy, the resulting software implementation and some exemplary results are shown in the following sections. Finally, two optimised antenna configurations are presented that benefit from the examination of the example sizing results.

10.1 SIZING STRATEGY

The chain like strategy is shown in Figure 60. After defining material parameters and requirements, the geometry of the main function carrier - the membrane - is computed.

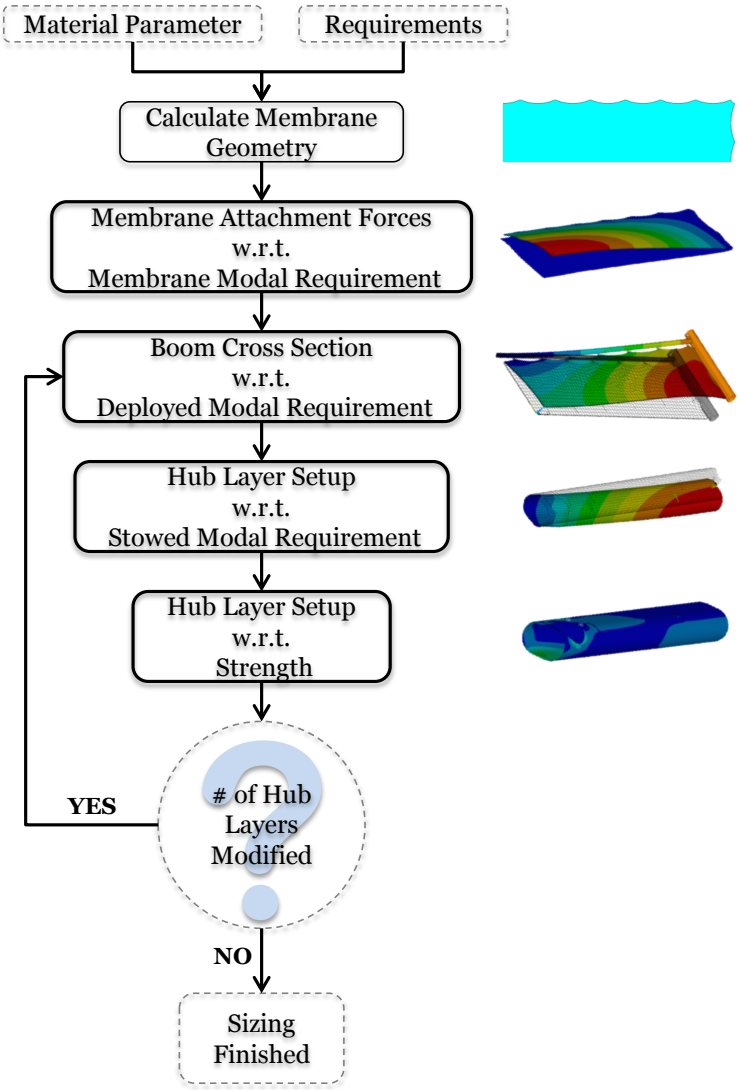

Figure 60.: Sizing Strategy

Afterwards, the membrane attachment forces, needed to fulfil the first mode frequency requirement of the pure membrane, are determined.

The next step is the sizing of the boom cross section according to the required first mode of the entire deployed antenna.

Then, the hub layer setup is tailored until the first mode frequency of the stowed antenna fulfils the launch requirements.

Subsequently, the hub layers are investigated on potential strength failures when loaded with the random vibration equivalent g_{RMS} static acceleration. If strength failures are detected, the layer setup is again modified until the strength behaviour is sufficient.

Thereby, the sizing of the hub layer setup and the boom cross section are affecting each other. For instance, a thicker hub laminate increases the mass of the hub and does require a stiffer boom to guarantee the deployed system stiffness. Contrary, an increased boom cross section does also increase the mass of the boom and thereby the additional mass applied to the hub for the modal and strength failure determination. Moreover, a larger boom cross section requires a larger boom feed through cut-out in the hub which increases the hub length and the hub cross section parameter d_h (see Figure 38 on page 68).

This interaction is the reason for the optional loop in Figure 60. If the hub sizing requires a change in the hub laminate, the sizing of the booms needs to be redone to account for the heavier hubs. The hubs sizing is done again to account then for the heavier booms.

Fortunately, this *cross-tailoring* does not involve the optimisation of two real numbers. Such an optimisation would require a lot of iterative calculation or a more sophisticated optimisation with two unknowns.

Instead, here the real number k_{eb1} and the integer number of additional hub face sheet layers are tuned. The integer number is therefore stabilising the entire optimisation and is thus enabling this sequence of two optimisations with each one unknown.

The boom cross section scaling parameter k_{eb1} is defined and explained on page 99

So, except of the *Calculate Membrane Geometry* task all other sizing tasks shown in the chain of Figure 60 are defined by an internal closed loop sizing that is able to tune an input sizing parameter in order to achieve the required output performance parameter.

Other previously performed calculations like buckling or thermo-mechanical analyses are not part of the closed loop sizing chain. This decision is made because those load cases did never result in

critical levels in all performed calculation. However, it is understood that a final detailed design shall be checked against these failure modes.

10.2 STRATEGY IMPLEMENTATION

As already mentioned before, the closed loop sizing chain approach is using conventional engineering software tools.

The core of all calculations is provided by MATLAB. FEAs are again performed in ANSYS. MATLAB has dedicated subroutines for each item of the sizing strategy as shown in Figure 60 in the previous section.

In contrast, the FEAs in ANSYS are all performed with the same script. ANSYS knows from a dedicated flag variable which calculation it has to perform. Thus, the related ANSYS script is relatively huge (2727 lines) and complex but all calculation are performed using the same basic geometry. So if a change in basic design (e.g. more membranes or another nominal hub layer setup) needs to be implemented, only one script needs to be changed. This ability of the ANSYS script was very practical during the development of this software tool in combination with up-coming ideas and new structural concepts.

A single FEA to calculate, for instance, the first mode of the deployed antenna, includes the following steps:

1. MATLAB sets a flag variable to specific value that informs ANSYS which calculation it has to perform,
2. MATLAB writes all available variables in an ASCII text file and sets a flag in an error handler file to 1,
3. MATLAB starts a universal ANSYS script in a fast batch mode,
4. ANSYS reads the previously written ASCII text file and stores all variables in its own workspace,
5. ANSYS builds up the model geometry according to the given variables (incl. flag variable), performs the required calculation, stores an image of the mode shape of the first mode in its work folder on the hard disc drive and writes the frequency of the first mode into another ASCII file,
6. ANSYS writes a 0 into the error handler file and terminates,

7. MATLAB reads the error handler file to see if ANSYS terminates regularly or if a failure in the calculation occurs,
8. If there was no failure MATLAB reads the result ASCII file of ANSYS and stores the frequency for later processing,
9. MATLAB looks for new plots stored on the hard disc drive by ANSYS, moves the figures to a dedicated result folder and changes the name of the file to an appropriate identifier including date, time and the title (e.g. first antenna mode) of the plot.

Performing a complete sizing requires different ANSYS runs initiated from different MATLAB subroutines. Thereby, a main routine in MATLAB is acting as user interface and managing the other subroutines.

10.2.1 *Details on Single Steps*

Details on the membrane geometry calculation are not given because it contains only basic mathematical calculations.

The optimisation approaches for the membrane attachment forces and the boom cross section have been both already explained extensively in the Sections 7.3.2 (membrane attachment forces) and 9.8.4 (boom sizing).

In contrast, for the hub sizing only the calculation of the first mode for one hub configuration has been performed in Section 9.6.4. The same is true for the verification of the hub design against strength failures in Section 9.6.5. However, the parameter to optimise for the hubs is only the integer number of additional 0° layers. The additional layers are added to each sandwich face sheet at the two outer sides of the sandwich. Thus, for example, one addition layer doubles the layers #1 and #7 in the hub shell layer setup.

The stacking of the hub laminate has been defined in the listing on page 75.

For the most antenna configurations the laminate with one additional layer turns out to be sufficient. No configuration does ever require more than four additional layer so that a complex optimisation approach as used for the boom cross section is not meaningful. Instead, the regarding MATLAB subroutine is simply starting with the basic hub laminate setup and adds 0° layers until the FEA results imply that the requirements are met.

For the transversal stiffeners the sizing does not require any kind of optimisation. Instead, the cross section geometry is calcu-

lated by MATLAB using the analytic Equations 9.9 and 9.5 from page 87.

10.2.2 *Parameter Study Add-On*

The before described program parts are so far only able to size an antenna for a given set of requirements. To perform parameter studies, another MATLAB main routine has been developed. This routine is able to read different sets of requirements and material variables from a Microsoft Excel file, perform a sizing for each set and write result parameters of interest back to the Excel file.

Annex A.11 shows such an exemplary Excel file for one reference design and six alternative designs. For each alternative design configuration, one key requirement has been changed.

The initialisation routine defines 142 material and requirement parameters.

Practically, at the start of each sizing MATLAB initialises all parameters needed for the program with an appropriate value that is set in an according initialisation routine. Subsequently, the routine overwrites the values that are also defined in the Excel file.

During the sizing process, all figures stored by ANSYS are again moved and renamed by the MATLAB routines as well. Thereby, the name of each file contains again the date, time and a identifier of the kind of simulation. Moreover, a prefix that indicates the regarding configuration is added to allow the user later to find a corresponding figure for each simulation of each configuration.

For the configuration prefix the variable `calcName` is used. This variable is specified in the Excel file (see first input line in Annex A.11)

10.3 EXAMPLES OR "WHAT IF ...?"

This section shows the closed loop sizing chain results for different sets of requirements. The first part of the examples is oriented to the listing on page 111. The second part shows other configurations that are already a consequence of the findings of the first part or simply other possible configurations that are not dedicated to the given antenna mission scenario but could be interesting for alternative applications.

Each subsection will contain a basic introduction on one requirement configuration and the results of the sizing chain. Both the requirements and the results will be presented in a table of the same kind for each case.

VARIABLE	VALUE	COMMENT
aLWR	0.25	Length to width ration of antenna array
mSThickness	0.1mm	Service membrane substrate thickness
mSSpecAddMass	0.448kg/m^2	Additional mass on service membrane
aFRequ	0.4Hz	Required first mode frequency for deployed antenna
mFRequ	0.52Hz	Required first mode frequency for tensioned membranes
aArea	40m^2	Antenna aperture area
mCutOutLen	1m	Preferred length of membrane cut-outs
hRad	0.1m	Hub radius (of circular cross section part)
hFSThIncr	0.1mm	Thickness of one hub UD layer
hCoreThickness	10mm	Thickness of hub honey comb core
bEsFactor	1.4	Boom E-modulus knock-down factor
bEllW	0.045m	Boom cross section parameter previously introduced as e_{b2} in Figure 41 on page 71

Table 13.: Input parameters for Conf0 - Reference Configuration

10.3.1 Conf0 - *Reference Configuration*

The first example is the reference design that requirements are similar to the so far used ones. Only two requirements have been changed according to previously gained system understanding.

1. The required first mode frequency of the membranes has been updated from 0.44Hz to 0.52Hz to account for the results of the previous chapter,

VARIABLE	VALUE	COMMENT
aMass	51.83kg	Mass of complete antenna
aSpecMass	1.30kg	Specific mass of complete antenna
bMass	1.87kg	Boom mass
stMass	0.85kg	Stiffener mass
hMassC	14.51kg	Complete hub mass (incl. edge stiffening elements)
mSMass	24.81kg	Service membrane mass
mAMass	9.61kg	Combined mass of the three antenna membranes
sIFMassComp	0.18kg	Combined mass of all frame to membrane interfaces
anW	4.07m	Width of deployed and stowed antenna
anL	13.30m	Length of deployed antenna
anLSto	0.65m	Length of stowed antenna
anVSto	$0.61m^3$	Volume of stowed antenna
mNFL	14	Number of membrane attachment points per boom
mNFW	4	Number of membrane attachment points per hub
hFSAdd0Layer	1	Additional 0° Layers in hub laminate
bCSScale	1.402	Boom cross section scaling factor (identical to previously used k_{eb1})
hOffset	0.090m	Hub geometry parameter, previously introduces as d_h in Figure 38 on page 68
compTime	17.0min	Computing time

Table 14.: Result parameters for Conf0 - Reference Configuration

2. The thickness of a single hub laminate layer has been decrease from 0.15mm to 0.10mm to reach a higher granularity of the layer setup.

The given requirements are shown in Table 13 while Table 14 shows the results from the sizing chain. In both tables the variable names used in ANSYS and MATLAB are used. The meaning of

the variables is only commented in these tables. Later tables in other configurations will only refer to the variable names.

Although the results are nearly reflecting the findings of the previous chapters, Table 14 motivates to examine the mass fracture of the different antenna parts with respect to the overall mass.

For this reference configuration the following proportionate masses apply:

- Service membrane: 47.86%
- Hubs: 27.99%
- Antenna membranes: 18.54%
- Booms: 3.62%
- Transversal stiffeners: 1.65%

The function carrying combined membranes deliver a mass fraction of two third (66.4%). It is moreover obvious that the service membrane provides almost the half of the antenna mass whereas the hubs provide a quarter. Thus, it could be expected that changed requirements on the service membrane or the hubs will have the most significant impact on the antenna overall mass.

Unless the important role of the boom on the deployed system stiffness, the fraction of the boom mass in relation to the system mass is low. This can be explained with the relatively low stiffness requirements for the deployed boom in contrast to the hub that is designed against the launch loads.

10.3.2 Conf1 - *Changed Deployed First Mode Frequency*

For this configuration the requirement on the deployed first mode frequency of the antenna has been reduced. Moreover, to account for the defined dependency between antenna and membrane frequency, also the target frequency for the pure antenna has been reduced. The changed input parameters are listed in Table 15. All non-listed parameters remain the same as previously defined in Table 13.

The same is true for the output parameter shown in Table 16. All variables not listed here but existing in Table 14 have not changed in comparison to the reference design. Moreover, a fourth column was added to quantify the difference between the Conf0 and Conf1 with respect to Conf0.

Interpreting the result table leads to the following conclusions:

VARIABLE	VALUE conf0	VALUE conf1
aFRequ	0.40Hz	0.30Hz
mFRequ	0.52Hz	0.39Hz

Table 15.: Input parameters for Conf1 - Changed Deployed First Mode Frequency

VARIABLE	VALUE conf0	VALUE conf1	Δ
aMass	51.83kg	50.75kg	−2.1%
aSpecMass	1.296kg/m^2	1.269kg/m^2	−2.1%
bMass	1.87kg	1.66kg	−11.2%
stMass	0.85kg	0.64kg	−25.0%
hMassC	14.51kg	13.85kg	−4.5%
anW	4.07m	4.02m	−1.3%
anLSto	0.650m	0.616m	−5.2%
anVSto	0.608m^3	0.569m^3	−6.4%
bCSScale	1.402	0.919	−34.4%
hOffset	0.090m	0.073m	−18.8%
compTime	17.0min	17.7min	+4.2%

Table 16.: Result parameters for Conf1 - Changed Deployed First Mode Frequency

1. All parts lost a bit of mass but the overall mass loss is at only 2.1% or 1.08kg
2. The mass of the transversal frame stiffeners decreases by 25% ⇒ The reduced membrane first mode requirement leads to smaller membrane tensioning forces that allow to downsize the transversal stiffeners.
3. The biggest change applies to the boom cross section scaling variable bCSScale which is decreased by more than a third. ⇒ This result is not surprising because the boom cross section is essential for the boom bending stiffness which is again essential for the first bending mode of the antenna.
4. Despite of the significant change in the cross section scaling parameter, the mass of all booms drops by only 11.2% or 0.21kg which is only about 20% of the overall lost mass ⇒ As the scaling parameter is just effecting one geometry

variable of the boom cross section, the change in boom mass is relatively low. The low impact on the antenna mass can be explained with the low mass fraction of the booms with respect to the overall antenna mass.

5. The hub mass decreases by 4.5% or 0.66kg. This mass is about 61% of the lost mass of the entire antenna and, therefore, the most significant loss of this comparison. Examining the results leads to the following conclusions:
   a) The decreased boom cross section allows the usage of a shorter hub (see `anW` which is identical to the hub length) in order to accommodate a boom that is less wide when flattened
   b) The reduced height of the deployed boom required a smaller cut-out in the hub that allows to reduce the `hOffset` variable,

Concluding these findings one can formulate that the reduction of the required first deployed antenna mode by 25% does reduce the mass and stowed volume of the antenna significantly but not with the same percentage. The explanation for the relatively small effect is that the major effect of the modified requirement is a boom cross section modification which leads to a minor geometry change of the hub.

As identified before, the hubs and the service membrane are contributing almost 76% of the overall antenna mass. Hence, it is reasonable, that a modified requirement that impacts mainly on the boom design does not change the overall mass in a very effectual way.

10.3.3 Conf2 - *Changed Stowed First Mode Frequency*

For this configuration the requirement on the first mode of the stowed antenna has been reduced by 20% (see Table 17).

VARIABLE	VALUE conf0	VALUE conf2
`hFRequ`	25Hz	20Hz

Table 17.: Input parameters for Conf2 - Changed Stowed First Mode Frequency

Interestingly, the only changed output parameter with respect to the Conf0 reference is the calculation time which has slightly

VARIABLE	VALUE conf0	VALUE conf2	Δ
compTime	17.0min	18.1min	+6.5%

Table 18.: Result parameters for Conf2 - Changed Stowed First Mode Frequency

increased (see Table 18). All other parameters remain constant. This is true because of the fact that the hub sizing is in general driven by the modal and the strength criteria.

The calculations were performed on a notebook PC with an Intel i7 2.2 GHz quad-core processor and 8 GB of RAM

Tracing the optimisation steps in MATLAB for both optimisations reveals the following:

1. For Conf0 the calculation for the first hub mode with its initial laminate setup results in a frequency of 24.56Hz. As the requirement for Conf0 was set to 25Hz, MATLAB adds an additional layer to the hub laminate and recalculates the first mode. The result changes to 28.66Hz which satisfies the modal requirement. The subsequent evaluation of the hub against strength failures from random vibration loads does show no critical failure indices.

2. For Conf2 the MATLAB routines deliver the same results as for Conf0 until the first mode of the hub needs to be compared to the requirement. Here MATLAB identifies that the obtained 24.56Hz are sufficient with respect to the requirement of 20Hz and continues with the random vibration simulation. During this simulation MATLAB evaluates that the hub with its basic laminate (no additional layer so far) is not able to bear the equivalent static load without exceeding the failure indices of one layer. Thus, it adds one additional layer to the face sheet laminate and redoes the calculation which delivers a positive result in this run.

The consequence of both sizing runs is a hub with 1 additional layer per face sheet. But in Conf0 this additional layer is already needed to fulfil the modal requirement whereas for Conf2 the need for an additional layer is identified during the strength criteria evaluation.

Moreover, the traced optimisation steps show why the calculation time has increased for Conf2: For Conf0 two modal and one strength calculations need to be done to size the hub. Instead, for the Conf2 one modal and two strength calculations are done. As the modal calculation is less complicated (no single layer result

evaluation) and time consuming than the strength computation, the change in calculation time is comprehensible.

10.3.4 Conf3 - *Changed Aperture Area*

As indicated in Table 19 below, here the required aperture area for the antenna has been reduced by 25%.

VARIABLE	VALUE conf0	VALUE conf3
aArea	$40m^2$	$30m^2$

Table 19.: Input parameters for Conf3 - Changed Aperture Area

The sizing results are given in Table 20. Interpreting both tables allows the following conclusions:

1. All parts lost significant amounts of mass and the overall mass loss reaches 24.6% or 12.75kg
2. With the aperture reduction by 25% also the masses of the service and antenna membranes reduce by almost this percentage (24.7%) ⇒ The low gap between both values can be explained with the nearly identical geometry of the membrane edge regions for Conf0 and Conf3. So the aperture area is scaled down while the outer interface regions are reduced in length but not in width. This results in a less effective ratio between interface related and aperture membrane parts.
3. Due to the reduced length of the antenna the number of boom to membrane interfaces per boom has been reduced from 14 to 12. In contrast the width reduction was not enough to reduce the interface number per hub.
4. For this configuration the hub does not require an additional layer to fulfil the modal and strength requirement. The optional loop shown in Figure 60 on page 112 was, therefore, not necessary which explains the drastically reduced computation time.
5. The only increased result variable is the specific mass that gains 0.5% ⇒ An explanation for this result is that the hubs options for downsizing are fully utilised for this szenario. Both the hub first mode frequency (31.6Hz) and the strength

VARIABLE	VALUE conf0	VALUE conf3	Δ
aMass	51.83kg	39.08kg	−24.6%
aSpecMass	1.296kg/m^2	1.303kg/m^2	+0.5%
bMass	1.87kg	1.42kg	−24.2%
stMass	0.85kg	0.49kg	−42.3%
hMassC	14.51kg	11.10kg	−23.5%
mSMass	24.81kg	18.68kg	−24.7%
mAMass∗3	9.61kg	7.23kg	−24.7%
sIFMassComp	0.18kg	0.16kg	−11.1%
anW	4.07m	3.59m	−11.7%
anL	13.30m	11.58m	−12.9%
anLSto	0.650m	0.610m	−6.1%
anVSto	0.608m^3	0.504m^3	−17.1%
mNFL	14	12	−14.3%
hFSAdd0Layer	1	0	−100.0%
bCSScale	1.402	0.846	−39.7%
hOffset	0.09m	0.07m	−21.9%
compTime	17.0min	8.0min	−52.7%

Table 20.: Result parameters for Conf3 - Changed Aperture Area

failure safety factor ($k_{s_{min}} \geqslant 1.35$) show the potential for further downscaling of the hub but the minimum laminate setup is already used.

Concluding this configuration a significant mass loss of 24.6% results out of an aperture area reduction by 25%. This mass reduction needs to be understood as a combination of:

1. The geometrical scaling of the membranes area and the boom and hub length,
2. The mechanically motivated boom cross section reduction and decreased number of face sheet layers in the hub.

Please refer to Annex A.2 to make aware the impact of the harness on the overall service membrane mass

10.3.5 Conf4 - *Changed Additional Mass on Service Membrane*

This configuration shows the effects of a drastic reduction of the additional service membrane mass (see Table 21) as it could

arise from a changed design that uses micro-strip lines for signal transfer instead of wires or even thinner wires.

Interpreting Table 22 gives the following findings:

1. Although, the additional service membrane mass has been reduced by 77.7% the service membrane mass is decreased by only 57.6% ⇒ Responsible for this effect is the still constant mass of the membrane substrate of 6.4kg.

2. The mass of the complete antenna is reduced by 32.6% to 34.9kg ⇒ This configuration fulfils the required maximum mass and specific mass limits defined in Section 4.2 on page 10.

3. Again the hubs first mode (29.6Hz) and the strength safety factors for the random vibration load ($k_{s_{min}} \geqslant 1.60$) imply

VARIABLE	VALUE conf0	VALUE conf4
mSSpecAddMass	$0.448\,kg/m^2$	$0.1\,kg/m^2$

Table 21.: Input parameters for Conf4 - Changed Additional Mass on Service Membrane

VARIABLE	VALUE conf0	VALUE conf4	Δ
aMass	51.83kg	34.94kg	−32.6%
aSpecMass	$1.296\,kg/m^2$	$0.874\,kg/m^2$	−32.6%
bMass	1.87kg	1.74kg	−7.0%
stMass	0.85kg	0.65kg	−23.6%
hMassC	14.51kg	12.25kg	−15.6%
mSMass	24.81kg	10.51kg	−57.6%
anW	4.07m	4.04m	−0.8%
anLSto	0.650m	0.629m	−3.2%
anVSto	$0.608\,m^3$	$0.584\,m^3$	−4.0%
hFSAdd0Layer	1	0	−100.0%
bCSScale	1.402	1.106	−21.1%
hOffset	0.09m	0.079m	−11.7%
compTime	17.0min	7.7min	−54.8%

Table 22.: Result parameters for Conf4 - Changed Additional Mass on Service Membrane

that the hub could be further downsized but the given options are already utilised.

Concluding this configuration it needs to be emphasised that this setup is the first antenna model that fulfils the defined requirement for the antenna mass. The therefore modified parameter was previously chosen according to a reasonable assessment but not related to a real antenna RF design. Thus, the here presented configuration could be possible.

10.3.6 Conf5 - *Change to Antenna Functionality*

The here presented configuration shows the results of a changed antenna functionality by neglecting the mission requirement for the antenna concept.

Hence, it includes RF concepts that does not require a fourth service membrane for harness and Low Noise Amplifier (LNA). Possible RF concepts that allow such modification could be:

1. A receive-only antenna without a capability for beam steering would not require a dedicated signal line to each patch and could be therefore designed using common signal lines as done by Huang in [30] and previously shown in Figure 17 on page 34,
2. A Reflect-Array concept that requires in general no signal lines for connection of the patches.

As shown in Table 23 the service membrane is actually not deleted from the model but the input parameters are modified in a way that the service membrane substrate thickness is reduced by a factor of 10^3 while the added specific mass is reduced to a marginally value of $10^{-4}\,kg/m^2$. Such significant parameter scaling factors are assumed to be less critical for the robustness of the used numeric calculation than setting masses and thicknesses to a clear zero.

VARIABLE	VALUE conf0	VALUE conf5
`mSThickness`	$10^{-4}\,m$	$10^{-7}\,m$
`mSSpecAddMass`	$0.448\,kg/m^2$	$10^{-4}\,kg/m^2$

Table 23.: Input parameters for Conf5 - Change to Antenna Functionality

VARIABLE	VALUE conf0	VALUE conf5	Δ
aMass	51.83kg	23.93kg	−53.8%
aSpecMass	1.296kg/m^2	0.598kg/m^2	−53.8%
bMass	1.87kg	1.66kg	−11.4%
stMass	0.85kg	0.45kg	−47.2%
hMassC	14.51kg	12.02kg	−17.1%
mSMass	24.81kg	0.01kg	−100.0%
anW	4.07m	4.02m	−1.3%
anLSto	0.650m	0.615m	−5.4%
anVSto	0.608m^3	0.568m^3	−6.6%
hFSAdd0Layer	1	0	−100.0%
bCSScale	1.402	0.908	−35.2%
hOffset	0.09m	0.072m	−19.4%
compTime	17.0min	7.9min	−53.6%

Table 24.: Result parameters for Conf5 - Change to Antenna Functionality

Interpreting Table 24 gives the following findings:

1. The mass of the antenna drops significantly by 53.8% or 27.9kg,
2. The main mass saving is resulting from the direct loss of the service membrane mass of 24.8kg. Another 2.49kg are won by a lighter hub which results from a thinner laminated setup and a shorting of the hub by 5cm due to the smaller required boom feed-though cut-outs.

This configuration shows, that the mass and specific mass of the antenna could be reduced to less than a half when defining another mission requirement for the antenna type.

However, it is again obvious that the used parameterised hub architecture is not sufficient to downsize the hub as far as possible. The first mode is 11.4Hz higher than required and the lowest safety factor against material failure due to random vibration loads is at 2.48. So for such very light membrane configuration a redesign of the hub shall be a good option for a detailed design.

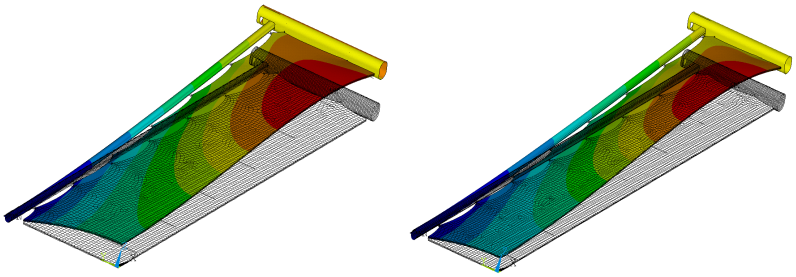

(a) Conf0 (b) Conf6

Figure 61.: First antenna modes of Conf0 and Conf6 shown to compare the different antenna shape and number of membrane attachment points along the booms

10.3.7 Conf6 - *Change of Length to Width Ratio*

The last basically changed configuration shows the impact of a modified antenna length to width ratio (see Table 25).

VARIABLE	VALUE conf0	VALUE conf6
aLWR	$\frac{1}{4}$	$\frac{1}{6}$

Table 25.: Input parameters for Conf6 - Change of Length to Width Ratio

The results of this change in antenna geometry is visualised in the Figures 61a and 61b. Some output parameters are given in Table 26.

Interpreting Table 26 gives the following findings:

1. The mass of the antenna shows no significant change
2. The antenna gets 12% narrower but about 21% longer which is directly related to the length of the booms and the hubs
3. The boom cross section and the boom mass are significantly increased which results from geometrically required 21% longer booms with a hub that lost only 5.7% of its mass due to hub shortening.
4. The hub loses only 5.7% of its mass (comparing to 12% in hub length loss) because the increased boom cross section required an increase of the `hOffset` parameter which increases the specific mass per hub length.

VARIABLE	VALUE conf0	VALUE conf6	Δ
aMass	51.83kg	51.61kg	−0.4%
aSpecMass	1.296kg/m^2	1.290kg/m^2	−0.4%
bMass	1.87kg	2.58kg	+37.6%
stMass	0.85kg	0.59kg	−31.3%
hMassC	14.51kg	13.68kg	−5.7%
mSMass	24.81kg	24.91kg	+0.4%
mAMass*3	9.61kg	9.65kg	+0.4%
sIFMassComp	0.18kg	0.20kg	+11.1%
anW	4.07m	3.56m	−12.4%
anL	13.30m	16.11m	+21.1%
anLSto	0.650m	0.687m	+5.7%
anVSto	0.608m^3	0.563m^3	−7.5%
mNFL	14	16	+14.3%
bCSScale	1.402	1.930	+37.7%
hOffset	0.09m	0.108m	+20.6%
compTime	17.0min	19.1min	+12.3%

Table 26.: Result parameters for Conf6 - Change of Length to Width Ratio

5. Due to the narrower deployed antenna shape, the stowed antenna is also more narrow, as well. The saving in antenna stowed volume anVSto of 7.5% is thereby not reaching the same percentage as the hub shortening. This is again related to the increased hOffset parameter that does also affect the stowed antenna length (anLSto).

Conf6 shows that a change in the antenna length to width ratio is nearly not affecting the mass of the antenna but significantly decreasing the volume or more specific the length of the stowed antenna.

10.4 EXAMPLE EVALUATION

For each of the previous six configurations only one major modification from the reference designs is made to see the direct effect on the overall structure. This section presents and concludes the achieved findings of these unique settings to support the identifi-

cation of other interesting candidate configurations for the next section.

1. Conf1 achieves a mass loss of 2.1% by a reduction of the target deployed mode frequency of 25% ⇒ Responsible for this comparatively low mass reduction is the significant impact of the changed requirement on the boom cross section but the very low fracture of the boom mass on the overall system mass.

2. Conf2 results in a structure that is fully identical to Conf0 although the target first mode frequency of the stowed antenna is reduced by 20% ⇒ The changed requirement is only of interest for the hub which is sized according to the changed modal requirement and random vibration strength criteria. For Conf2 the strength criteria turned out to be the more critical requirement for the sizing so that an impact of the changed modal requirement is not given.

3. Conf3 achieves a mass loss of 24.6% by a reduction of the antenna aperture area by 25% ⇒ This global size reduction reduces the mass of all parts due to the resulting geometrical downscaling of all parts and the reduced mechanical loads due to smaller dimensions and masses of all parts.

4. Conf4 saves 32.6% of the overall mass by a reduction of the additional service membrane mass by 77.7% ⇒ The reduction of this parameter is identified to be very effective on the mass reduction of all antenna parts. Moreover, this parameter is very attractive for parameter studies because it is so far not defined by a detailed RF design but only by a reasonable assessment. So, the antenna reacts very sensitive to changes of a parameter that is so far not well defined. It is furthermore assumed that the result could be further optimized by using a thinner substrate for the service membrane.

5. Conf5 continues the idea of Conf4 and totally eliminates the service membrane which results in a mass loss of 53.8% of the overall mass ⇒ As also true for Conf4, the mass saving is thereby mainly related to the mass of the lost membrane. The savings on boom and hub masses are comparatively low.

6. Conf6 shows no significant mass reduction but a reduction of the stowed volume by 7.5% by changing the antenna aper-

ture length to width ratio from 1/4 to 1/6 ⇒ The changed envelope results in shorter and lighter hubs (−0.83kg) as well as longer and stiffer/heavier booms (+0.71kg). Both mass changes are nearly compensating each other. In contrast, the reduced stowed volume and length are significant and very attractive.

So the different configurations reveal a high impact of parameters that change the mass of the membranes and comparatively low impact of modified launch loads and stowed or deployed stiffness requirements.

Moreover, the calculations reveal that the downsizing capabilities of the hubs are limiting the efficiency of the design. It is possible to improve the downsizing capability by using thinner UD layers.

10.5 RESULTING FINAL CONFIGURATIONS

Here the gained system understanding from the previous two sections is used to create two final concepts by combined modifications of different input parameters.

One is addressing a phased array antenna that's patches need to be fed by conventional wired lines and LNAs. The second concept is related to an non-phased array antenna concept that's patches are fed by micro-strip lines on the antenna membranes or a reflect array configuration. Thus, the last configuration does not require a service membrane but is - in contrast to the phased array concept - not compliant with the defined requirements for this thesis. Hence, it should be seen as an outlook for an adaption of this basic structural concept towards a modified mission scenario.

10.5.1 Conf7 - *Final Phased Array Concept*

An overview on the modified input parameters for Conf7 is given in Table 27.

As a result of the findings from Conf6 the aperture length to width ratio `aLWR` has been decreased to reduce the stowed antenna volume and length.

The results of Conf4 and Conf5 motivated the combined reduction of the additional service membrane mass `mSSpecAddMass` and the service mass substrate thickness `mSThickness`.

Consequently, this configuration is violating the second subrequirement of requirement #4 on the service membrane thick-

VARIABLE	VALUE conf0	VALUE conf7
aLWR	$\frac{1}{4}$	$\frac{1}{6}$
mSThickness	$0.1 \cdot 10^{-3}\,\mathrm{m}$	$0.05 \cdot 10^{-3}\,\mathrm{m}$
mSSpecAddMass	$0.448\,\frac{\mathrm{kg}}{\mathrm{m}^2}$	$0.1\,\frac{\mathrm{kg}}{\mathrm{m}^2}$
hFSThicknessIncrement	$0.1 \cdot 10^{-3}\,\mathrm{m}$	$0.05 \cdot 10^{-3}\,\mathrm{m}$

Table 27.: Input parameters for Conf7 - Final Phased Array Concept

VARIABLE	VALUE conf0	VALUE conf7	Δ
aMass	51.83kg	29.61kg	−42.9%
aSpecMass	$1.296\mathrm{kg/m^2}$	$0.740\mathrm{kg/m^2}$	−42.9%
bMass	1.87kg	2.28kg	+21.4%
stMass	0.85kg	0.41kg	−51.8%
hMassC	14.51kg	9.73kg	−32.9%
mSMass	24.81kg	7.34kg	−70.4%
mAMass∗3	9.61kg	9.65kg	+0.4%
sIFMassComp	0.18kg	0.20kg	+11.1%
anW	4.07m	3.50m	−14.0%
anL	13.30m	16.11m	+21.1%
anLSto	0.650m	0.649m	−0.1%
anVSto	$0.608\mathrm{m^3}$	$0.523\mathrm{m^3}$	−14.1%
mNFL	14	16	+14.3%
bCSScale	1.402	1.40	+0.1%
hOffset	0.090m	0.089m	−0.4%
compTime	17.0min	18.6min	+9.6%

Table 28.: Result parameters for Conf7 - Final Phased Array Concept

ness, defined in section 4.2 on page 10. It is thereby assumed that a reduction of the substrate thickness by a factor of 2.0 is applicable when reducing the additional service membrane mass by a factor of 4.48.

The reduction of the layer thickness of a single hub UD face sheet layer hFSThicknessIncrement is a result of calculations done for Conf3, Conf4 and Conf5. For all of those configurations the final design shows that the basic hub laminate is sufficient or even oversized. Thus, the here used reduction of the layer

thickness refines the granularity of the achieved result and should, therefore, result in a lighter hub. However, such a thin layer thickness will complicate the manufacturing of the hub but, with the present experience on thin boom manufacturing at DLR, it is assumed that this should be possible.

Table 28 shows the results of this sizing run.

In general the overall mass is reduced to 29.61kg and the specific mass reaches a value of only 0.74kg/m^2. This is possible by significant losses in service membrane and hub mass.

The hub mass drops from 14.51kg for Conf0 and 13.68kg for Conf6 to a value of only 9.73kg for the here presented Conf7. This result is mainly deriving from the reduced thickness of the single UD layers for the hub face sheets. Although, this thickness is reduced to the half value, the sizing chain routines deliver a laminate stacking that is identical to the one from Conf0. Hence, the thickness of the face sheet - and thereby its mass - is reduced by a factor of 2.0. Moreover, the hub is directly shortened due to the modified `aLWR`.

The face sheet layer mass of both hubs is reduced by 57% from 7.48kg for Conf0 to 3.20kg Conf7.

The stowed volume of the antenna is reduced by 14.1%. This significant effect is reasoned by the reduced hub length and the reduced hub cross section parameter `hOffset`.

Thus, this configuration is one possible configuration for the here discussed membrane antenna. The reduced service membrane thickness seems to be reasonable when respecting the potential loss of additional service membrane mass by a detailed RF design.

10.5.2 Conf8 - *Final Non-Phased or Reflect Array Concept*

This configuration assumes, that the service membrane is no longer required. Thus, the regarding membrane thickness and the additional service membrane mass are reduced to insignificant values (see Table 29).

As done for Conf7 the aperture length to width ratio and the thickness of a single UD layer for the hub face sheet layer stacking are adapted to more promising values.

In addition, the boom cross section parameter `bEllW` has been modified. It defines the width of the half elliptic part of the boom cross section. This reduction is assessed to be valid because of the expected reduction of the required boom stiffness that derives from the further reduced membrane mass.

The achieved results are shown in Table 30. The overall mass is further reduced to a value close to 20kg. When comparing these

VARIABLE	VALUE conf0	VALUE conf7
aLWR	$\frac{1}{4}$	$\frac{1}{6}$
mSThickness	$0.1 \cdot 10^{-3}\,\mathrm{m}$	$5.0 \cdot 10^{-8}\,\mathrm{m}$
mSSpecAddMass	$0.448\,\frac{\mathrm{kg}}{\mathrm{m}^2}$	$1.12 \cdot 10^{-4}\,\frac{\mathrm{kg}}{\mathrm{m}^2}$
hFSThicknessIncrement	$0.1 \cdot 10^{-3}\,\mathrm{m}$	$0.05 \cdot 10^{-3}\,\mathrm{m}$
bEllW	$0.045\,\mathrm{m}$	$0.035\,\mathrm{m}$

Table 29.: Input parameters for Conf8 - Final Non-Phased or Reflect Array Concept

VARIABLE	VALUE conf0	VALUE conf8	Δ
aMass	51.83kg	20.98kg	−59.5%
aSpecMass	$1.296\,\mathrm{kg/m^2}$	$0.524\,\mathrm{kg/m^2}$	−59.5%
bMass	1.87kg	2.03kg	+8.5%
stMass	0.85kg	0.34kg	−59.8%
hMassC	14.51kg	8.74kg	−39.7%
mSMass	24.81kg	0.01kg	−100.0%
mAMass∗3	9.61kg	9.65kg	+0.4%
sIFMassComp	0.18kg	0.20kg	+11.1%
anW	4.07m	3.45m	−15.2%
anL	13.30m	16.11m	+21.1%
anLSto	0.650m	0.637m	−1.9%
anVSto	$0.608\,\mathrm{m^3}$	$0.506\,\mathrm{m^3}$	−16.8%
mNFL	14	16	+14.3%
hFSAdd0Layer	1	0	−100.0%
bCSScale	1.402	1.24	−11.8%
hOffset	0.090m	0.084m	−7.0%
compTime	17.0min	14.3min	−15.9%

Table 30.: Result parameters for Conf8 - Final Non-Phased or Reflect Array Concept

results to the one of Table 30 from the previous configuration one can easily see that the majority of the lost mass again contributed by the lost service membrane mass of 7.33kg. The booms lose about 0.25kg, the stiffeners 0.07kg and the hubs about 0.99kg.

Generally, this result is a very promising one that emphasises the potentials and flexibility of the presented closed loop sizing chain.

10.6 CONCLUSION

This chapter introduced an approach for a closed loop sizing chain that uses a combined software tool of MATLAB, ANSYS, and EXCEL.

Different example configurations are sized to gain a better system understanding and derive two final improved designs for each a phased array and a non-phased array/reflect array configuration.

11 CONCLUSION

In this thesis a novel sizing method for a gossamer space antennas has been introduced and demonstrated by using this method for a new antenna concept.

The regarding basic design of the antenna is a further enhanced version of a classic structural concept [21, 40, 30]. Thereby, previous concepts use inflatable and sometimes rigidisable booms for realising the packaging and deployment capabilities. In contrast, the presented concept substitutes those pressurized or in-orbit cured booms by on-ground rigidised, elastically deformed CFRP-booms. Such booms are also deployed by inflation but the inflation is only working as a pneumatic actuator that drives the deployment. Once the antenna is fully deployed, the inflation hoses are vented and the booms CFRP-shell are instantly carrying the full mechanical loads.

The use of such on-ground cured composite booms generated the following advantages:

- Enhanced structural efficiency by very light carbon composites that are fully cured in a controlled manufacturing environment,
- The flight model can be tested on ground in stowed and *deployed* configuration,
- Outstanding deployment repeatability and shape accuracy of the deployed antenna.

After the brief introduction into the global design concept the design and sizing of fundamental antenna components of the antenna has been explained in dedicated chapters. The order of the chapters is thereby also an indicator for a reasonable sequence of sizing steps that was revisited when the closed loop sizing chain has been defined. This chain pictures again a valid order of sizing steps and describes how these steps can be automated by combining the capabilities of different available engineering software tools.

Although the antenna design is characterized by a large number of adjustable variables that would usually require a multi-dimensional optimisation, the sizing chain introduces a straight-

forward approach that allows a sizing of the structure as a sequence of different one-dimensional optimisations.

This simplification was possible by the gained general understanding of the antenna structure as well as of the interactions of the different antenna components and lead to a combined tool that allows a fully automated resizing of the given antenna design in less than 20 minutes.

The hypotheses of this thesis have been previously defined in Chapter 2 on page 4

Considering the basic hypotheses of this work the following statements are considered to be valid:

- HYPOTHESIS I: A design for the membrane antenna is presented that more than meets the required specific mass of $1\frac{kg}{m^2}$. This result needs to be seen under the perspective of a generic RF-design.
- HYPOTHESIS II: A sizing method is presented that allows a rapid resizing of all fundamental antenna parts as a reaction on changing requirements.

The presented methods and strategies shall enable other engineers to size a deployable membrane antenna in a reasonable way to react on upcoming design changes from RF side or changed launcher requirements.

Moreover, the design considerations and the sizing strategies shall be adaptable to other gossamer structures like solar sails, solar arrays, reflectors or even instrument booms.

12 OUTLOOK

Given by the very broad character of this thesis a lot of aspects could not be investigated as deep as it is required for a final design of a space structure. Consequently, a lot of ideas for alternative concepts on different levels came up while compiling this thesis. Thus, a non-exhaustive list of potential future research topics and recommended design changes is given hereunder:

1. Membranes
    - Impacting charged particles will charge the membranes or the applied parts → This could influence membrane spacing by induced electrostatic forces between the parallel layers.
    - A future RF design for the membrane antenna has to consider that the expected temperature differences between the membranes will shear-deform the single patch elements by relative in-plane travelling of the membrane layers. This effect will be most critical at the edge regions close to the hubs.
    - The given design uses the same membrane tensioning force values at the long and short membrane edges → It needs to be investigated if this approach is the most efficient (membrane first mode vs. frame loading)
    - The variation of the factor between the target membrane and system first mode frequency showed that a higher membrane target frequency does not necessarily result in a higher antenna mass → This need to be further investigated to understand the effects and find a further advanced configuration.
    - The interaction between the transversal stiffeners and the membranes in stowed configuration needs to be investigated to prevent membrane damaging during launch and stowed lifetime.

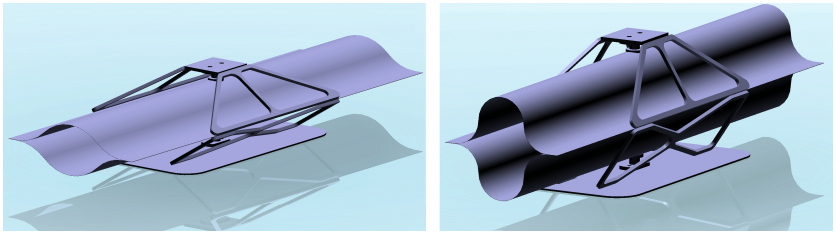

Figure 62.: Alternative boom interface concept in stowed (left) and deployed (right) configuration using flexure joints (designed for GOSSAMER-1 solar sail demonstrator)

2. Interfaces
    - The presented boom interfaces are relatively heavy and suffer from high play values to guarantee their function under space conditions → Figure 62 shows an alternative interface that uses no conventional hinges or bearings but deformable, flexure hinges that have no play but can compensate thermal deformations.
3. Hubs
    - The hub shell is made of a CFRP/aluminium honeycomb sandwich material of constant thickness and laminated setup along the entire hub shell → A detailed design with adapted laminate setups for different hub sections should further decrease the mass. Moreover, the substitution of the sandwich material by an aircraft like stringer/skin shell or an (an)isogrid concepts could result in a lighter antenna. For sure, the stiffening aluminium parts in the hub design should be substituted by composite or Titanium parts.
    - The high hub stiffness (and thereby mass) is mainly needed to achieve a sufficient bending stiffness to comply with the launch loads while the hub is only supported at its two ends → Another hub support concept for the stowed antenna with multiple support points along the hub or even a constant support of the hub along the entire length would enable lighter hubs. However, again this step requires a previously RF design for the membrane to assess options for intermediate support points.
    - The current hub shell consist of face sheets out of 0° and 90° CFRP UD layers and aluminium honeycomb that material data has been extracted form ESAComps

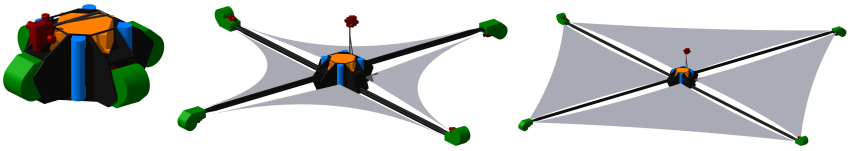

(a) Stowed (b) Deploying (c) Deployed

Figure 63.: GOSSAMER-I demonstrator

standard library → The uses of other UD orientations (e.g. ±45°) and better performing fibres for the face sheets or better performing honeycomb could further enhance the structural efficiency.

4. General
   - Driven by the cost extensive testing of gossamer space structures, the presented work is based on a limited number of tests. This seems to be a general trend for gossamer structures but it is an outcome of this work to recommend at least some tests on part level to obtain results on stiffness, strength and buckling behaviour of primary structure elements and interfaces.
   - The presented membrane antenna frame could also fit the requirements for a deployable solar array that uses thin film solar cells. Considering the given results, such a solar array should weigh not more than 30kg.
   - An investigation on the robustness of this design with respect to MMODs or manufacturing uncertainties should be performed for a final design

Besides the antennas, the gained experience of the here presented work will contribute to the future development of deployable gossamer structures at DLR. For 2014 two on-orbit technology demonstration mission are planned and already funded that will both use modified versions of DLR's CFRP-booms: DLR's GOSSAMER-I solar sail deployment demonstrator [24] and the DEORBIT SAIL demonstrator under lead of the University of Surrey [37].

Moreover, an ESA co-funded study on "Robust and Tolerant Gossamer Structures" started in 2012 and will last 3 years. The 3 year EU project DEPLOYTECH is also led by the University of Surrey and started in 2012 as well. DLR's contribution is aiming on the further increase of the Technology Readiness Level (TRL) of the booms and their deployment mechanisms.

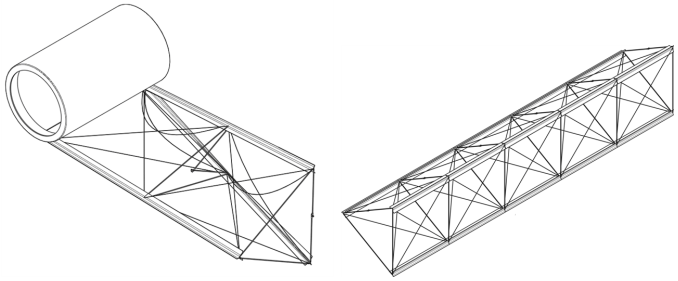

(a) Deploying (b) Deployed

Figure 64.: CTT - Collapsible Tape Truss

In addition to the ongoing improvement of DLR's classic shell boom, the recently presented work of Hillebrandt et al. in [29] shows the continuation of the work on gossamer structures at DLR by introducing a novel deployable truss concept for various gossamer structures.

So, it is obvious that the interest in Gossamer Structures is still there and even rising. This new demand can be answered best by further advancing current technologies and remain open for new ideas.

A

APPENDIX

A.1 RADAR WAVE PENETRATION DEPTH

- referred at page 7 -

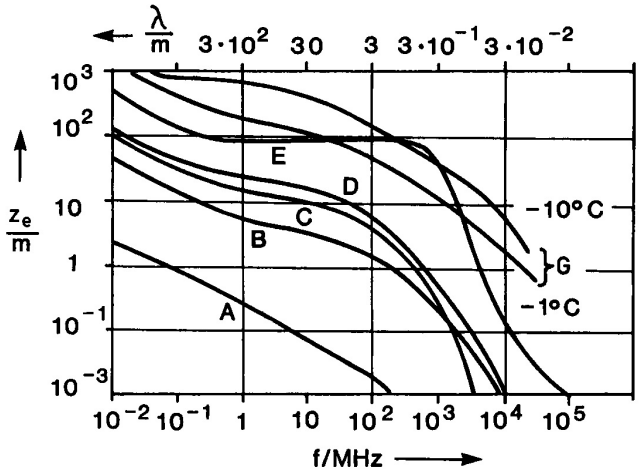

Figure 65.: Frequency (f in MHz) and/or wave length (λ in m) depending penetration depth (z_e in m) of electro-magnetic waves for different materials like A: sea water, B: wet soil, C: fresh water, D: middle dry soil, E: very dry soil, G: ice from fresh water (graph extracted from [34])

A.2 ANTENNA MEMBRANE MASS CALCULATION

- referred at page 35 and 124 -

The mass values from Table 2 on page 36 are derived here.

A.2.1 *Membrane Substrate*

In contrast to the concept by Huang the thickness of the membranes layers have been increased to 50 µm to improve the robustness of the antenna. The mass m_M of the pure Kapton® membrane results from

$$m_M = \rho_M \cdot e_M \cdot A_{AA} \cdot (1 + M_M) = 3.120\text{kg} \tag{A.1}$$

where

ρ_M	membrane material density, here $1300\frac{kg}{m^3}$ for Kapton®
e_M	membrane material thickness, here $50\mu m$
A_{AA}	array area, here $40m^2$
M_M	membrane margin, here 20%

The membrane margin M_M is thereby representing the increased size of the membrane in contrast to the array and the additional weight for stiffened regions at the membrane edges for tear prevention or wrinkling minimization.

A.2.2 *LNAs*

In contrast to the membrane and the patches the calculation of the LNA mass is very unspecific as there is no standard of the shelf product that data could be used. Therefore, an estimated value is used that results from assessments of antenna experts. The mass of one LNA element is thereby estimated to $m_{LNAe} = 0.8g$. The mass of all LNAs m_{LNA} is:

$$m_{LNA} = m_{LNAe} \cdot N_{LNA} = 0.4656\text{kg} \tag{A.2}$$

where

N_{LNA}	number of LNAs, here 582

A.2.3 *Harness*

The mass of the cable is also a estimated value from antenna experts. It has been assumed that the power and signal cable have a specific weight of about $\gamma_c = 30g/m$. The average length of each cable is estimated to $l_C = 5m$. Thus the following harness mass m_H evolves:

$$m_H = l_C \cdot \gamma_C \cdot N_C = 17.46kg \tag{A.3}$$

where

N_C	number of cables, here 582

A.3 MEMBRANE WRINKLING TEST

- referred at page 44 -

For complex membranes with force attachment angles that are not exactly vertical or horizontal, the positioning of the pulleys is not trivial. Therefore, a MATLAB program was programmed that is able to calculate the exact position for each pulley out of defined membrane attachment points and the angle for the supporting force.

An output of the regarding program is plotted in Figure 66.

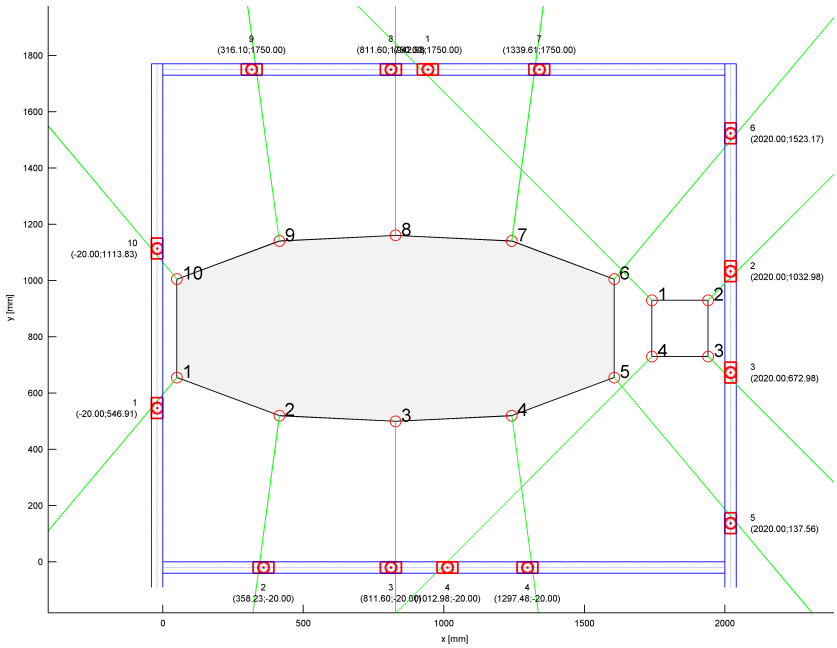

Figure 66.: Output of MATLAB script for pulley position calculation

In addition, Figure 67 shows the result of such a scan.

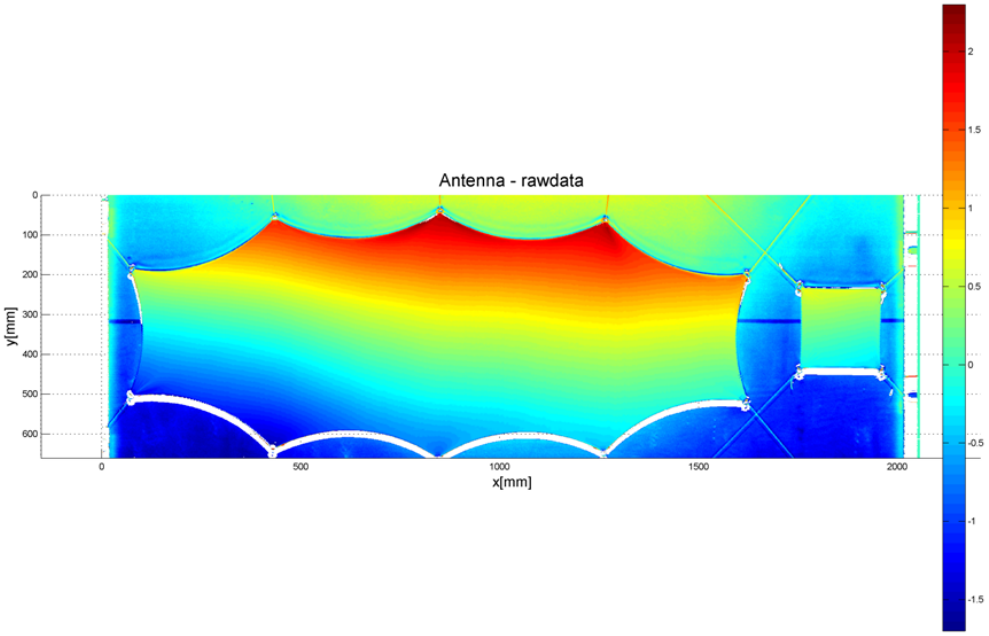

Figure 67.: Wrinkling test scan results

A.4 MEMBRANE ANTENNA BREADBOARD MODEL

- referred at page 27 and 56 -

The below shown photographs result from the realisation of a previous antenna concept that does not use structural integrated hubs for coiling but considered the usage of hubs that are jettisoned after deployment. This jettisoning would decrease the deployed mass of the antenna significantly but the concept was skipped due to the generation of space debris.

Moreover, transversal stiffeners were not used for this model which results in the strong boom cross section deformations shown in Figure 68d.

(a) Full view on 6m x 1.3m breadboard model

(b) Corner section of breadboard model (boom to beam interface)

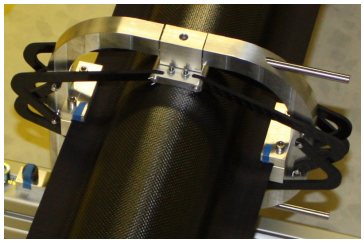

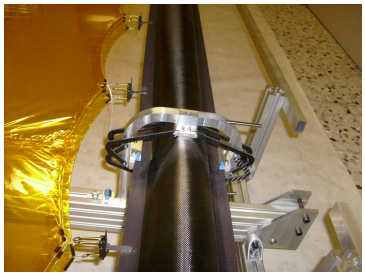

(c) detailed view on spacecraft to boom interface (referred at page 27)

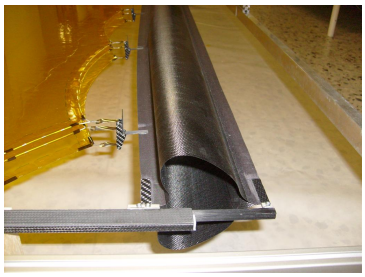

(d) detailed view on boom to beam interfaces

Figure 68.: Details of membrane antenna breadboard

A.5 CFS CHARACTERISATION

- referred at pages 61 and 91 -

During breadboard design different types of CONSTANT FORCE SPRINGS (CFS) have been ordered for breadboard assembly and CFS characterization. Figure 69 shows the setup of the 1N CFS during characterization. A conventional tensile testing machine was used to apply and monitor the deflection as well as monitor the force. A breadboard frame to membrane interface mechanism was used to get realistic friction effects.

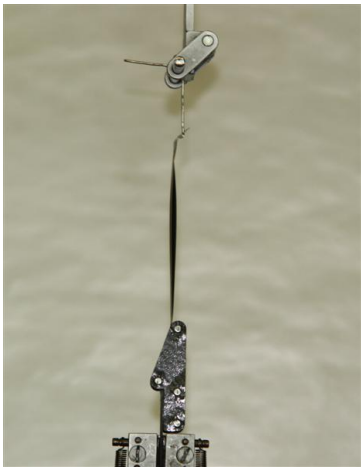

(a) front view

(b) left front view

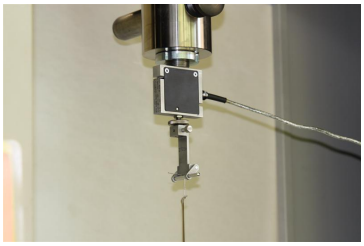

(c) details on force sensor (10N maximum force)

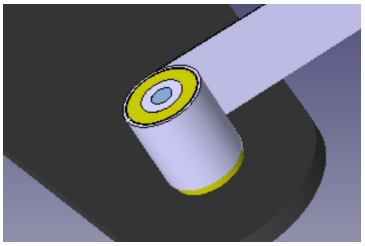

(d) details on the CFS bearing (CAD model)

Figure 69.: CFS testing

Figure 69d shows details of the used bearing concept. From inside to outside the following elements are shown: central screw (dark gray), stainless steel sliding shell (light gray), PTFE bearing (yellow), and CFS (light gray).

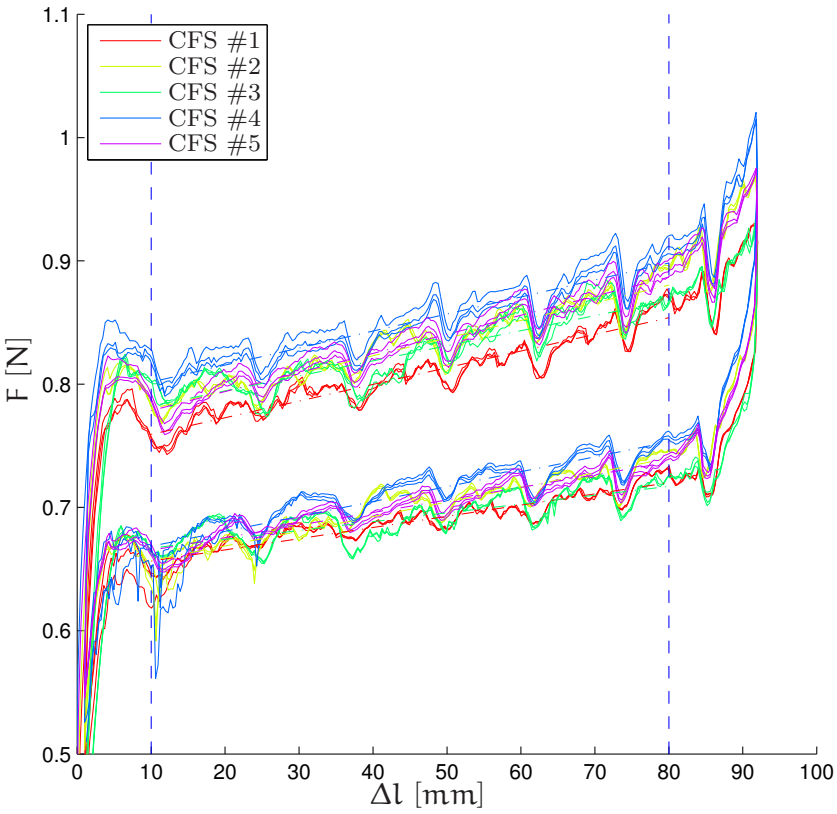

Figure 70.: Hysteresis characteristic of CFSs 1 till 5

Figures 70 and 71 show the results of these tests. Each spring was tested with a deflection speed of $1.667 \frac{\mathrm{m}}{\mathrm{s}}$ and cycled 3 times. All ten tests show a strong hysteresis effect. This is a clear indicator for friction within the system. It is understood that the friction will derive from not perfect friction-less bearing conditions and internal material friction.

The periodic peaks that can be observed along the entire working range can be explained with the coiling process of these non-endless stripes of sheet metal. At each full rotation the inner end of the coiled spring is passing the loaded contact region between the spring and the inner bearing which leads to a temporary increased or decreased rotation resistance that need to be overcome. This assumption is supported by the made observation that the distance between two peaks is identical with the perimeter of the coiled spring.

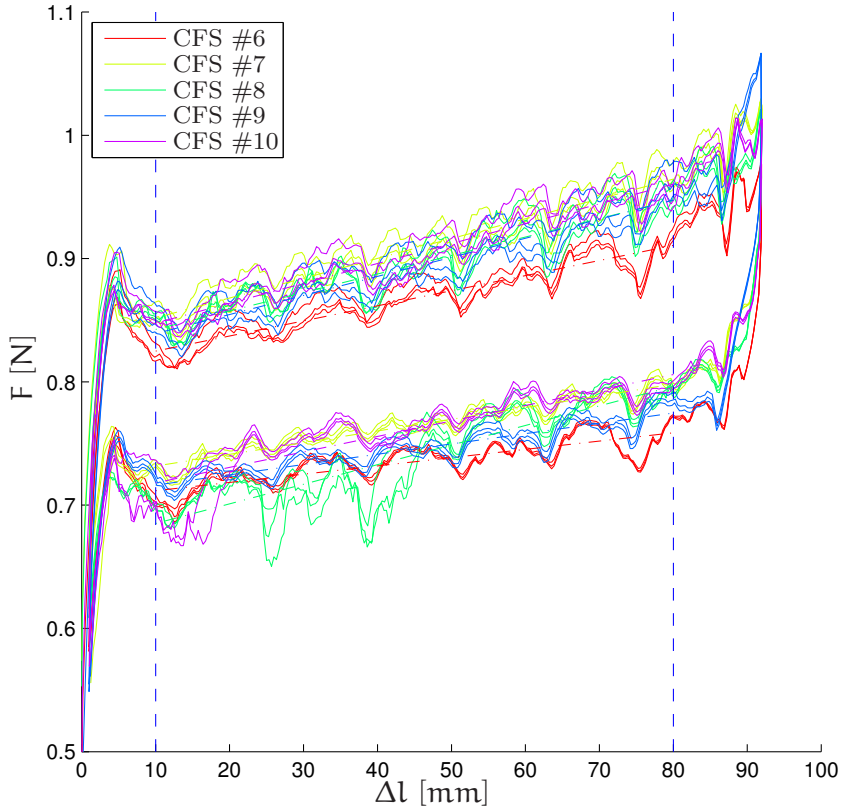

Figure 71.: Hysteresis characteristic of CFSs 6 till 10

A.6 FRAME TO MEMBRANE INTERFACES

- referred at pages 62 and 65 -

Details on the boom to membrane interface are given in Fig 72.

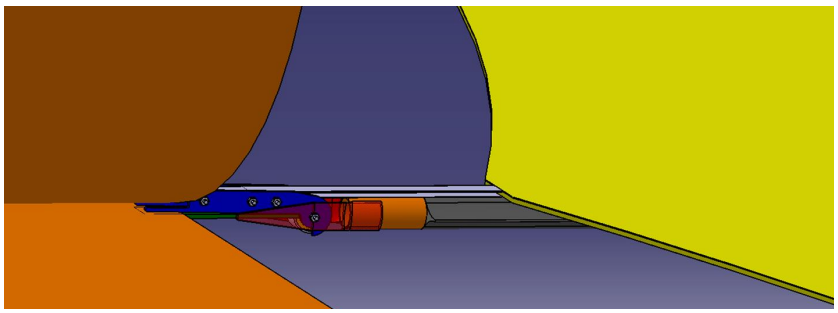

(a) stowed configuration (≈ 1° tilt angle)

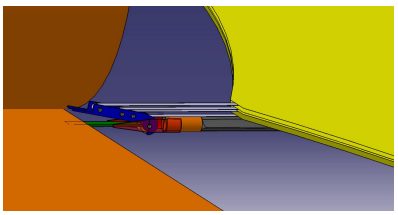

(b) partially deployed configuration (10° tilt angle)

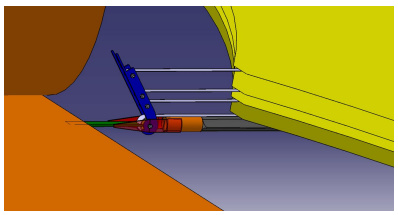

(c) partially deployed configuration (60° tilt angle)

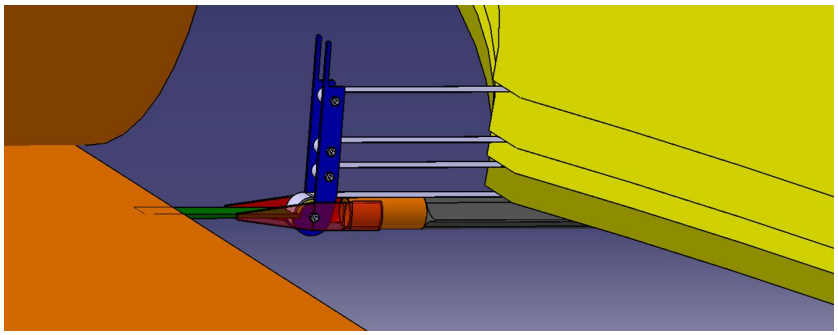

(d) deployed configuration (90° tilt angle)

Figure 72.: Boom to membrane interface

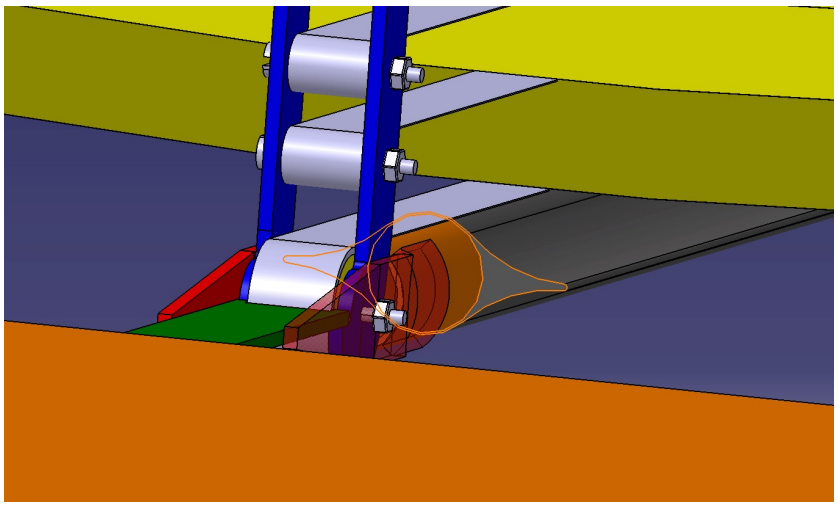

Figure 73.: Detailed view on protective cover applied to transversal stiffeners to not damage membranes during coiling

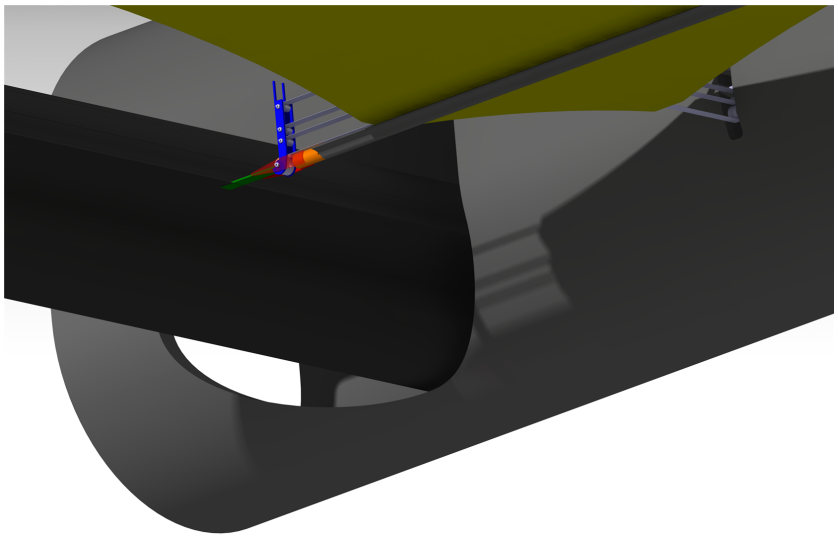

Figure 74.: Both frame to membrane interface types integrated in the antenna corner

A.7 LOAD AND REQUIREMENT DEFINITION FOR THE STOWED ANTENNA

- referred at page 74 -

In general, two sources for loads and requirements are available for the given antenna concept: The *VEGA User's Manual*[53] and the ECSS norm on testing [19].

A definition of the term verification is given in section 4.1.1 in [20]

The ECSS definitions are more general and can be used for *verification* of space equipment for use at different satellites on different launchers. The ECSS loads for equipment are defined in the ECSS norm on testing [19, section 5.1].

In case of the here designed antenna, VEGA has been already selected as baseline launcher. Thus, the mentioned *VEGA User's Manual* could be used for selection of adequate launch loads.

However, to let the antenna comply with different launchers, it is a suitable approach to compare the load requirements in both documents and choose the highest value for each load case.

A.7.1 *Steady State Acceleration Loads*

According to the *VEGA User's Manual* the maximum expected steady state accelerations are [53, chapter 3.2.1]:

$$a_{VEGA\_long} = 5.5g$$
$$a_{VEGA\_lat} = 0.9g$$

But according to ECSS the qualification testing of space equipment shall be performed at [19, Section 5.1.9.4]:

$$a_{ECSS\_long} = 7.5g$$
$$a_{ECSS\_lat} = 7.5g$$

Moreover, ECSS demands a qualification factor of $f_Q = 1.25$ [19, Section 4.8.1.2] that should be multiplied to the expected load. To cover both limit loads, the maximum of the loads in each direction is chosen and multiplied by the qualification factor:

$$\begin{aligned} a_{long} &= \max\left\{a_{VEGA\_long}, a_{ECSS\_long}\right\} \cdot f_Q \qquad \text{(A.4)} \\ &= 9.375g \\ a_{lat} &= \max\{a_{VEGA\_lat}, a_{ECSS\_lat}\} \cdot f_Q \qquad \text{(A.5)} \\ &= 9.375g \end{aligned}$$

So a combined maximum acceleration a_{SA} for all axis can by defined to:

$$a_{SA} = a_{long} = a_{lat} = 9.375g \tag{A.6}$$

A.7.2 *Acoustic & Random Vibration Loads*

According to ECSS qualification testing of an antenna need to include either acoustic test or random vibration tests but it is not necessary to do both [19, Table 5]. Hence, it needs to be decided which load case should be used for the sizing.

Table 31 shows the acoustic loads as they are defined for VEGA and for equipment testing in the ECSS.

CENTER FREQUENCY	LEVEL (VEGA)	LEVEL (ECSS)
31.5Hz	124dB	130dB
63Hz	129dB	135.5dB
125Hz	135dB	139dB
250Hz	132dB	143dB
500Hz	131dB	138dB
1000Hz	120dB	132dB
2000Hz	100dB	128dB
4000Hz	—	124dB
8000Hz	—	120dB
OASPL	138.5dB	147dB

OASPL: Overall Acoustic Sound Pressure Level

Table 31.: Acoustic test levels from VEGA User's Manual [53, Table 3.2] and ECSS on testing[19, Table 13]

Obviously, all test levels for ECSS are higher than the one defined for VEGA. Therefore, one should use the ECSS loads to be on the safe side.

A similar comparison of the random vibration loads for VEGA and ECSS is not possible as only ECSS provides such loads. For VEGA only a statement is made that the acoustics will cover all random vibration loads for payload above 300kg [53, chapter 3.2.3].

Contrary, ECSS specifies the in Table 32 defined spectra for equipment of more than 50kg mass. It also contains a value for the representative g-RMS value that can be used to transform

a random vibration spectrum into an equivalent steady state acceleration.

The authors of the *NASA's FEMCI Website*[1] define the g-RMS value as:

ASD: Acceleration Spectral Density

> *"[...] the square root of the area under the ASD vs. frequency curve [...]"*
>
> *[1, 1st paragraph]*

Theoretically, 68.3% of the accelerations of the time history of a stationary Gaussian random signal are smaller than the g-RMS value. This value is called the 1-Sigma-g-RMS value and will be further referred here as $a_{1\sigma GRMS}$. To cover the very majority of the possible accelerations, the value need to be multiplied by 3 to create the 3-Sigma-g-RMS value (or $a_{3\sigma GRMS}$) that contains 99.7% of the exspected peaks. Please rerfer to [1] to get more information on this value and its calculation.

The referred Table 11 in [19] contains an obvious mistake. The level in the third row is given with 3db/octave. Table 10 in the same document shows that the last part of the spectrum is always characterised by a falling and not by a rising slope. Thus, -3dB/octave is assumed to be the correct value.

FREQUENCY	LEVEL (ECSS)	REMARK
20...110Hz	+3dB/octave	
110...700Hz	$0.09g^2/Hz$	$a_{1\sigma GRMS} = 11.12$
700...2000Hz	−3dB/octave	

Table 32.: Random vibration test levels for equipment with a mass of more than 50kg [19, Table 11]

It is important to understand, that the $a_{1\sigma GRMS}$ value is a special kind of mean value for a random spectrum that is often used in space engineering to size a spacecraft or spacecraft attached equipment by a representative but not identical steady state acceleration.

For the here given work the decision has been made to use the $a_{3\sigma GRMS}$ value as design load for random vibration and acoustic loads. Reasons for that assessment are:

1. Unspecific design of the membranes, which would be expected to be the most interesting parts for acoustic loads.
2. Less complex and, therefore, faster calculation of FE models for static acceleration instead of random vibration.
3. The used random spectrum derives from a general ECSS norm for space equipment that does neither respect the dedicated VEGA random spectrum nor the amplifying or

damping influence of the satellite that transfers the launch loads from the launcher to the antenna. Thus, it is assumed that the ECSS spectrum is very conservative and will overestimate the real loads on a VEGA launchers significantly. The difference between the complex random spectrum and the less complex $a_{3\sigma GRMS}$ value shall be thereby acceptable.

Therefore, the following equivalent steady state acceleration $a_{3\sigma GRMS}$ is used for the further design:

$$a_{3\sigma GRMS} = 3 \cdot a_{1\sigma GRMS} = 33.36g = 327.26\frac{m}{s^2}. \tag{A.7}$$

A.7.3 *Modal Requirements*

Usually, antennas that are mounted to spacecrafts are considered as *equipment* and needs to be design according to ECSS. Depending on the size, ECSS recommends first mode frequencies of 100Hz to 150Hz.

But those high frequencies are only suitable for small antennas attached to comparable big satellites. For the here discussed SAR antenna, the antenna structure will contribute a significant part of the satellite's mass and is, therefore, not only an attached equipment but a part of the satellite's structure itself.

According to the VEGA User's Manual the cantilevered fundamental mode frequencies of the hard-mounted *spacecraft* have to fulfil the following requirements [53, section 4.2.3.4]:

- In lateral launcher direction, all spacecrafts of 2500kg or less, need to have a first mode of $\geqslant$ 15Hz
- In longitudinal launcher direction, all spacecrafts of 2500kg or less, need to have a first mode between 20Hz and 45Hz

To respect both requirements, the design modal frequency of the stowed antenna $f_{1_{SA}}$ is set to:

$$f_{1_{SA}} = 25Hz$$

A.7.4 *Launch Lock Related Static Loads*

The chosen launch lock configuration is given in Figure 75a. It fixes each hub at two support blocks aided by two belts. As the hubs are not screwed or bonded to the blocks, the belts have to provide enough tension to ensure that the hub is never losing

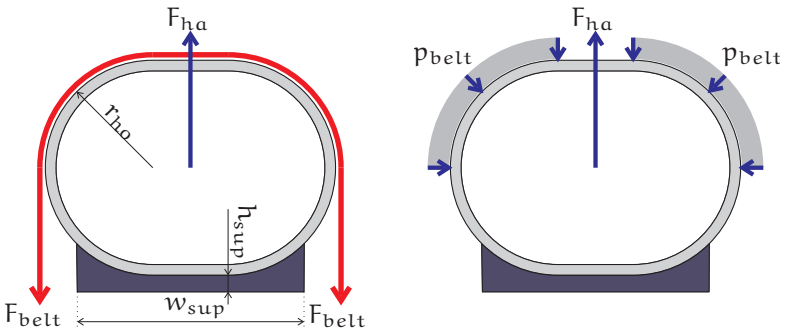

(a) with securing belt (b) with equivalent pressure

Figure 75.: Launch lock configuration

its contact to the blocks. Thereby, the worst case scenario is an acceleration applied in a direction perpendicular to the contact surface between hub and block.

So, for the following calculations it is assumed that:

$$F_{belt} = F_{ha} \cdot k_{hS} \tag{A.8}$$

$$= \frac{m_{hSA}}{2} \cdot a_{maxL} \cdot k_{hS} \tag{A.9}$$

where

F_{belt}	Belt tension force
F_{ha}	Hub acceleration/inertia force
m_{hSA}	mass of one hub in stowed configuration (plus all wrapped around parts and integrated interfaces)
a_{maxL}	maximum expected accelaration
k_{hS}	factor of safety for belt pretension

The maximum expected load has been already defined in Equation A.7 on page 157. It's the quasi static equivalent to the random vibrations and it can apply to all direction.

$$a_{maxL} = a_{3\sigma GRMS} = 33.36g = 327.26\frac{m}{s^2} \tag{A.10}$$

The mass of *one* stowed hub m_{hS} for the given basic configuration calculates to:

$$m_{hS} = m_{hs} + m_B + \frac{m_{st} + 3 \cdot m_{MA} + m_{MS}}{2} + 2 \cdot m_{bhIF} \tag{A.11}$$

where

m_{hs}	shell mass of one hub
m_B	combined mass of two half booms)
m_{st}	combined mass of the half of all transversal stiffeners
m_{MA}	mass of one antenna membrane
m_{MS}	mass of the service membrane
m_{bhIF}	mass of one boom to hub interface

The FEA based modelling of the configuration displayed in Figure 75a is possible but the friction affected interaction between belt and hub would add an uncomfortably high amount of complexity to the model and would, therefore, increase the calculation time significantly.

This equivalent concept neglects friction effects between hub and belt

Assuming that the resulting hub cross section deformation is very small in contrast to the overall dimensions, the simplification shown in Figure 75b is valid. This analogue setup uses a hub shell perpendicular pressure to substitute the tensioned belt and its effects on the hub. The equivalent pressure is added only for regions of the hub cross section that are in direct contact with the hub *and* that are curved. So it only effects the two upper circle quarters of the hubs cross section (see again Figure 75b)

To transform the in Equation A.9 define belt force F_{belt} to a pressure p_{belt} one part of the so called BOILER EQUATION is used. This set of equations is valid for a cylindrical boiler or vessel under defined inner pressure:

$$\sigma_{circ} = \frac{p \cdot r}{e} \tag{A.12}$$

$$\sigma_{long} = \frac{p \cdot r}{2 \cdot e} \tag{A.13}$$

where

σ_{circ}	shell stress in circumferential direction
σ_{long}	shell stress in longitudinal direction
p	pressure in the boiler
r	radius of the boiler
e	thickness of the boiler shell material

For the intended analogy only the definition of σ_{circ} Equation A.12 is of interest. The circumferential tension in a cylindric

boiler is equivalent to the longitudinal stress in the hub launch lock belt σ_{belt} loaded by the belt force F_{belt}:

$$\sigma_{belt} = \sigma_{circ} \tag{A.14}$$

The longitudinal stress in the belt σ_{belt} is thereby defined as followed:

$$\sigma_{belt} = \frac{F_{belt}}{e_{belt} \cdot w_{belt}} \tag{A.15}$$

where

e_{belt}	belt material thickness
w_{belt}	belt width

Inserting the Equations A.12 and A.15 in Equation A.14 results in:

$$\frac{p \cdot r}{e} = \frac{F_{belt}}{e_{belt} \cdot w_{belt}} \tag{A.16}$$

One can assume that the boiler radius r is equivalent to the bending radius of the belt and for $r_{ho} \gg e_{belt}$ it is also equivalent to the hubs outer radius r_{ho}. Moreover the thickness of the belt material t_{belt} is equivalent to the boiler material thickness t_{belt}. Applying these assumptions to Equation A.16 and solve it for p_{belt} results in:

$$\frac{p_{belt} \cdot r_{ho}}{\not{e}_{belt}} = \frac{F_{belt}}{\not{e}_{belt} \cdot w_{belt}} \tag{A.17}$$

$$p_{belt} = \frac{F_{belt}}{w_{belt} \cdot r_{ho}} \tag{A.18}$$

A.8 LOAD AND REQUIREMENT DEFINITION FOR THE DEPLOYED ANTENNA

- referred at page 74 -

A.8.1 *Membrane Tensioning Loads*

According to Table 6 and Equation 7.13 on page 52 a combined membrane tensioning force F_M of

$$F_M = 3 \cdot F_{MA} + F_{MS} = 9.709N \tag{A.19}$$

is expected at each frame to membrane interface. For the chosen configuration a total number of 36 interfaces are distributed over the entire frame, whereas 8 of them are attached to the hubs and 28 to the booms.

However, in contrast to the other loads, this one is strongly linked to the design of the membranes and therefore not fixed. So the used number of interfaces and the tensioning forces are just an example for the configuration described in chapter 7.

A.8.2 *Modal Requirements*

The first mode frequency for the deployed antenna $f_{1_{DA}}$ is defined in bullet #8 on page 11 to:

$$f_{1_{DA}} = 0.4Hz$$

A.9 HUB AND HUB SUPPORT BLOCK MATERIALS

- referred at page 69, 78 and 79 -

Table 33 contains the properties of the UD layer used for layup of the hub face sheet material. It is made of T800 fibre and a standard Epoxy resin. The values have been extracted from the standard ESAComp material data base (type `T800; Epoxy; UD-.200/216/60`).

ESAComp *is software able to calculate the combined properties of different composites (for details please refer to www.esacomp.com)*

The local Cartesian coordinate system is defined as followed:

- x and y direction are the laminates in-plane directions
- The fibres of the UD laminate are aligned with the x-axis
- the z-axis defines the out-of-plane direction and is therefore perpendicular to the ply

Table 34 gives the first failure stresses and strains that are used to asses the factor of safety against material damage.

Tables 35 and 36 contain the properties and failure criteria of the UD layer used for the hub core material. It is a aluminium honeycomb layer. The values have been extracted again from the standard ESAComp material data base (type `1/4-2024-0.0015; HON-/45`).

Moreover, the Tables 37 and 38 contain the properties and failure criteria of the aluminium used for the stiffener rings at the hub ends as well as the support blocks. The values have been extracted again from the standard ESAComp material data base (type `7178-T6`).

PROPERTY	SYMBOL	UNIT	VALUE
Elastic Modulus (x-direction)	E_{FSx}	$\frac{N}{m^2}$	$155.0 \cdot 10^9$
Elastic Modulus (y and z-direction)	E_{FSy}, E_{FSz}	$\frac{N}{m^2}$	$8.5 \cdot 10^9$
Shear Modulus (xy-direction)	G_{FSxy}	$\frac{N}{m^2}$	$5.5 \cdot 10^9$
Shear Modulus (yz-direction)	G_{FSyz}	$\frac{N}{m^2}$	$3.3 \cdot 10^9$
Shear Modulus (xz-direction)	G_{FSxz}	$\frac{N}{m^2}$	$5.5 \cdot 10^9$
Poisson's Ratio (yz-direction)	ν_{FSyz}	1	0.03
Poisson's Ratio (xy-direction)	ν_{FSxy}	1	0.3
Poisson's Ratio (xz-direction)	ν_{FSxz}	1	0.3
Density	ρ_{FS}	$\frac{kg}{m^3}$	1550.0
Fibre Volume Content	ψ_{FS}	%	60

Table 33.: Hub face sheet material - general properties

PROPERTY	SYMBOL	UNIT	VALUE
Maximum Tension (x-direction)	$\sigma_{FStx_{max}}$	$\frac{N}{m^2}$	$2000.0 \cdot 10^6$
Maximum Tension (y and z-direction)	$\sigma_{FSty_{max}}$, $\sigma_{FStz_{max}}$	$\frac{N}{m^2}$	$40.0 \cdot 10^6$
Maximum Compression (x-direction)	$\sigma_{FScx_{max}}$	$\frac{N}{m^2}$	$1500.0 \cdot 10^6$
Maximum Compression (y and z-direction)	$\sigma_{FScy_{max}}$, $\sigma_{FScz_{max}}$	$\frac{N}{m^2}$	$220.0 \cdot 10^6$
Maximum Shear (xy and xz-direction)	$\tau_{FSxy_{max}}$, $\tau_{FSxz_{max}}$	$\frac{N}{m^2}$	$80.0 \cdot 10^6$
Maximum Shear (yz-direction)	$\tau_{FSyz_{max}}$	$\frac{N}{m^2}$	$39.2 \cdot 10^6$

Table 34.: Hub face sheet material - first failure stresses and strains

PROPERTY	SYMBOL	UNIT	VALUE
Elastic Modulus (x and y-direction)	E_{Corex}, E_{Corey}	$\frac{N}{m^2}$	$1.0 \cdot 10^{-9}$
Elastic Modulus (y and z-direction)	E_{Corez}	$\frac{N}{m^2}$	$0.758 \cdot 10^{9}$
Shear Modulus (xy-direction)	G_{Corexy}	$\frac{N}{m^2}$	$1.0 \cdot 10^{-9}$
Shear Modulus (yz-direction)	G_{Coreyz}	$\frac{N}{m^2}$	$131.0 \cdot 10^{6}$
Shear Modulus (xz-direction)	G_{Corexz}	$\frac{N}{m^2}$	$290.0 \cdot 10^{6}$
Poisson's Ratio (yz-direction)	ν_{Coreyz}	1	0.5
Poisson's Ratio (xy-direction)	ν_{Corexy}	1	0.0
Poisson's Ratio (xz-direction)	ν_{Corexz}	1	0.0
Density	ρ_{Core}	$\frac{kg}{m^3}$	45.0

Table 35.: Hub core material - general properties

PROPERTY	SYMBOL	UNIT	VALUE
Maximum Compression (z-direction)	$\sigma_{Corecz_{max}}$	$\frac{N}{m^2}$	$1.724 \cdot 10^{6}$
Maximum Shear (xz-direction)	$\tau_{Corexz_{max}}$	$\frac{N}{m^2}$	$1.379 \cdot 10^{6}$
Maximum Shear (yz-direction)	$\tau_{Coreyz_{max}}$	$\frac{N}{m^2}$	$0.827 \cdot 10^{6}$

Table 36.: Hub core material - first failure stresses and strains

PROPERTY	SYMBOL	UNIT	VALUE
Elastic Modulus	E_{Alu}	$\frac{N}{m^2}$	$71.0 \cdot 10^{9}$
Shear Modulus	G_{Alu}	$\frac{N}{m^2}$	$27.0 \cdot 10^{9}$
Poisson's Ratio	ν_{Alu}	1	0.33
Density	ρ_{Alu}	$\frac{kg}{m^3}$	2820.0

Table 37.: Aluminium solid material - general properties

PROPERTY	SYMBOL	UNIT	VALUE
Maximum Stress	$\sigma_{Alu_{max}}$	$\frac{N}{m^2}$	$510.0 \cdot 10^6$
Maximum Shear	$\tau_{Alu_{max}}$	$\frac{N}{m^2}$	$300.0 \cdot 10^6$

Table 38.: Aluminium solid material - first failure stresses and strains

A.10 STATIC DEFORMATION OF DEPLOYED ANTENNA

- referred at page 89 -

The following figure show the static deformation of the deployed antenna in its reference configuration (later referred as conf0). The deformations in all figures are scaled with a factor of 200 to emphasise the otherwise very small deformations.

The *deflection sums* in the Figures 76 till 79 show the deflection of each element as a vectorial sum of the x, y, and z-deflection components or respectively the length of the related deflection vector.

The numbers in the figures are given in SI-units. So deflections are shown in Meter whereas strain is given as dimensionless factor.

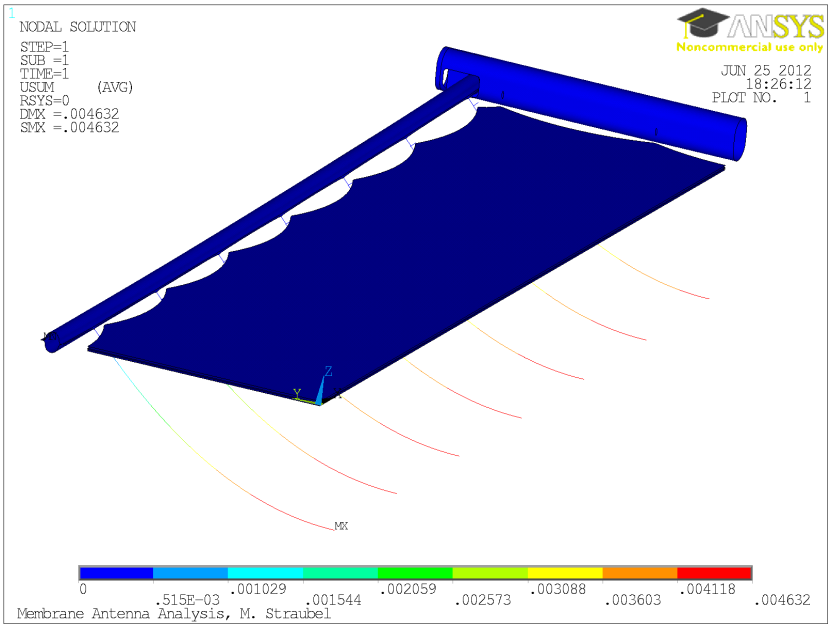

Figure 76.: Deflection sum for the entire antenna

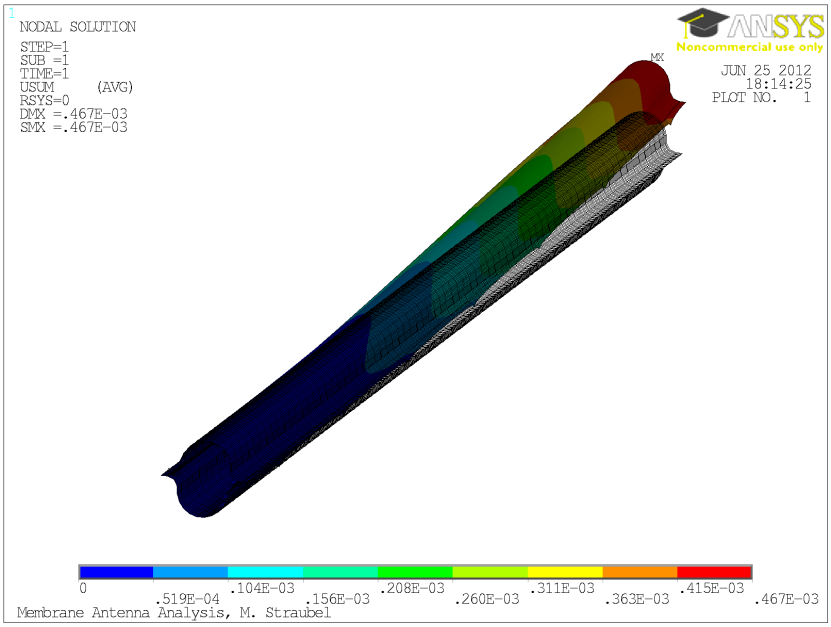

Figure 77.: Deflection sum of the boom

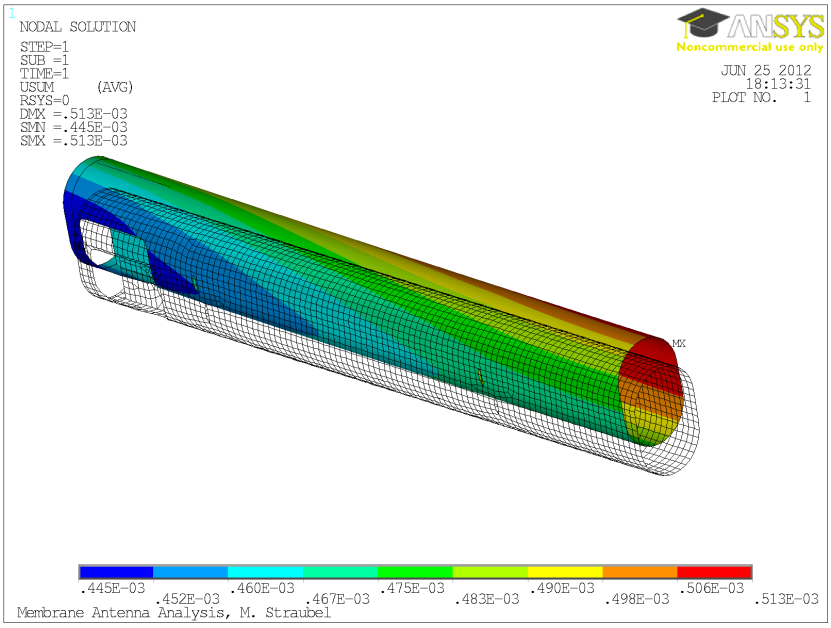

Figure 78.: Deflection sum of the hub

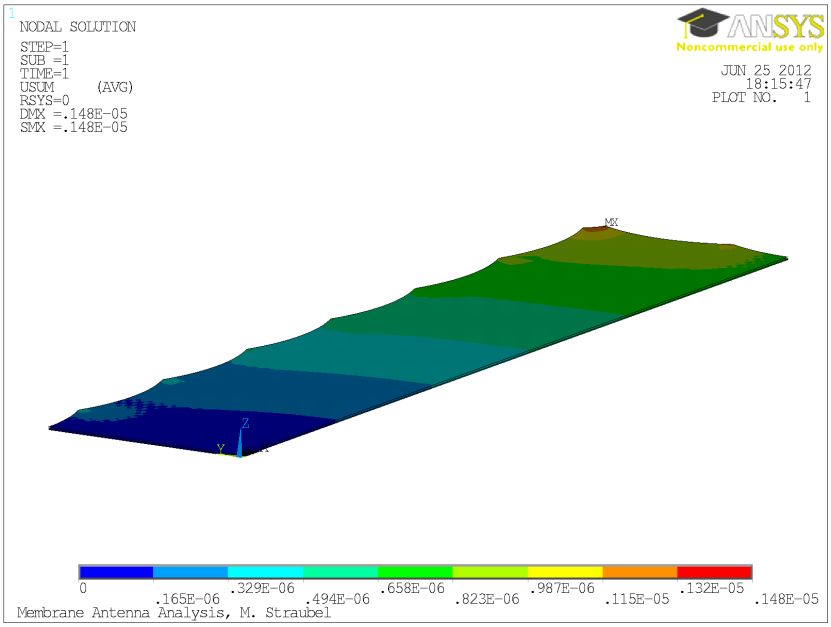

Figure 79.: Deflection sum of the membranes

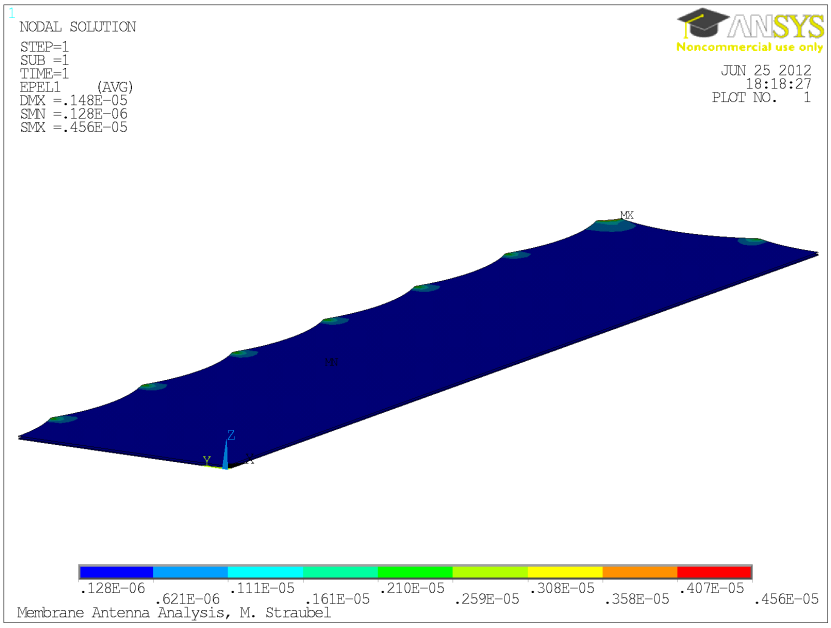

Figure 80.: First principle strain of the membranes

A.11 CLOSED LOOP SIZING CHAIN

- referred at page 116 -

The used Excel file for MATLAB input and output parameter handling is given here. To see all parameters of the above discussed configurations in one table. Moreover, parameters that are not discussed before are given.

This file has been split here manually to fit the pages and remain readable. Each column represents one configuration.

INPUTS	Comment on Variable	conf0	conf1	conf2	conf3	conf4	conf5	conf6	conf7	conf8
calcName	Identifier for automated result file naming									
aLWR	Length to width ration of antenna array	0.2500	0.2500	0.2500	0.2500	0.2500	0.2500	0.1667	0.1667	0.1667
mSThickness	Service membrane substrate thickness	1.00E-04	1.00E-04	1.00E-04	1.00E-04	1.00E-04	1.00E-07	1.00E-04	5.00E-05	5.00E-08
mSSpecAddMass	Additional mass on service membrane	4.48E-01	4.48E-01	4.48E-01	4.48E-01	1.00E-01	1.00E-04	4.48E-01	1.00E-01	1.12E-04
aFRequ	Required first mode frequency for deployed antenna	0.4	0.3	0.4	0.4	0.4	0.4	0.4	0.4	0.4
mFRequ	Required first mode frequency for tensioned membranes	0.52	0.39	0.52	0.52	0.52	0.52	0.52	0.52	0.52
hFRequ	Required first mode frequency for hub (stowed antenna)	25	25	20	25	25	25	25	25	25
aArea	Antenna aperture area	40	40	40	30	40	40	40	40	40
mCutOutLen	Preferred length of membrane cut outs	1	1	1	1	1	1	1	1	1
hRad	Hub radius (of circular cross section part)	0.1	0.1	0.1	0.1	0.1	0.1	0.1	0.1	0.1
hFSIncrement	Thickness of one hub UD layer	1.00E-04	1.00E-04	1.00E-04	1.00E-04	1.00E-04	1.00E-04	1.00E-04	5.00E-05	5.00E-05
hCoreThickness	Hub honey comb core thickness	0.01	0.01	0.01	0.01	0.01	0.01	0.01	0.01	0.01
bEsFactor	Boom E-modulus knockdown factor	1.4	1.4	1.4	1.4	1.4	1.4	1.4	1.4	1.4
bEllW	Boom geometry parameter	0.045	0.045	0.045	0.045	0.045	0.045	0.045	0.045	0.035

Figure 81.: Input part of Excel file used for data handling of the closed loop sizing chain

OUTPUTS										
calcName	*Identifier for automated result file naming*	*conf0*	*conf1*	*conf2*	*conf3*	*conf4*	*conf5*	*conf6*	*conf7*	*conf8*
aMass	*Antenna mass*	*51.83*	*50.75*	*51.83*	*39.08*	*34.94*	*23.93*	*51.61*	*29.61*	*20.98*
aSpecMass	Antenna specific mass	1.296	1.269	1.296	1.303	0.874	0.598	1.290	0.740	0.524
bMass	*Boom mass*	*1.87*	*1.66*	*1.87*	*1.42*	*1.74*	*1.66*	*2.58*	*2.28*	*2.03*
stMass	*Frame stiffener mass*	*0.85*	*0.64*	*0.85*	*0.49*	*0.65*	*0.45*	*0.59*	*0.41*	*0.34*
hMassC	*Combined hub mass*	*14.51*	*13.85*	*14.51*	*11.10*	*12.25*	*12.02*	*13.68*	*9.73*	*8.74*
mSMass	*Service membrane mass*	*24.81*	*24.81*	*24.81*	*18.68*	*10.51*	*0.01*	*24.91*	*7.34*	*0.01*
*mAMass*3*	*Membrane antenna mass (of three membranes)*	*9.61*	*9.61*	*9.61*	*7.23*	*9.61*	*9.61*	*9.65*	*9.65*	*9.65*
sIFMassComp	*Frame to membrane IF mass*	*0.18*	*0.18*	*0.18*	*0.16*	*0.18*	*0.18*	*0.20*	*0.20*	*0.20*
anW	*Antenna deployed width*	*4.07*	*4.02*	*4.07*	*3.59*	*4.04*	*4.02*	*3.56*	*3.50*	*3.45*
anL	*Antenna deployed length*	*13.30*	*13.30*	*13.30*	*11.58*	*13.30*	*13.30*	*16.11*	*16.11*	*16.11*
anLSto	Antenna stowed length	0.650	0.616	0.650	0.610	0.629	0.615	0.687	0.649	0.637
anVSto	Antenna stowed volume	0.608	0.569	0.608	0.504	0.584	0.568	0.563	0.523	0.506
mNFL	*Number of membrane attachment points in antenna length direction*	*14*	*14*	*14*	*12*	*14*	*14*	*16*	*16*	*16*
mNFW	*Number of membrane attachment points in antenna width direction*	*4*	*4*	*4*	*4*	*4*	*4*	*4*	*4*	*4*
hFSAdd0Layer	*Additional 0° Layers in hub laminate*	*1*	*1*	*1*	*0*	*0*	*0*	*1*	*1*	*0*
bCSScale	*Boom cross section scaling parameter*	*1.402*	*0.919*	*1.402*	*0.846*	*1.106*	*0.908*	*1.930*	*1.402*	*1.237*
compTime	*Calculation time in minutes*	*17.0*	*17.7*	*18.1*	*8.0*	*7.7*	*7.9*	*19.1*	*18.6*	*14.3*
hOffset	Hub geometry parameter	0.090	0.073	0.090	0.070	0.079	0.072	0.108	0.089	0.084
hF1	*First hub mode frequency*	*28.66*	*28.84*	*28.66*	*31.62*	*29.64*	*36.42*	*33.80*	32.90	*34.08*
hFSThickness	*Hub laminate face sheet thickness*	*0.00040*	*0.00040*	*0.00040*	*0.00030*	*0.00030*	*0.00030*	*0.00040*	*0.00020*	*0.00015*
mAAttF	*Antenna membrane attachment forces*	*0.880*	*0.494*	*0.880*	*0.681*	*0.879*	*0.879*	*0.669*	*0.669*	*0.821*
mSAttF	*Service membrane attachment forces*	*6.812*	*3.827*	*6.812*	*5.273*	*2.884*	*0.003*	*5.178*	*1.528*	*0.002*
bEllH	*Half height of ellipse in boom cross section*	*0.049*	*0.032*	*0.049*	*0.030*	*0.039*	*0.032*	*0.068*	*0.049*	*0.043*
hArea	*Hub surface area*	*1.509*	*1.429*	*1.509*	*1.263*	*1.460*	*1.428*	*1.368*	*1.290*	*1.256*
errorInd	*Error code (no errors if 0)*	*0*	*0*	*0*	*0*	*0*	*0*	*0*	*0*	*0*

Figure 82.: Output part of Excel file used for data handling of the closed loop sizing chain

PUBLICATIONS

Some ideas and figures have appeared previously in the publications [65], [66], [67], [68], [69], [70], [71], [12], [54], [59] and [60]

BIBLIOGRAPHY

[1] NASA FEMCI website. URL http://femci.gsfc.nasa.gov/random/randomgrms.html. Viewed on Nov 1st 2011. (Cited on page 156.)

[2] RADARSAT Systems: Satellite Characteristics. URL http://www.asc-csa.gc.ca/eng/satellites/radarsat/radarsat-tableau.asp#r2. Viewed on July 26th 2011. (Cited on page 14.)

[3] NASA Image Gallery. URL http://www.nasa.gov/multimedia/imagegallery/image_feature_924.html. viewed at Sep 17, 2011. (Cited on page 1.)

[4] A. L. Adler, M. M. Mikulas, and J. M. Hedgepeth. Static and Dynamic Analysis of Partially Wrinkled Membrane Structures. In *41st AIAA/ASME/ASCE/AHS/ASC Structures, Structures Dynamics, and Material Conference*, Atlanta, GA, USA, April 2000. paper reference AIAA-2000-1810. (Cited on page 46.)

[5] Gregory S. Agnes, Robert D. Abelson, Robert Miyake, John K. H. Lin, Joe Welsh, and Judith J. Watson. Preliminary Analysis of the 30-m Ultraboom Flight Test Article. In *46th Structural Dynamics and Materiels Conference*, Austin, TX, Apr 18-21 2005. Pasadena, CA : Jet Propulsion Laboratory, National Aeronautics and Space Administration, 2005. (Cited on page 21.)

[6] R.E. Allred, A.E. Hoyt, and P.M. McElroy. UV Rigidizable Carbon-Reinforced Isogrid Inflatable Booms. In *43rd AIAA/ASME/ASCE/AHS/ ASC Structures, Structural Dynamics, and Materials Conference*, Denver, Colorado, USA, Apr 22-25 2002. (Cited on page 21.)

[7] Weir Edward Arthur and Mee Francis Herbert Arthur. US-Patent 3,144,104, Coilable Tube Device, August 1964. URL http://www.freepatentsonline.com/3144104.html. (Cited on page 15.)

[8] V. Barbet. Inflatable Structures Technology. Summary report (non confidential abstract), Alcatel Alenia Space,

Aug 19 2005. Summary Report on ESA CONTRACT No 16627/02/NL/CK. (Cited on page 18.)

[9] V. Barbet, S. Guionie, G. Laduree, S. Langlois, R. Potes, and S. Lienard. Mechanical Testing of Inflatable Space Structure Beams. In *European Conference on Spacecraft Structures, Materials and Mechanical Testing*, Noordwijk, The Netherlands, May 10-12 2005. URL http://articles.adsabs.harvard.edu//full/2005ESASP.581E..98B/0000098.003.html. (Cited on pages 17 and 18.)

[10] Max D. Benton and Jr. William M. Robbins. US-Pantent 4,599,832, Extendible Structures, Jul 15 1986. (Cited on page 20.)

[11] J.T. Black. Videogrammetry Using Projected Circular Targets: Proof-of-Concept Test. In *21st International Modal Analysis Conference (IMAC)*, Kissimmee, Florida, February 3-6 2003. (Cited on page 42.)

[12] Joachim Block, Marco Straubel, and Martin Wiedemann. Ultralight Deployable Booms for Solar Sails and Other Large Gossamer Structures in Space. In *60th International Astronautical Congress*, Oct 12-16 2009. (Cited on page 171.)

[13] Thierry Bonnefond, G. Taubmann Montes, and P. Coste. Inflatable Capture Mechanism (ICM) for the Mars Sample Return (MSR) mission. In *ESA Workshop on Inflatable and rigidizable Structrues*, Oct 11 2006. Presentation. (Cited on pages 16 and 18.)

[14] Michael Brooks. *13 Things That Don't Make Sense*. Doubleday, Aug 12 2008. ISBN-10: 0385520689, ISBN-13: 978-0385520683. (Cited on page v.)

[15] D.P. Cadogan and M.S. Grahne. Deployment Control Mechanisms for Inflatable Space Structures. In *33 rd Aerospace Mechanisms Conference*, May 1999. (Cited on pages 25 and 26.)

[16] D.P. Cadogan, J.K. Lin, and M.S. Grahne. Inflatable Solar Array Technology. In *37th Aerospace Sciences Meeting and Exhibit*, Reno, NV, USA, Jan 11-14 1999. (Cited on page 19.)

[17] Mark V. Douglas. US-Patent 5,267,424, Module for an Articulated Stowable and Deployable Mast, AEC-Able Engineering Co., Inc., Dec 7 1993. (Cited on page 20.)

[18] DuPont. Summary of properties for Kapton® polyimide films. URL http://www2.dupont.com/Kapton/en_US/assets/downloads/pdf/summaryofprop.pdf. Viewed on August 8th, 2011. (Cited on page 60.)

[19] ECSS. ECSS-E-10-03A - space engineering - testing, Feb 15 2002. (Cited on pages 154, 155, and 156.)

[20] ECSS. ECSS-E-ST-10-02C - space engineering - verifikation, Mar 06 2009. (Cited on page 154.)

[21] H. Fang, M. Lou, and J. Huang. Design and Development of an Inflatable Relectarry Antenna. Technical report, JPL, May 15 2002. IPN Progress Report 42-149. (Cited on pages 19, 24, 27, and 137.)

[22] R.E. Freeland, C.D. Bilyeu, and M.D. Steiner. Large Inflatable Deployable Antenna Flight Experiment Results. *ACTA Astronautica*, 41:267–277, 1997. (Cited on page 16.)

[23] R.E. Freeland, C.D. Bilyeu, and G.R. Veal. Inflatable Deployable Space Structures Technology Summary. In *49 th International Astronautical Congress*, Melbourne, Australia, Sept 28 - Oct 2 1998. (Cited on pages 19 and 23.)

[24] U. Geppert, B. Biering, F. Lura, J. Block, M. Straubel, and R. Reinhard. The 3-Step DLR-ESA Gossamer Road to Solar Sailing. *Advances in Space Research*, 48:1695–1701, Dec 1 2011. ISSN 0273-1177. doi: DOI:10.1016/j.asr.2010.09.016. URL http://www.sciencedirect.com/science/article/pii/S0273117710006332. (Cited on page 141.)

[25] K.-H. Grote and J. Feldhusen. *DUBBEL - Taschenbuch fi¿½r den Maschinenbau*, volume 21. Spinger, 2005. ISBN 3-540-22142-5. (Cited on page 37.)

[26] Northrop Grumman. STEM TIP DRUM - Data Sheet. URL http://www.as.northropgrumman.com/products/aa_stem/assets/DS-202-STEMTIPdrum.pdf. (Cited on page 15.)

[27] Martin Hillebrandt. Experimentelle Verifikation von Low-Cost-CfK-Booms (engl. Experimental Verification of Low-Cost-CFRP-Booms). student research, DLR-IB 131-2012/21, August 2009. (Cited on page 96.)

[28] Martin Hillebrandt. Development of a New Deployable Mast for Gossamer Space Structures. Diploma Thesis, DLR-IB 131-2012/22, Jul 2011. (Cited on page 22.)

[29] Martin Hillebrandt, Marco Straubel, Christian Hï¿½hne, and Martin Wiedemann. A New Deployable Truss for Gossamer Space Structures. In *53nd AIAA/ASME/ASCE/AHS/ASC Structures, Structural Dynamics and Materials Conference at 13th AIAA Gossamer Systems Forum*, number 1584, Honolulu, Hawaii, USA, Apr 23-26, 2012. (Cited on pages 22 and 142.)

[30] J. Huang. The Development of Inflatable Array Antennas. *Antennas and Propagation Magazine*, 43:44–50, Aug 2001. (Cited on pages 25, 26, 27, 33, 34, 35, 126, 137, and 144.)

[31] J. Huang, V. A. Feria, and H. Fang. Improvement of the Three-Meter Ka-Band Inflatable Reflectarray Antenna. In *IEEE Antennas & Propagation Symposium*, Boston, MA, USA, Jul 2001. URL http://trs-new.jpl.nasa.gov/dspace/bitstream/2014/16439/1/00-2472.pdf. (Cited on page 25.)

[32] K. Iqbal and Sergio Pellegrino. Bi-stable Composite Shells. In *41st AIAA/ASME/ASCE/AHS/ASC Structures, Structural Dynamics, and Materials Conference and Exhibit*, Atlanta, GA, USA, Apr 3-6 2000. URL http://www-civ.eng.cam.ac.uk/dsl/publications/bistable.pdf. (Cited on page 15.)

[33] William J. Jorden. Soviet Fires Earth Satellite Into Space; It Is Circling the Globe at 18,000 M.P.H.; Sphere Tracked in 4 Crossings Over U.S. *The New York Times*, October 5 1957. URL http://www.nytimes.com/partners/aol/special/sputnik/sput-01.html. (Cited on page 1.)

[34] H. Klausing, E. Baur, S. Buckreuï¿½, W. Holpp, P. Honold, W. Keydel, and A. Moreira. *Radar mit Realer und Synthetischer Apertur*. Oldenbourg Wissenschaftsverlag GmbH, 2000. ISBN: 3-486-23475-7. (Cited on pages 23 and 143.)

[35] Gerhard Krieger and Alberto Moreira. Multistatic SAR Satellite Formations: Potentials and Challenges. In *IEEE Geoscience and Remote Sensing Symposium*, pages 2680–2684, Seoul, Korea, Jul 25-29 2005. (Cited on page 8.)

[36] S. Langlois and R. Roumï¿½as. European Perspectives for Inflatable Structures. In *European Conference on Spacecraft Structures, Materials & Mechanical Testing*, Toulouse, France, Dec 12 2002. (Cited on page 19.)

[37] Vaios Lappas. Gossamer Systems for Satellite Deorbiting: The CUBESAIL and DEORBITSAIL Space Missions. Gossamer Systems Forum 2012 Keynote: Systems for Satellite Deorbiting (presented at the AIAA SDM conference, Honolulu, USA), April 26, 2012. URL http://www.deorbitsail.com/media.html. presentation can be downloaded from the given web site. (Cited on page 141.)

[38] Y. M. Lefevre, S. Lienard, M. Eymard, and R. Roumeas. Materials and Wall Concepts for UV-Curable Inflatable Space Structures. In *European Conference on Spacecraft Structures, Materials and Mechanical Testing*, Noordwijk, The Netherlands, May 10-12 2005. URL http://articles.adsabs.harvard.edu//full/2005ESASP.581E..97L/0000097.002.html. (Cited on page 18.)

[39] John K. H. Lin, David P. Cadogan, John Huang, and V. Alfonso Feria. An Inflatable Microstrip Reflectarray Concept for Ka-Band Applications. In *41st AIAA/ASME/ASCE/AHS/ASC Structures, Structural Dynamics, and Materials Conference & Exhibit*, Atlanta, Georgia, USA, April 3-6 2000. (Cited on page 24.)

[40] B. C. Lopez, M. C. Lou, J. Huang, and W. Edelstein. Development of an Inflatable SAR Engineering Model. In *AIAA/ASME/ASCE/AHS/ASC Structures, Structural Dynamics, and Materials Conference and Exhibit*, volume AIAA-2001-1618, Seattle, WA, USA, Apr. 16-19 2001. (Cited on pages 25, 26, 27, and 137.)

[41] M. C. Lou and H. Fang. Development of Inflatable Antenna Structures. In *European Conference of Spacecraft Structures, Materials and Mechanical Testing*, Toulouse, France, Dec 11 2002. URL http://trs-new.jpl.nasa.gov/dspace/bitstream/2014/10683/1/02-2792.pdf. (Cited on pages 18, 19, and 24.)

[42] M. C. Lou and V. A. Feria. Development of Space Inflatable/Rigidizable Structures Technology. In *IUTAM-IASS Symposium on Deployable Structures: Theory and Applications*, Cambridge, U.K., September 1998. URL http://trs-new.jpl.nasa.gov/dspace/bitstream/2014/18818/1/99-2110.pdf. (Cited on page 19.)

[43] H.M.Y.C. Mallikarachchi and S. Pellegrino. Deployment Dynamics of Composite Booms with Integral Slotted Hinges.

In *50th AIAA/ASME/ASCE/AHS/ASC Structures, Structural Dynamics, and Materials Conference*, Palm Springs, CA, USA, May 4-7 2009. (Cited on pages 21 and 22.)

[44] H.M.Y.C. Mallikarachchi and S. Pellegrino. Design and Validation of Thin-Walled Composite Deployable Booms with Tape-Spring Hinges. In *52nd AIAA/ASME/ASCE/AHS/ASC Structures, Structural Dynamics and Materials Conference*, Denver, CO, USA, Apr 4-7 2011. (Cited on page 22.)

[45] Feoffrey W. Marks, Micheal T. Reilly, and Richard L. Huff. The Lightweight Deployable Antenna for the MARSIS Experiment on the Mars Express Spacecraft. In *36th Aerospace Mechanisms Symposium*, May 14-17 2002. (Cited on page 22.)

[46] Michael E. McEachen. Validation of SAILMAST Technology and Modeling by Ground Testing of a Full-Scale Flight Article. In *48th AIAA Aerospace Sciences Meeting Including the New Horizons Forum and Aerospace Exposition*, Orlando, Florida, USA, Jan 4 - 7 2010. (Cited on pages 19 and 20.)

[47] Akira Meguro, Akio Tsujihata, Naokazu Hamamoto, and Masanori Homma. Technology Status of the 13 m Aperture Deployment Antenna Reflectors for Engineering Test Satellite VIII. *Acta Astronautica*, 47(2-9):147 – 152, 2000. ISSN 0094-5765. doi: DOI:10.1016/S0094-5765(00)00054-0. URL http://www.sciencedirect.com/science/article/pii/S0094576500000540. Space an Integral Part of the Information Age. (Cited on page 23.)

[48] Alberto Moreira, Gerhard Krieger, Hauke Fiedler, Irena Hajnsek, Marian Werner, Manfred Zink, and Marwan Younis. TanDEM-X: A Satellite Formation for High Resolution Radar Interferometry. In *International Astronautical Congress (IAC)*, Oct 02-06 2006. (Cited on page 8.)

[49] T. W. Murphey. *Recent Advances in Gossamer Spacecraft - Booms and Trusses*, volume 212. AIAA, 2006. Editor: C. H. Jenkins, ISBN-10: 1-56347-777-7, ISBN-13: 978-1-56347-777-5. (Cited on pages 16, 20, and 22.)

[50] T. W. Murphey. Historical Perspectives on the Development of Deployable Reflectors. In *50th AIAA/ASME/ASCE/AHS/ASC Structures, Structural Dynamics, and Materials Conference*, Palm Springs, California, May 4 - 7 2009. (Cited on page 23.)

[51] Northrop Grumman. Telescopic mast data-sheet, 2010. URL http://www.as.northropgrumman.com/products/aa_telescopic_boom/assets/DS-401-TeleMast7301.pdf. (Cited on page 21.)

[52] R.S. Pappa, J.T. Black, and J.R. Blandino. Dot-Projection Photogrammetry and Videogrammetry of Gossamer Space Structures. In *21st International Modal Analysis Conference (IMAC)*, Kissimmee, Florida, February 3-6 2003. (Cited on pages 42 and 43.)

[53] E. Perez. *VEGA User's Manual*. ARIANESPACE, issue 3 / revision 0 edition, Mar 2006. URL http://www.arianespace.com/launch-services-vega/VEGAUsersManual.pdf. (Cited on pages 154, 155, and 157.)

[54] Ernst K. Pfeiffer and Marco Straubel. Advanced Materials and Architectures of Large Deployabel Antennas. In *Advance Lightweight Structures and Reflector Antennas*, Tbilisi, Georgia, Oct 14-16 2009. (Cited on page 171.)

[55] Allan G. Piersol and Thomas L. Paez. *Harris' Shock and Vibration Handbook*. McGraw-Hill Professional, 6th edition, 2010. ISBN: 978-0-07-150819-3. (Cited on page 95.)

[56] Mark K. Pryor and Jeremy O. Newlin. US-Patent US2006\0207189 A1, Deployable Structural Assemblies, Systems for Deploying Such Structural Assemblies and Related Methods, Sep 21 2006. (Cited on page 20.)

[57] M. Rodriguez-Cassola, P. Prats, D. Schulze, N. Tous-Ramon, U. Steinbrecher, L. Marotti, M. Nannini, M. Younis, P. Lopez-Dekker, M. Zink, A. Reigber, G. Krieger, and A. Moreira. First Bistatic Spaceborne SAR Experiments With TanDEM-X. *Geoscience and Remote Sensing Letters, IEEE*, 9(1):33 –37, Jan 2012. ISSN 1545-598X. doi: 10.1109/LGRS.2011.2158984. URL http://elib.dlr.de/70071/. (Cited on page 8.)

[58] S. Schwartz. Space Rigidization Techniques for Expandable Structures. *Modern Plastics, Volume*, 46(11), Nov 1969. (Cited on page 19.)

[59] C. Sickinger, H. Assing, H. Kï¿½ke, and M. Straubel. Verification Methology for Self-Deploying Support Frames. In *1st CEAS European Air and Space Conference*, Berlin, Germany, Sep 11-13 2007. (Cited on page 171.)

[60] C. Sickinger, M. Straubel, H. Kï¿½ke, and M. Leipold. Mechanical Concepts on Large Membrane Array Antenna Architectures. In *29th ESA Antenna Workshop*, ESA-ESTEC, Noordwijk, The Netherlands, April 18-20 2007. (Cited on page 171.)

[61] Christoph Sickinger. *Verifikation entfaltbarer Composite-Booms fï¿½r Gossamer-Raumfahrtsysteme*. Dissertation, Technische Universitï¿½t Carolo-Wilhemina zu Braunschweig, Mar 2009. URL http://www.shaker.de/de/content/catalogue/index.asp?lang=en&ID=8&ISBN=978-3-8322-8049-9&search=yes. Publisher: Shaker, ISBN: 978-3-8322-8049-9. (Cited on pages 16, 60, 70, 106, and 107.)

[62] P.D Soden, A.S Kaddour, and M.J Hinton. Recommendations for Designers and Researchers Resulting from the World-Wide Failure Exercise. *Composites Science and Technology*, 64:589 – 604, 2004. ISSN 0266-3538. doi: 10.1016/S0266-3538(03)00228-8. URL http://www.sciencedirect.com/science/article/pii/S0266353803002288. Failure criteria in fibre reinforced polymer composites Part C: Additional theories conclusions and recommendations. (Cited on page 79.)

[63] Kay Sommerwerk. Design and Modelling of a support and stabilizing cylinder for a very large stable membrane antenna. student research project thesis, DLR-IB 131-2012/47, Sep 02 2009. (Cited on pages 59 and 68.)

[64] O. R. Stohlman and S. Pellegrino. Effects of Component Properties on the Accuracy of a Joint-Dominated Deployable Mast. In *52nd AIAA/ASME/ASCE/AHS/ASC Structures, Structural Dynamics and Materials Conference*, Denver, CO, USA, Apr 4-7 2011. Paper ID: AIAA 2011-2163. (Cited on page 20.)

[65] Marco Straubel and Michael Sinapius. *Adaptive, Tolerant and Efficient Composite Structures (Editors: Martin Wiedemann and Michael Sinapius)*, volume 1 of *Research Topics in Aerospace*, chapter Boom Concepts for Gossamer Deployable Space Structures, pages 237–250. Spinger, Jun 30 2012. ISBN 978-3-642-29189-0. doi: 10.1007/978-3-642-29190-6. URL http://www.springer.com/engineering/mechanical+engineering/book/978-3-642-29189-0. (Cited on page 171.)

[66] Marco Straubel, Christoph Sickinger, and Stï¿½phane Langlois. Large Deployable Membrane Structures. In *1st CEAS European Conference on Spacecraft Structures, Materials & Mechanical Testing*, Berlin, Germany, Sep 11-13 2007. (Cited on pages 44 and 171.)

[67] Marco Straubel, Christoph Sickinger, and Stï¿½phane Langlois. Trade-Off on Large Deployable Membrane Antennas. In *30th ESA Antenna Workshop*, Noordwijk, The Netherlands, May 27-30 2008. (Cited on pages 27, 41, 46, and 171.)

[68] Marco Straubel, Michael Sinapius, and Stï¿½phane Langlois. On-Ground Rigidised, Deployable Masts for Large Gossamer Space Structures. In *European Conference on Spacecraft Structures, Materials & Mechanical Testing*, Toulouse, France, Sep 15-17 2009. (Cited on pages 16 and 171.)

[69] Marco Straubel, Stï¿½phane Langlois, Michael Sinapius, and Christian Hï¿½hne. Simulation and Test on Mechanical Behavior of a Deployable Membrane Antenna. In *32th ESA Antenna Workshop*, Noordwijk, The Netherland, Oct 5-8 2010. (Cited on pages 68 and 171.)

[70] Marco Straubel, Joachim Block, Michael Sinapius, and Christian Hï¿½hne. Deployable Composite Booms for Various Gossamer Space Structures. In *52nd AIAA/ASME/ASCE/AHS/ASC Structures, Structural Dynamics and Materials Conference*, number 2023, Denver, Colorado, USA, Apr 4-7 2011. (Cited on pages 16 and 171.)

[71] Marco Straubel, Christian Hï¿½hne, Christine Arlt, Stephane Langlois, and Michael Sinapius. Design and Sizing of a 40m² Deployable Membrane SAR Space Antenna. In *European Conference on Spacecraft Structures, Materials and Environmental Testing*, Noordwijk, NL, Mar 2012. (Cited on page 171.)

[72] G. Tibert. *Deployable Tensegrity Structures for Space Application*. PhD thesis, Royal Institute of Technology - Department of Mechanics, Stockholm, Sweden, July 11 2003. ISSN 0348-467X. (Cited on pages 15 and 20.)

[73] G. Veal and R. Freeland. IN-STEP Inflatable Antenna Description. In *AIAA Space Programs and Technologies Conference*, Huntsville, AL, USA, Sept 26-28 1995. (Cited on page 16.)

[74] C.G. Wang, H.F. Tan, X.W. Du, and Z.M. Wan. Wrinkling Prediction of Rectangular Shell-Membrane under Transverse In-Plane Displacement. *International Journal of Solids and Structures*, 44(20):6507 – 6516, 2007. ISSN 0020-7683. doi: DOI:10.1016/j.ijsolstr.2007.02.036. URL http://www.sciencedirect.com/science/article/pii/S0020768307001059. (Cited on page 46.)

[75] Y. W. Wong and Sergio. Pellegrino. Wrinkled Membranes. Part I: Experiments. *Journal of Mechanics of Materials and Structures*, 1:1–23, 2006. (Cited on page 42.)

[76] Y.W. Wong and S. Pellegrino. Amplitude of Wrinkles in Thin Membranes. *New Approaches to Structural Mechanics, Shells and Biological Structures, Kluwer Academic Publishers*, 1: 257–270, 2002. (Cited on page 46.)

[77] Y.W. Wong, S. Pellegrino, and K.C. Park. Prediction of Wrinkle Amplitudes in Solar Sails. In *44th AIAA/ASME/ASCE/AHS Structures, Structural Dynamics, and Materials Conference*, Norfolk, VA, USA, April 7-10 2003. paper reference AIAA-2003-1982. (Cited on pages 44, 45, and 46.)

[78] Manfred Zink, Gerhard Krieger, and Thierry Amiot. Interferometric Performance of a Cartwheel Constellation for TerrySAR-L. In *Fringe 2003 Workshop*, Frascati, Italy, Dec 1-5 2003. (Cited on page 8.)

[79] Andreas Zï¿½rnig. Numerische und experimentelle Optimierung von Spannungszustï¿½nden in dï¿½nnen Membranen. student research project thesis, DLR-IB 131-2012/48, Apr 9 2008. (Cited on pages 44, 45, and 46.)

[80] Andreas Zï¿½rnig. Entwurf und Modellierung einer Leichtbau-Radarantenne unter Berï¿½cksichtigung der Startlasten einer Trï¿½gerrakete vom Typ VEGA. diploma thesis, DLR-IB 131-2009/12, Sep 18 2008. URL http://elib.dlr.de/58425/. (Cited on pages 46, 47, 58, and 65.)

Marco Straubel

born March 2nd 1982 in Zerbst, Germany

Career

General

since 2006 DLR Institute of Composite Structures and Adaptive Systems

2011 Awarded by the DLR Board of Directors with a three month research semester at NASA's Langley Research Center in Hampton, VA, USA

since 2012 *Program Architect Space* at the DLR Institute of Composite Structures and Adaptive Systems and *Head of the Deployable Structures Team* of the Composite Design Department

Projects

2007 - 2010 Sponsorship from ESA-NPI on *Very Large Stable Membrane Antenna Architectures*

2009 In charge of DLR's boom deployment test during a parabolic flight campaign

since 2010 In charge of boom deployment mechanisms for the European solar sail demonstration mission GOSSAMER-1

Education

School

1989 - 2000 School education incl. primary school and gymnasium (high school), finished with German *Abitur*

University

2001 - 2006 Mechatronics at Otto-von-Guericke Universität, Magdeburg, Germany

Okt. 2006 Diploma Thesis

Title *Robust Vibration Control on a Parallel Robot Using Piezo Ceramics*

Institution DLR Institute of Composite Structures and Adaptive Systems

✉ *marco.straubel@gmail.com*